Scholar Commons
USF University of South Florida

University of South Florida
Scholar Commons

Graduate Theses and Dissertations | Graduate School

2005

# Theoretical And Experimental Investigation Of Phase Behavior Of Polymeric Systems In Supercritical Carbon Dioxide And Their Modeling Using SAFT

Ratka Damnjanovic
*University of South Florida*

Follow this and additional works at: https://scholarcommons.usf.edu/etd

 Part of the American Studies Commons

## Scholar Commons Citation

Damnjanovic, Ratka, "Theoretical And Experimental Investigation Of Phase Behavior Of Polymeric Systems In Supercritical Carbon Dioxide And Their Modeling Using SAFT" (2005). *Graduate Theses and Dissertations.*
https://scholarcommons.usf.edu/etd/2845

This Thesis is brought to you for free and open access by the Graduate School at Scholar Commons. It has been accepted for inclusion in Graduate Theses and Dissertations by an authorized administrator of Scholar Commons. For more information, please contact scholarcommons@usf.edu.

# Theoretical And Experimental Investigation Of Phase Behavior Of Polymeric Systems In Supercritical Carbon Dioxide And Their Modeling Using SAFT

by

Ratka Damnjanovic

A thesis submitted in partial fulfillment
of the requirements for the degree of
Master of Science in Chemical Engineering
Department of Chemical Engineering
College of Engineering
University of South Florida

Major Professor: Aydin K. Sunol, Ph.D.
John T. Wolan, Ph.D.
Vinay K. Gupta, Ph.D.

Date of Approval:
March 1, 2005

Keywords: polymers, solubility, methyl methacrylate, poly (methyl methacrylate), statistical associating fluid theory

© Copyright 2005 , Ratka Damnjanovic

# DEDICATION

I dedicate this Thesis to my family, my dear husband Aleksandar and our son Nenad, and my parents Milica and Ilija Kolevi, who have always been very supportive and encouraging in anything I tried to accomplish in life, and who are always proud with every success I achieve.

ACKNOWLEDGMENTS

I am grateful to my advisor Dr. Aydin K. Sunol and his wife, Dr. Sermin G. Sunol, for making this work possible, for their continuous support, encouragement, and guidance throughout the course of this study. I am extremely grateful to my husband Aleksandar, and my son Nenad, as well as the rest of my family, for their unconditional love, support, continuous encouragement, understanding, and patience during my studies. My colleagues have been extremely invaluable providing assistance, friendly atmosphere and optimism, especially Naveed Aslam with his advices and assistance, and for providing the code for the modeling part of this work, Raquel, Brandon, and Eddy who were always ready to offer their help with all the little details, and to my fellow class-mates, Jeffy, Keyur, and others, for the good spirits, humor, and positive attitude. I am also grateful to all my teachers and advisors from the past for bringing up in me the spirit and love for science, and for guiding me onto the path I've taken, especially my ex-mentors at the University of Witwatersrand in South Africa, Dr. Diane Hildebrandt and Dr. David Glasser. I am enormously thankful to our Graduate Coordinator, Dr. John Wolan, for being always helpful regarding all matters related to academic admission, academic advising, course selection, etc., second for teaching us a great class in Reacting Systems, and third for referring me for admission to the Omega Chi Epsilon Honor's

Society. Last but not least, I am grateful to Dr. McHugh and his group for their email correspondence, and for acknowledging my findings that the measured data that they have published in Fluid Phase Equilibria, 157 (1999), 285-297 is not reproducible. Dr. McHugh and his group are not sure why their solubility data are not reproducible, but they plan on repeating their measurements and publishing a short paper with a new data. They will reference me in their updated paper as the one who brought this discrepancy to their attention. I am truly honored by their gesture. Also, I want to thank my committee members, Dr. John T. Wolan and Dr. Vinay K. Gupta, for their valuable suggestions and help. And, again, I am grateful to Dr. Sunol and to the Chemical Engineering Department at USF for the Graduate Research Assistantship, and the appropriate financial support they provided which helped me going during the course of this study.

TABLE OF CONTENTS

LIST OF TABLES

LIST OF FIGURES

LIST OF SCHEMES

## LIST OF SYMBOLS

| | |
|---|---|
| $a$ | parameter in a cubic equation of state; activity |
| A | Helmholtz energy |
| $b$ | parameter in a cubic equation of state |
| M | molecular weight, g/mol |
| $M_w$ | weight-average molecular weight |
| $M_n$ | number-average molecular weight |
| P | pressure, bar |
| $P_c$ | critical pressure, bar |
| $P_r$ | reduced pressure, $P/P_c$ |
| $P^{vap}$ | pure component saturation pressure |
| $P^{sub}$ | pure component sublimation pressure |
| $R$ | gas constant |
| T | temperature, °C, K |
| $T_c$ | critical temperature, °C, K |
| $T_r$ | reduced temperature, $T/T_c$ |
| $T_g$ | glass transition temperature, °C, K |
| $T_m$ | melting temperature, °C, K |
| $T_c$ | crystallization temperature, °C, K |
| v | molar volume, $cm^3/mol$ |

| | |
|---|---|
| V | volume, $cm^3$ |
| Z | compressibility factor, Pv/RT |
| $\rho$ | density, $g/cm^3$ |
| $f_i$ | fugacity of species *i* in a mixture |
| $\hat{\varphi}$ | fugacity coefficient |
| $\mu_i$ | chemical potential |
| G | molar Gibbs free energy of a mixture (or of pure component) |
| S | entropy |
| $x$ | liquid-phase mole fraction |
| $y$ | vapor-phase mole fraction |
| $y_A$ | solubility of the solute in the supercritical fluid |
| $n$ | number of moles |
| $m$ | number of segments in a molecule |
| $r_{ij}$ | distance between molecules *i* and *j* |
| $k_{ij}$ | binary interaction parameter |
| $v$ | volume of site-site association |
| $w$ | Pitzer's acentric factor |

THEORETICAL AND EXPERIMENTAL INVESTIGATION OF PHASE BEHAVIOR OF POLYMERIC SYSTEMS IN SUPERCRITICAL CARBON DIOXIDE AND THEIR MODELING USING SAFT

Ratka Damnjanovic

## ABSTRACT

Environmentally friendly processing of materials is becoming an increasingly important consideration in a wide variety of emerging technologies. Polymer processing, in particular, has benefited tremendously in this venue from numerous advances achieved using high-pressure carbon dioxide ($CO_2$) as a viscosity modifier, plasticizing agent, foaming agent, and reaction medium. Polymer processing in supercritical fluids has been a major interest for a portfolio of materials processing applications including their impregnation into porous matrices. Also, SCF solvents are being examined as a media for polymerization processes, polymer purification and fractionation, and as environmentally preferable solvents for solution coatings. Pressurized $CO_2$ is inexpensive, sustainable, relatively benign, and versatile due to its gas-like viscosity and liquid-like densities, which can be controllably tuned through appropriate choice of temperature and pressure. Addition of high-pressure $CO_2$ to polymer systems can have a profound impact on their thermodynamic properties and phase behavior, since the number of interacting species increases due to the high-pressures, so that the compressibility also increases, as well as the plasticity effects. Even then, polymers are only sparingly soluble in $CO_2$ unless one uses an entrainer or surfactant. An addition of a liquid monomer co-solvent results in greatly enhanced polymer solubility in the

supercritical fluid at rather mild conditions of lower temperatures and reduced pressures. The focus of this research is to measure, evaluate and model the phase behavior of the methyl methacrylate-$CO_2$ and the poly (methyl methacrylate)-$CO_2$-methyl methacrylate system, where methyl methacrylate plays role of a co-solvent. Cloud-point data are measured in the temperature range of 30-80°C, pressures as high as 300 bar, co-solvent concentrations of 27 and 48.4 wt% MMA, and varying PMMA concentrations of 0.1, 0.2, 0.5, and 2.5 wt%. Solubility data is reported for these systems. The experimental results are modeled accurately using the Statistical Associating Fluid Theory (SAFT) for multi-component polymer/solvent mixtures. The measured solubility data appears to be significantly different than previously published results by McHugh et al, Fluid Phase Equilibria, 1999. Thorough investigation, re-calibration of the equipment, and repetition of the measurements has proved that the measured data is entirely correct and the reference data is significantly off, which indirectly gives credit to this work and opens room for amendments of those results. In addition, a reasonably closer qualitative match is achieved with the SAFT model used in this work as opposed to the modeling results published by the McHugh group.

# CHAPTER 1

# INTRODUCTION

## 1.1. Background

Solubility is a key fundamental property in studying phase behavior of multi-component mixtures. Phase behavior dictates feasibility of various separation techniques as well as material processing pathways. In polymer processing, particularly, the phase behavior of polymer solutions play important role, primarily because many polymers are produced in solution and the final product may contain some residual solvent. The physical properties of polymers are usually affected by the amount and type of the low-molecular-weight components they contain. A frequent technical problem is to remove essentially all the low-molecular-weight components; a common procedure is to volatilize them through a removal process called polymer devolatilization [10]. Total removal of solvent is particularly important for polymeric films, and other applications such as impregnation of porous materials with polymers. Therefore, proper solvent selection for any solubility process is a very important step as it can greatly influence and determine the homogeneity of the mixture, the degree of dissolution of the solute, in this case the polymer, and the effective removal of the residual solvent. Liquefied gases are potentially good candidates as they can be easily removed by varying the pressure.

Intuitively, we all know that gases are not considered as good solvents. However, many gases can exhibit significant solvent strength when they are compressed to liquid-like densities above their critical point. By operating in the critical region, the pressure and temperature can be used to control density, which regulates the solvent power of the supercritical fluid. This implies that it is the interaction between the solvent and solute molecules that determines how much solute dissolves in the SCF solvent. By compressing the solvent to liquid-like densities, we have only increased the probability that solvent and solute molecules will interact. The types of interactions (e.g., dispersion, polar, hydrogen bonding) depend on the physical characteristics of each of the species in the mixture [1].

Supercritical fluid technology has made tremendous strides, in the past decade, in terms of commercial application and fundamental understanding of solution behavior. Significant contribution has come from the continuing pressure on industry to move away from volatile organic compounds (VOC) and ozone depleting substances (ODS) as processing solvents [4]. Besides their environmentally friendly nature, there are additional advantages of a supercritical fluid process such as lower energy requirements, improved product quality, simplified reaction/separation scheme, higher selectivity, and higher recovery of the supercritical solvents compared to liquid solvents. Furthermore, popular supercritical solvents, such as carbon dioxide and water, are inflammable. Due to higher mobility compared to solvents and liquid-like solvency power compared to gases, the supercritical solvents have advantages such as easy control and manipulation of process parameters, favorable mass transfer and kinetic considerations for supercritical

processes [7]. While all of these characteristics are touted as “potential” advantages of a supercritical fluid process, hurdles remain to instill it as a viable choice in process design. However, the existence of several small and growing companies (Novasep, Trexel, Micell, Phasex, Thar Technologies) confirms that the recent successes are starting to carve out a market segment [4].

Some initial applications of supercritical fluids are the separation of caffeine from green coffee beans using supercritical carbon dioxide [7], deasphalting heavy residual oils with supercritical propane [1], and removing adsorbed materials from activated carbon with supercritical carbon dioxide [7]. The most current industrial applications make use of supercritical carbon dioxide in extraction and fractionation of food and biomaterials. The food and pharmaceutical industries use this technology more often than others since the nontoxic nature of $CO_2$ provides a strong impetus. Other applications being carried in a fluid phase include several of the particle generation technologies wherein material is dissolved in $CO_2$ or an organic solvent and precipitated from the solution via a pressure or solvent composition change. Particle generation is certainly an intense inquiry and is receiving attention primarily from the pharmaceutical and biotechnology industries, although there are significant polymer and inorganic material applications of these techniques [4].

Specific examples of recent successes are the new DuPont facility for producing fluoropolymers in a supercritical carbon dioxide-based solvent. Dry cleaning technology based on liquid $CO_2$, is competing in the textile market with both Washpoint (ICI/Linde) and Micare (Cool Clean Technologies), representing viable alternatives with chlorinated

solvents. Furthermore, there are several efforts underway to commercialize cleaning technologies in the microelectronics industry. Many new developments have arisen of the use of $CO_2$ as a novel reaction solvent. Novel construction of $CO_2$-phillic catalysts and surfactants have allowed both traditional and new reaction pathways to be explored. In fact, the development of novel polymeric surfactants for use with $CO_2$ has resulted in two Presidential Green Chemistry Awards [4].

## 1.2. Research Objectives

As it will be described in this work, it is believed that the largest potential application of supercritical solvents and supercritical fluid technology is in the area of polymerization and polymer processing, such as impregnation, particle formation, encapsulation, separation, foaming (batch and extrusion), blending, foam injection molding, etc. In this work, the use of $CO_2$ as a processing solvent for nonreactive processes, and more particularly for the physical processing and solubility of polymeric materials is studied.

Due to the increasing interest in the various emerging supercritical technologies, both the existing and the upcoming new applications require fundamentally correct description and quantification of physical, transport, and thermodynamic properties of components of interest.

Understanding the underlying physics and chemistry of SCF-polymer solution behavior provides the opportunity to fully exploit the potential of SCF-based polymer processing. Although a detailed understanding of the physics and chemistry of polymer-

liquid mixture has emerged in the past decades, significant challenges remain for developing the same level of understanding of polymer-SCF solution behavior [3].

At present, efficient development of SCF-based polymer processing technology suffers from the limitation that equations of state utilized for process simulation and modeling still do not adequately describe the unique characteristics of a long-chain polymer solution. The underlying issue is how to account for the intra- and intersegmental interactions of the many segments of the polymer connected to a single backbone relative to the small number of segments in a solvent molecule [3].

In this research, a review of the strengths and limitations of equation of state modeling of SCF-polymer system are studied. The advantages of using molecular thermodynamics and statistical associating fluid theory (SAFT) for modeling of SCF-polymer systems are presented. The SAFT model [19] used in this work has proven to produce better prediction of the solubility behavior of the $CO_2$-poly(methyl methacrylate) system used in this study than previous modeling attempts reported in the literature.

Fundamental properties of $CO_2$-polymer systems are discussed in this work with an emphasis on available data and measurement technologies. Available data from literature is compared to the experimental data obtained in this work, specifically the solubility of poly(methyl methacrylate) in $CO_2$ with the addition of a monomeric co-solvent such as methyl methacrylate. Much more accurate experimental data is obtained in this study for the solubility of the monomer and the polymer in $CO_2$.

## 1.3. Overview

In Chapter Two, a literature review is presented for the design of SCF-polymer systems, polymer blend thermodynamics, experimental techniques and measurement of solubility of polymers, equations of state and modeling of SCF-polymer behavior.

In Chapter Three, the experimental system description, equipment, parts and components description, experimental set-up and calibration, experimental procedures, preparation of chemicals and temperature-controlled environment are discussed.

In Chapter Four, the experimental system components, independently and integrated, are analyzed, and the experimental results are presented and discussed.

In Chapter Five, a conclusion of the results and future work perspectives are presented.

In the Appendices, the modeling algorithm description, modeling equations and sample calculations are presented and analyzed.

# CHAPTER 2

# LITERATURE REVIEW: SOLUBILITY MEASUREMENTS, CORRELATIONS AND PREDICTIVE METHODS

In this chapter, the measurement techniques, correlations and theoretical models used in literature are discussed with a brief fundamental and historic background. The solubility measurement methods and techniques are presented, followed by the prediction methods, correlations and theoretical models. The focus is on supercritical carbon dioxide-polymer systems.

## 2.1. Design of Polymer Blends

Although much progress has been made since the time of Flory and Huggins in the understanding of polymer blend thermodynamics, an ongoing research continues to elucidate how polymer blend phase behavior is affected by the presence of small-molecule solvents or exposure to elevated pressures.

In fact, many commercially relevant polymers are blends i.e. multicomponent systems, containing secondary components that impart desirable or improved properties such as color (dyes), flame resistance, toughness, tensile and impact strength, reduced cost (fillers), reduced oxidizability (antioxidants), and improved processability

(plasticizers and mold release agents). Blends are physical mixtures without any chemically linked sequences between the different species in the mixture. Polymer blends can be divided into one of two categories: *compatible* or *incompatible*. Compatible blends are those in which the chemically dissimilar macromolecules are combined to produce a mixture with a desirable set of physical properties. Such blends can be further classified as either *miscible* or *immiscible*. The term miscible is defined as being mixed at the molecular level.

Immiscible blends commonly exist as micrometer-scale spheroidal or fibrous dispersions of one component within a matrix of the other. The blend morphology characteristics are sensitive to blend composition, interfacial tension, and molecular weight. Compatible but immiscible blends are commonly referred as polymer alloys if one or more compatibilizing agents are present and the components cannot be physically separated after mixing.

Most mixtures of polymers are immiscible, if not strongly incompatible, due to a combination of the existence of long chains that effectively limit the entropy of mixing, and the natural tendency for either athermal or endothermic mixing. Polymer blends are miscible only if specific attractive interactions between dissimilar chains provide sufficient driving force for mutual dissolution of the constituents.

The kinds of factors that effect polymer miscibility are as follows: (i) entropy of mixing, (ii) dispersion forces, (iii) specific interactions, and (iv) free-volume differences. The dispersion forces lead always to positive heats of mixing and they are the main reason for phase separation in blends at low temperatures. Their effect weakens with

increasing temperature and, at some point, they are overcome by the entropy of mixing, leading to the appearance of the upper critical solution temperature (UCST). The specific interactions can be sufficiently strong leading to negative heats of mixing and polymer miscibility. Free-volume differences between the polymers, or between the polymer solute and the solvent, lead to negative volume of mixing favoring demixing, i.e. these free-volume differences can be sufficient to cause phase splitting. This effect, referred to also as equation of state (EOS) effect, becomes more important at higher temperatures, where the intermolecular interactions become weaker, leading to the lower critical solution temperature (LCST), [13]. Thus, at low temperatures and in the absence of specific interactions, polymer blends are not miscible due to dispersion forces. As the temperature increases, their effect diminishes and mixing occurs as a result of the entropy of mixing until the free-volume effects become important and immiscibility occurs, not necessarily at temperatures that can always be reached experimentally.

A liquid cosolvent can greatly enhance polymer solubility in a supercritical fluid solvent if it has an intermolecular potential that matches closely with that of a polymer repeat unit. In addition, a cosolvent that has a much higher density than that of the SCF solvent reduces the free volume difference between the polymer and the solvent. However, increasing the pressure also reduces the free volume difference between the solvent and the polymer and increases the probability of interaction between polymer, solvent, and cosolvent segments [2].

In this work, the impact of methyl methacrylate (MMA) cosolvent on the solubility of poly(methyl methacrylate) (PMMA) in supercritical $CO_2$ is studied and

analyzed. The addition of polar MMA to $CO_2$ provides enhanced polar interactions between PMMA, which is a weak polar polymer, and the mixed solvent. This enhanced interaction power is manifested through the decrease in the cloud-point temperatures and pressures for the system.

## 2.2. Solubility in Carbon Dioxide

The use of carbon dioxide as a solvent or diluent in the preparation and processing of polymers has found extensive interest. While it is a nonsolvent for most polymers, it is a very effective plasticizer, as discussed earlier [4]. The attractive qualities of carbon dioxide include the relatively low toxicity, tunable solvent properties (due to its compressibility), and low critical point ($T_c$ = 31.1°C, $P_c$ = 73.8 bar). The low critical point of $CO_2$ near the critical point makes the supercritical region easily accessible. Supercritical fluids are useful for their liquid like densities (solvating power) and their gas-like diffusivities (easy transport). The extensive compressibility that $CO_2$ possess near its critical point makes the solvent and transport properties of $CO_2$ easily tunable with modest changes in pressure or temperature.

Carbon dioxide has been shown to affect several pure polymer properties. Since $CO_2$ acts as a plasticizer, free volume and chain mobility increase in the presence of $CO_2$ and thus viscosity and glass transition temperature decrease. Also, with increased mobility, the chains can more easily arrange themselves into crystalline structures so crystallinity can increase upon addition of $CO_2$. Adding $CO_2$ increases polymer free volume and the effective surface tension of a polymer with absorbed $CO_2$ decreases [8].

## 2.3. Experimental Techniques for Solubility Measurement

Polymer miscibility in macromolecular systems is determined by variety of analytical methods, but most easily by measuring the thermal signature of the system: a miscible system will exhibit a single glass transition temperature ($T_g$) that lies between those of the pure components, if they were all polymers. If low molecular solvent is present in the mixture, other analytical methods routinely used to establish blend compatibility and miscibility are used, such as: dynamic mechanical analysis, cloud-point technique, gel permeation chromatography, electron microscopy, light scattering, small-angle X-ray diffraction, neutron scattering, carbon-13 NMR, ultrasonic velocity, and excimer fluorescence [8, 11]. For polymer-SCF systems, in order to be able to characterize polymer configurational properties in SCF solvents across wide ranges of pressure-temperature space, the major issue is in the application of these techniques to a high-pressure system setup.

Polymer chain conformation on its own has a major impact on the accessibility of the solvent to the repeat units in the polymer coil. Information on the role of chain conformation on solubility is slowly emerging as light, X-ray, and neutron scattering studies are reported quantifying the impact of polymer chain dimensions and polymer-SCF solvent interactions on the breadth of the single-phase region. These scattering techniques are themselves challenging since a radiation source and detector must be coupled to a high-pressure cell with well-defined geometrical characteristics so that artifacts of the apparatus are kept to a minimum. However, the benefits of these techniques can be significant since SCF properties are tunable, which means that it is

possible to traverse the entire good-to-poor solvent quality spectrum by adjusting solvent density with changes in pressure at a single temperature and in a single solvent. These kinds of studies can provide deeper insight into the role of microscopic level interactions on macroscopically observed phase behavior [3].

From a theoretical point of view, solution thermodynamic theories have been extended to discuss polymer miscibility.

## 2.4. Polymer Characteristics and Morphology

Differential Scanning Calorimetry Analysis (DSC) provides a method to analyze polymer morphologies through changes in the heat capacity of a sample. Specific polymer characteristics such as the glass transition temperature ($T_g$), melting temperature ($T_m$), degree of crystallinity, and phase separation behavior (polymer blends) can be monitored by DSC.

The glass transition temperature of a polymer is the point at which local segmental motion begins. Above this temperature, a polymer will behave as a rubbery material, below the $T_g$ it is in a glassy state were the chains are “frozen” in place. This is known as the viscoelastic behavior of polymers. The long chains of macromolecules in the amorphous phase exhibit a wide range of properties, from viscous flow to rigid solid, depending on the temperature. The properties change most rapidly, but continuously, through the $T_g$ region. For example, the viscosity typically changes by up to several orders of magnitude over this region. So, at the high-temperature end of the $T_g$ region, the molecules can easily flow, while at the low-temperature end the chains are rigid.

DSC is used to study the *thermal transitions* of a polymer, i.e. the changes that take place in a polymer when it is heated. The device is depicted in Figure 2.1 below.

In the most popular DSC design, two pans sit on a pair of identically positioned platforms connected to a furnace by a common heat flow path. In one pan, the polymer sample is placed. The other one is the reference pan, and it is left empty. The furnace can be turned on through the computer. The computer is programmed to heat the two pans at a specific rate, usually $10^{o}$C per minute, which is held constant throughout the experiment. This ensures that the two separate pans heat at the same rate as each other, even though the contents in the two pans are different, i.e. one has polymer in it, and one doesn't. Since there is extra material in the sample pan, the polymer sample, it will take more heat to keep the temperature of the sample pan increasing at the same rate as the reference pan. Just how much more heat is needed is what the DSC is measuring.

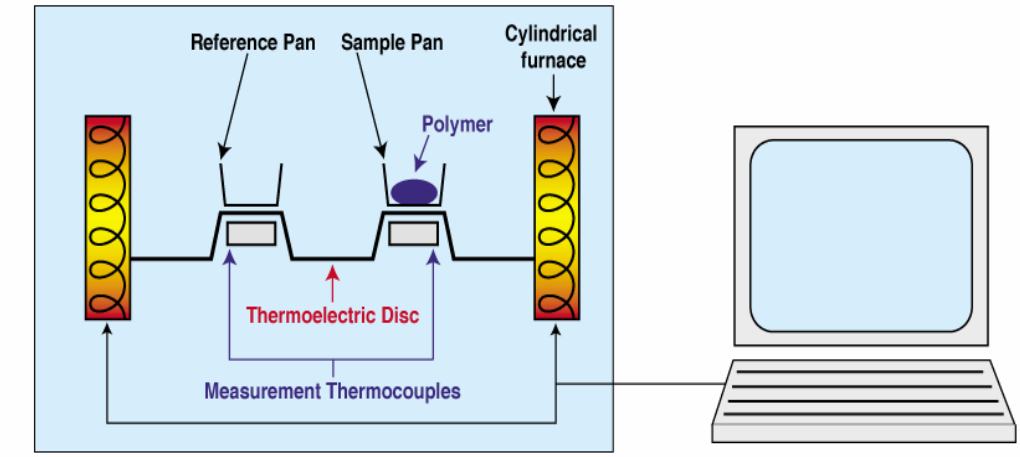


Figure 2.1 Differential Scanning Calorimetry (DSC)

Out of this measurement, a plot is obtained as the temperature increases. On the *x*-axis is the temperature. On the *y*-axis is the difference in heat flow between the sample and reference.

### 2.4.1. Heat Capacity

When the instrument starts heating the two pans, the computer will plot the difference in heat flow against temperature, which is the heat absorbed by the polymer against temperature. At first, the plot looks like the one given in Figure 2.2

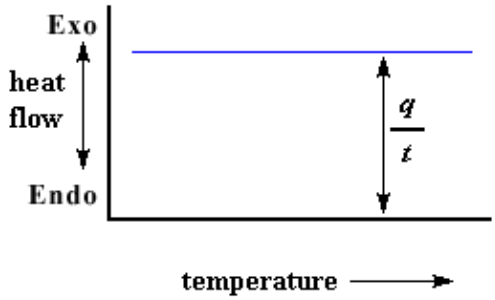


Figure 2.2 Heat Capacity

The heat flow at a given temperature is shown in units of heat, $q$ supplied per unit time, $t$. The heating rate is temperature increase $\Delta T$ per unit time, $t$.

$$Heat\ flow = \frac{heat}{time} = \frac{q}{t}$$

$$Heating\ rate = \frac{temperature\ increase}{time} = \frac{\Delta T}{t}$$

When the heat flow $q/t$ is divided by the heating rate $\Delta T/t$, results in heat supplied, divided by the temperature increase.

The amount of heat it takes to get a certain temperature increase is called the *heat capacity*, or $C_p$, which can be easily figured out from the DSC plot.

$$\frac{\frac{q}{t}}{\frac{\Delta T}{t}} = \frac{q}{\Delta T} = C_p = heat\,capacity$$

2.4.2. The Glass Transition Temperature

When the polymer is heated a little more, after a certain temperature, the plot will shift downward suddenly, as shown in Figure 2.3

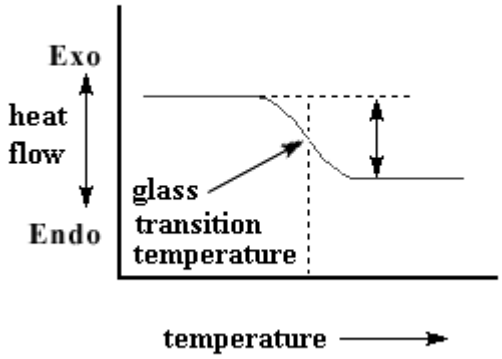


Figure 2.3 Glass Transition Temperature

This means heat is being absorbed by the sample. It also means that there is a change (increase) in its heat capacity. This happens because the polymer has just gone through the glass transition. Polymers have a higher heat capacity above the glass transition temperature than they do below it. Because of this change in heat capacity that occurs at

the glass transition, DSC can be used to measure a polymer's glass transition temperature. That change doesn't occur suddenly, but takes place over a temperature range. Usually, the middle of the incline is taken to be the $T_g$.

### 2.4.3. Crystallization

Above the glass transition, the polymers have a lot of mobility, and never stay in one position for very long. When they reach the right temperature, they will have gained enough energy to move into very ordered arrangements, crystals. When polymers fall into these crystalline arrangements, they give off heat. This can be seen as a big peak in the plot of heat flow versus temperature.

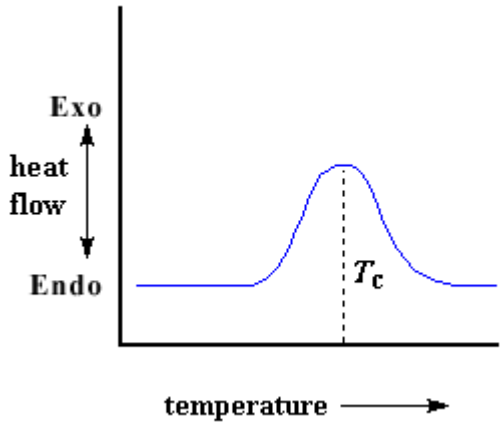


Figure 2.4 Crystallization Temperature

The temperature at the highest point is usually considered to be the polymer's crystallization temperature, or $T_c$. The area of the peak, however, represents the latent energy of crystallization for the polymer. But most importantly, this peak tells us that the

polymer can in fact crystallize. If it is analyzed a 100% amorphous polymer, like atactic polystyrene, we wouldn't get one of these peaks, because such materials don't crystallize. The optimum crystallization temperature occurs between the $T_g$ and $T_m$. Crystallization is also called an *exothermic* transition because the polymer gives off heat when it crystallizes.

### 2.4.4. Melting

Heat may allow crystals to form in a polymer, but too much of it can do the opposite. If we keep heating the polymer past its $T_c$, eventually we'll reach another thermal transition, one called melting. When we reach the polymer's melting temperature, or $T_m$, those polymer crystals begin to fall apart, that is they melt. The chains come out of their ordered arrangements, and begin to move around freely.

The heat that the polymer gave off when it crystallized, is needed back when the melting temperature, $T_m$, is reached. There is a latent heat of melting as well as a latent heat of crystallization. When the polymer crystals melt, they must absorb heat in order to do so. Melting is a first order transition, which means that when you reach the melting temperature, the polymer's temperature won't rise until all the crystals have melted. This also means that the furnace is going to have to put additional heat into the polymer in order to melt both the crystals *and* keep the temperature rising at the same rate as that of the reference pan. This extra heat flow during melting shows up as a large dip in the DSC plot as heat is absorbed by the polymer. It looks like this:

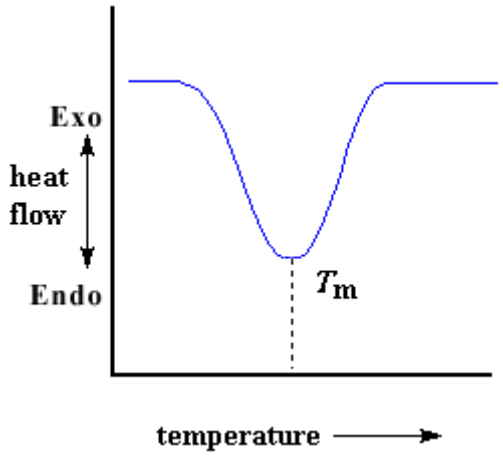


Figure 2.5 Melting Temperature

The heat of melting can be determined by measuring the area of this dip. Usually, the temperature at the apex of the dip is considered to be the point where the polymer is completely melted. Melting is also called an *endothermic* transition, because it is required to add energy to the polymer to make it melt.

### 2.4.5. Differential Scanning Calorimetry of Polymers

Summarizing the above, the first step in the plot is when the polymer is heated past its glass transition temperature, then there is a big peak when the polymer reaches its crystallization temperature, then finally there is a big dip when the polymer reaches its melting temperature. Putting them all together, a whole plot often looks something like this:

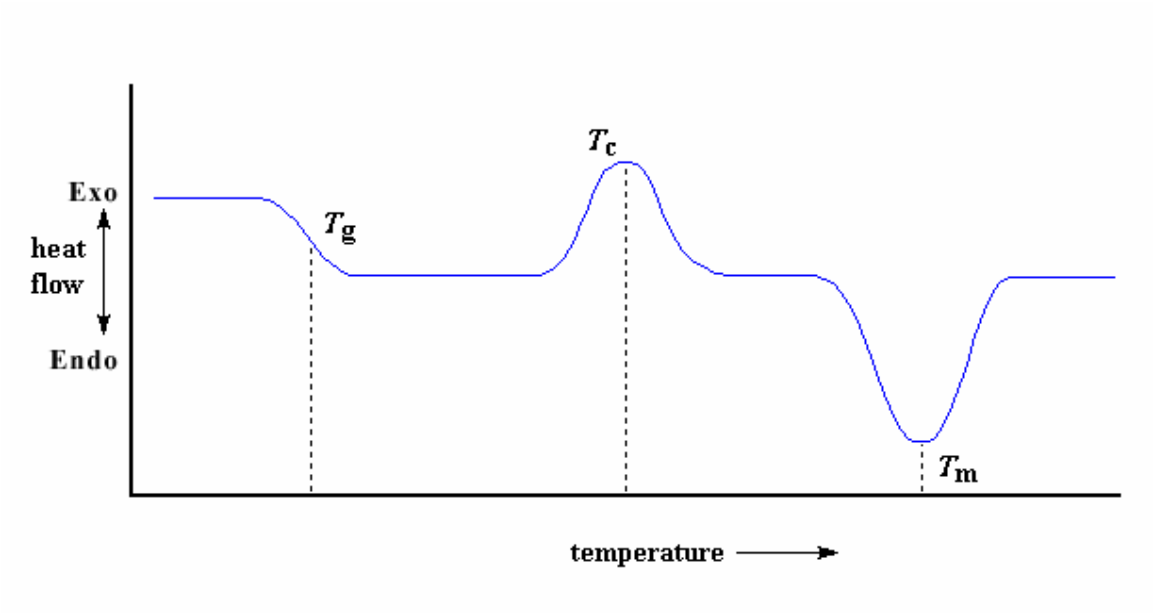


Figure 2.6 DSC Thermal Signature of a Specific Polymer

Of course, not every peak shows on every DSC plot. The crystallization peak and the melting dip will only show up for polymers that can form crystals. Completely amorphous polymers won't show any crystallization, or any melting either. But polymers with both crystalline and amorphous domains, will show all the features that are seen above. Most polymers are either completely amorphous or have an amorphous like component even if they are crystalline.

By looking at the DSC plot, a big difference can be seen between the glass transition and the other two thermal transitions, crystallization and melting. For the glass transition, there is no peak, and there's no dip, either. This is because there is no latent heat given off, or absorbed, by the polymer during the glass transition. Both melting and crystallization involve absorbing or giving off heat. The only thing we do see at the glass transition temperature is a change in the heat capacity of the polymer.

Because there is a change in heat capacity, but there is no latent heat involved with the glass transition, the glass transition is called a *second order transition*. The mechanical properties of polymers change drastically when the temperature crosses the $T_g$. For example, the Elastic Modulus may decrease by a factor of 1000 times as the temperature is raised through the $T_g$. Transitions like melting and crystallization, which do have latent heats, are called *first order transitions*.

To summarize, the basic theory and terminology of polymers was presented in this section. This review is important to understand the basic rheological phenomena associated with polymers and their behavior at high temperatures.

## 2.5. Thermodynamic Phase Behavior of Polymer Blends

The phase behavior of polymer blends can be described by the Gibb's free energy of mixing ($\Delta G_{mix}$), which is dependant on both the enthalpic ($\Delta H_{mix}$) and entropic ($\Delta S_{mix}$) changes on mixing, and is negative for favorable processes.

$$\Delta G_{mix} = \Delta H_{mix} - T\Delta S_{mix} < 0 \qquad (2.1)$$

The coexistence curve and the limit of stability are the boundaries of the T-Φ (Temperature-Segment Fraction Polymer) phase diagram separating the miscible, metastable and immiscible regions. The coexistance curve (binodal) is described by the equality of chemical potential of component *i* ($\mu_i$) in the two phases:

$$\mu_i' = \mu_i'' \qquad (2.2)$$

while the limit of stability (spinodal) is described by the second derivative of the Gibb's molar free energy change of mixing with respect to composition (mole fraction).

$$\left(\frac{\partial^2 g_{mix}}{\partial x^2}\right)_{T,P} < 0 \qquad (2.3)$$

A decrease in the Gibbs energy of a binary mixture due to phase separation can occur only if a plot of the Gibbs energy change of mixing against mole fraction is, in part, concave downward [10]. In blends, phase separation can occur either upon cooling or upon heating, or both. Speaking in polymers terminology, the analogous process to phase separation is called ordering, i.e. the individual polymer constituents start to organize themselves around the backbone of the polymer, beginning to condense within themselves which causes pull-back, rejection and splitting from the other components in the mixture [8]. This process can also occur upon cooling, heating, or both. If a blend separates upon cooling, this transition is labeled an upper critical solution temperature (UCST). However, if phase mixing or disordering (opposite of ordering) occurs upon cooling, the transition is labeled a lower critical solution temperature (LCST). In a T-x diagram, the highest point on the phase diagram is the critical solution temperature, $T^c$. At temperatures $T > T^c$, the mixture is completely miscible because for all mole fractions $\left(\partial^2 \Delta_{mix} g / \partial x^2\right)_{T,P} > 0$. At $T < T^c$, the mixture is partially miscible because in part of the mole fraction range $\left(\partial^2 \Delta_{mix} g / \partial x^2\right)_{T,P} < 0$. The binodal curve is the boundary between the one-phase region and the two-phase region. Within the two-phase region, the spinodal curve [$\left(\partial^2 \Delta_{mix} g / \partial x^2\right)_{T,P} = 0$] distinguishes the unstable region [$\left(\partial^2 \Delta_{mix} g / \partial x^2\right)_{T,P} < 0$] from the metastable region [$\left(\partial^2 \Delta_{mix} g / \partial x^2\right)_{T,P} > 0$]. If the overall mole fraction of the mixture falls within the unstable region, spontaneous demixing occurs when going from the one-phase to the two-phase region [10].

An understanding of what causes each of these types of transitions in each blend system facilitates an understanding of how the presence of carbon dioxide could affect the phase behavior of a given polymer blend.

## 2.6. Thermodynamic Modeling of Polymer Solutions and Blends

At the foundation of any process modeling and simulation are the property models used to describe physical properties of the components involved. The selection of model and its parameters profoundly affect every step in the simulation. In the case of modeling polymer processing and production processes, this task becomes particularly challenging because in such processes one encounters mixtures of solvents made of small conventional molecules, and polymers, which have long-chain structure. It is essential to use models that can simultaneously describe the behavior of both polymers and conventional molecules with acceptable accuracy. Equations of state (EOS) are very attractive tools for such property modeling.

Understanding the phase behavior of polymer solutions in supercritical fluids (SCF) is of great theoretical and practical interest. Predicting phase boundaries and phase compositions (e.g. solubilities) for such systems is difficult because the molecules of the polymer and solvent greatly differ in size, and their mixtures are highly non-ideal at high pressures. The thermodynamic models for polymer solutions that are being used in practice basically belong to two categories, *lattice models* and *perturbation models*. In lattice models, the molecules are assumed to have one or more segments, and the partition function of the system can be obtained by counting the possible configurations

when these segments are arranged in hypothetical cells that are like the lattices in the solid materials. Then the thermodynamic properties can be calculated on the basis of statistical mechanics. A number of models reported in the literature are based on this approach. For polymer solutions under high pressure, a good lattice model to use could be the Sanchez-Lacombe model, which can correlate the experimental data for a range of molecular weights [16, 17, 18].

On the other hand, a good perturbation model to use would be the model known as SAFT or statistical associating fluid theory, which was recently developed by Chapman et al. and Huang and Radosz [21]. The SAFT theory is based on the relationship between the residual Helmholtz free energy due to association and the monomer density, which is again related to the association strength. Detailed description of these models can be found in the literature.

The objective of this work is the observation of the phase behavior of polymers in the high-pressure $CO_2$ solvent, as well as the examination of the validity of an appropriate EOS and mixing rules for such polymer/supercritical fluid system. This process is an authentic example of how the principles of thermodynamics can be extended to high-pressure processes.

Undoubtedly, the largest potential application of supercritical fluid technology is in the area of polymer processing, although polymer/SCF phase equilibrium calculations confront us with the situation where the solute molecule can have a molecular weight in the hundreds of thousands for high molecular weight polymers. Therefore, some modifications to the thermodynamics calculation scheme must take place. While the

fundamental equations remain the same as those for small molecule systems, the equation of state is different. We must now deal with mixtures of components that differ substantially in molecular size.

### 2.6.1. High-Pressure Vapor-Liquid Equilibria

Various modeling procedures have been proposed in the literature to predict the phase behavior of vapor-liquid systems at high pressures. (The designation vapor is used synonymously with supercritical fluid in this context). Regardless of the modeling procedure, the following thermodynamic relationships, or their equivalent relationships in terms of chemical potentials, must be satisfied for two phases to be in equilibrium.

$$f_i^V(T,P,y_i) = f_i^L(T,P,x_i), \qquad i = 1,\ 2,\ 3 \ldots\ m \tag{2.4}$$

The most thermodynamically consistent method for calculating high-pressure phase behavior is to choose an equation of state to model both the liquid and the vapor of SCF phases. With this approach, the fugacity in each component can be written as

$$f_i^V(T,P,y_i) = y_i \varphi_i^V P \tag{2.5}$$

$$f_i^L(T,P,x_i) = x_i \varphi_i^L P \tag{2.6}$$

therefore,

$$y_i \varphi_i^V = x_i \varphi_i^L \tag{2.7}$$

where subscripts $L$ and $V$ refer to liquid and vapor phases respectively, $f$ is the fugacity and $\varphi$ is the fugacity coefficient. The equilibrium ratios (K-factors) are given by:

$$K = \frac{y_i}{x_i} = \frac{\varphi_i^L}{\varphi_i^V} \tag{2.8}$$

To compute the fugacity coefficients for the vapor and liquid phase, the exact thermodynamic relationships (Prausnitz, 1969) can be used.

For the vapor:

$$\ln \varphi_i^V = \frac{1}{RT} \int_{v^V}^{\infty} \left[ \left( \frac{\partial P}{\partial n_i} \right)_{T,V,n_i} - \frac{RT}{V} \right] dv - \ln \left( \frac{Pv^V}{RT} \right) \tag{2.9}$$

and for the liquid:

$$\ln \varphi_i^L = \frac{1}{RT} \int_{v^L}^{\infty} \left[ \left( \frac{\partial P}{\partial n_i} \right)_{T,V,n_i} - \frac{RT}{V} \right] dv - \ln \left( \frac{Pv^L}{RT} \right) \tag{2.10}$$

where $R$ is the gas constant, $v^V$ is the molar volume of the vapor phase, $v^L$ is the molar volume of the liquid phase, $n_i$ is the number of moles of component $i$,

$Z = \frac{Pv}{RT}$ in each equation is the compressibility factor of the mixture, while $\left( \frac{\partial P}{\partial n_i} \right)_{T,V,n_i}$ can be determined analytically from the appropriate equation of state for the system.

In many cases, high-pressure phase behavior can be reasonably represented with a cubic EOS if the components in the mixture do not differ too substantially in intermolecular strengths or in size, structure, or shape. Then, the Peng-Robinson (1976), or the Soave-Redlich-Kwong (1972) equations of state would produce satisfactory results.

However, for polymer-SCF high-pressure systems, a more sophisticated model is needed, such as the lattice-gas model, where the *P-V-T* properties of a pure component are calculated assuming that the component is broken into parts or “mers” that are placed into a lattice, and appropriate number of holes (gas) are also placed in specific lattice

sites, to obtain the correct system density. Also, a molecular perturbation model can be used for better representation of the system.

There are two requirements for the success of EOS models: they must accurately predict the saturation pressure of pure components, and suitable mixing rules must be available to extend their use to multicomponent mixtures.

### 2.6.2. Equations of State

There are two major types of equations of state that are capable of representing solvent-polymer mixtures, with some specific limitations. Those are the lattice models (eg. Sanchez-Lacombe), and the perturbation models (SAFT). The principles and governing equations of each of these models are reviewed in this section in greater detail.

#### 2.6.2.1. Lattice Fluid Models (The Sanchez-Lacombe Equation of State)

The early lattice models, such as the older Flory-Huggins theory (1953), do not apply very well to systems where there are strong specific interactions and to dilute or semi-dilute solutions. Also, it neglects the so-called free volume effect. This theory, which ignores the equation of state properties of the pure components, completely fails to describe LCST behavior in polymer solutions [15]. Freeman and Rowlinson (1960) observed experimentally that many hydrocarbon polymers dissolved in hydrocarbon solvents phase separated at high temperatures. These non-polar polymer solutions exhibited what are known as lower critical solution temperatures (LCST), a critical-point phenomena that is rare among low molecular weight solutions. It was recognized that the

common appearance of LCST behavior in polymer solutions must be related to the large size difference between polymer and solvent molecules. Soon after the discovery of the universality of LCST behavior in polymer solutions, Flory and co-workers (1964-1970), developed a new theory of solutions that considers the "equation of state" properties of the pure components. This new theory of solutions, the Flory theory, demonstrates that mixture thermodynamic properties depend on the thermodynamic properties of pure components. In particular LCST behavior can be understood in terms of the dissimilarity of the equation of state properties of polymer and solvent. Patterson (1971) has also shown that LCST behavior is related to the dissimilarity in polymer-solvent properties by using the general corresponding states theory of Prigogine and collaborators [15].

Thus, the lattice theory of solutions, although first developed for monoatomic molecules, can be extended to molecules of more complex structure using well-defined assumptions, as shown by Guggenheim, Flory, and others. This extension makes it particularly useful for solutions of molecules that differ appreciably in size, such as polymer solutions. However, the concept of a lattice for liquid structure is a vast oversimplification; and as a result, lattice theory becomes increasingly inappropriate as attention is focused on temperatures remote from the melting point. Also, for each binary system, lattice theory requires as an input parameter the interchange energy $w$ (or its equivalent, the Flory parameter $\chi$), that is difficult to predict and that, unfortunately, is temperature-dependant [10]. More recently, a newer equation of state theory of pure fluids [16, 17] and their solutions [18] has been formulated by Sanchez and Lacombe (1977), characterized as *lattice fluid* theory. In general, it defers from a corresponding

states theory. It does not require separation of internal and external degrees of freedom as does the Flory theory and the Prigogine corresponding states theory. External degrees of freedom are assumed to depend only on intermolecular forces, whereas internal degrees of freedom are associated with intramolecular chemical bond forces. Nevertheless, the lattice fluid theory has much in common with the Flory theory. Both theories require three equation of state parameters for each pure component. For mixtures, both reduce to the Flory-Huggins theory at very low temperatures.

The Sanchez-Lacombe model is a lattice-fluid model in which vacancies, i.e. empty lattice sites are introduced in the lattice to account for the compressibility and density changes. It is given by the expression,

$$\tilde{\rho}^2 + \tilde{P} + \tilde{T}\left[\ln(1-\tilde{\rho}) + \left(1-\frac{1}{r}\right)\tilde{\rho}\right] = 0 \tag{2.11}$$

where $\tilde{P}, \tilde{T}, \tilde{\rho}, \text{and}\, \tilde{v}$ are the reduced pressure, temperature, density and volume, respectively, that are defined as,

$$\begin{aligned} \tilde{T} &= \frac{T}{T^*}, & T^* &= \varepsilon^* / k \\ \tilde{P} &= \frac{P}{P^*}, & P^* &= \varepsilon^* / v^*, \\ \tilde{\rho} &= \frac{\rho}{\rho^*} = \frac{1}{\tilde{v}} = \frac{V^*}{V}, & V^* &= N(rv^*), \\ & & \rho^* &= M/(rv^*), \end{aligned} \tag{2.12}$$

where $\varepsilon^*$ is the mer-mer interaction energy, $v^*$ is the close-packed molar volume of a mer, $M$ is the molecular weight, $N$ is the number of molecules, $r$ is the number of sites (mers) a molecule occupies in the lattice, $R$ is the universal gas constant.

The characteristic temperature, pressure and close-packed mass density are given as $T^*$, $P^*$, and $\rho^*$. When dealing with mixtures it is necessary to define combining rules for $\varepsilon^*_{mix}$, $v^*_{mix}$, and $r_{mix}$ to use the equation of state to calculate properties of a mixture. For that matter, the so-called van der Waals-1 rules are used. These assume random mixing of the components, as for small molecule system. The mixing rule for the characteristic close-packed molar volume of a mer of the mixture $v^*_{mix}$ is given by

$$v^*_{mix} = \sum_{i=1}\sum_{j=1} \Phi_i \Phi_j v^*_{ij} \tag{2.13}$$

with

$$v^*_{ij} = \frac{v^*_{ii} + v^*_{jj}}{2}\left(1 - \eta_{ij}\right) \tag{2.14}$$

where $\eta_{ij}$ corrects for deviations from the arithmetic mean and where subscripts $i$ and $j$ are the components in the solution. The volume fraction (i.e. segment fraction) of component $i$, $\Phi_i$, is defined as

$$\Phi_i = \frac{m_i}{\rho^*_i v^*_i} \Bigg/ \sum_{j=1}\left(\frac{m_j}{\rho^*_j v^*_j}\right) \tag{2.15}$$

where $m_i$ is the mass fraction of component $i$ in the mixture, and $\rho^*_i$ and $v^*_i$ are the characteristic mass density and close-packed molar volume of component $i$, respectively. The mixing rule for the characteristic interaction energy for the mixture $\varepsilon^*_{mix}$ is given by

$$\varepsilon^*_{mix} = \frac{1}{v^*_{mix}} \sum_{i=1}\sum_{j=1} \Phi_i \Phi_j \varepsilon^*_{ij} v^*_{ij} \tag{2.16}$$

$$\varepsilon^*_{ij} = \left(\varepsilon^*_{ii}\varepsilon^*_{jj}\right)^{1/2}\left(1 - k_{ij}\right) \tag{2.17}$$

where $\varepsilon_{ii}^{*}$ and $\varepsilon_{jj}^{*}$ are the characteristic mer-mer interaction energies for components *i* and *j*, and $k_{ij}$ is a mixture parameter that accounts for specific binary interactions between components *i* and *j*. The mixing rule for number of sites occupied by a molecule of the mixture, $r_{mix}$, is given by

$$\frac{1}{r_{mix}} = \sum_{j=1} \frac{\Phi_j}{r_j} \tag{2.18}$$

where $r_j$ is the number of sites molecule *j* occupies in the lattice.

Expressing Sanchez-Lacombe EOS in terms of the compressibility factor, yields

$$Z^2 - (1-d)Z + \left(\frac{RT}{P} d^2\right) \log\left[\left(Z - \frac{P}{RT}\frac{b}{d}\right) \Big/ Z\right] + \frac{P}{R^2 T^2} a \tag{2.19}$$

where the correction factors *a*, *b*, and *d* are problem specific for each polymer-SCF process (appropriate correlations for polymer-$CO_2$ system are derived empirically, taking into consideration the components mole fractions and binary interaction parameters).

Solving Equation (2.19) as a quadratic equation in terms of Z, and then substituting the Z term in Equation (2.9), yields

$$\ln \varphi_i^V = \frac{1}{RT} \int_{v^V}^{\infty} \left[\left(\frac{\partial P}{\partial n_i}\right)_{T,V,n_i} - \frac{RT}{V}\right] dv - \ln Z \tag{2.20}$$

These calculated fugacity coefficients are used to calculate the equilibrium solubility mole fractions of polymer in the $CO_2$ system under different experimental conditions (temperature, pressure, composition). The experimentally measured solubility data can be regressed using the Sanchez-Lacombe EOS with conventional mixing rules, as already discussed, to determine the pressure term.

The linearly temperature dependent binary interaction coefficients $k_{ij}$, which is associated with the intermolecular interactions between a pair of unlike species, can be regressed to incorporate temperature dependence. The value of this parameter usually never gets larger than about 0.150. It can also be negative, although a negative value usually indicates the presence of specific chemical interactions (hydrogen bonding). Appropriate $k_{ij}$ expressions for various polymer-$CO_2$ systems are available in the literature. Fairly more sophisticated than the lattice fluid models are the perturbation models, which are described further in this review.

2.6.2.2. Perturbation Models (SAFT)

Reasonable, but nevertheless approximate, theories are now available for mixtures that contain chain-like molecules in addition to "normal", essentially spherical, or globular, molecules. These theories (perturbed hard chain, statistical associating fluid, perturbed hard chain of spheres) have a wider range of applicability than those based on a hole-free lattice because they are based on equations of state that, unlike a hole-free lattice, give the segment density as a function of temperature, pressure, and composition. Further, these EOS theories can incorporate association between like molecules and solvation between unlike molecules. Regrettably, even for nonpolar fluids, these EOS theories require several (typically 3 or 4) pure-component molecular parameters; and if the molecules associate, additional parameters are needed. The need of so many parameters follows from our inadequate understanding of intermolecular forces [10].

One of the major challenges faced in adapting the supercritical solvents as greener

substitutes is the unavailability of phase equilibrium data and design information for new systems. This is because most of the available methods and simulations are problem specific. Thus, the motivation for development of a conceptual design tool for supercritical products and processes is strong among the research community.

In recent decades, molecularly based equations of state have been developed which to some extent provide some predictive capabilities. The background for these equations of state is statistical thermodynamics, which gives the relation between properties of single molecules and the macroscopic properties of an ensemble of molecules. While this approach is formally exact, it cannot be applied rigorously because of its mathematical complexity. Several approximations have to be made. A common approximation is, for example, to describe the macroscopic properties based on pair interactions while neglecting the many body potentials.

The first widely applied equation of state based on this molecular view was the Perturbed Hard-Chain Theory (PHCT) equation of state developed by Beret and Prausnitz (1975) and by Donohue and Prausnitz (1978). Multi-polar interactions were considered by Vimalchand and Donohue (1985). The success of their work has been the inspiration for further developments. A more recent equation of state concept for chain molecules is based on Wertheim's Thermodynamic Perturbation Theory (1984). By applying Wertheim's theory and extending it to mixtures, Chapman et al. (1990) derived the Statistical Associating Fluid Theory (SAFT) equation of state for chain mixtures. Although many modifications of the SAFT model were suggested, one of the most successful modifications remains to be the SAFT model suggested by Huang and Radosz

(1991). Chapman et al. (2000) have developed a new theory, based on a perturbation theory of Barker and Henderson (1967) by extending it to chain molecules, referred to as the Perturbed-Chain SAFT (PC-SAFT), where the chain structure of the molecules, which are assumed to be chains of freely joined spherical segments, is now considered also in the dispersion term. Gross and Sadowski applied this theory to associating and polymeric systems.

The PC-SAFT molecular model is given in Figure 2.7,

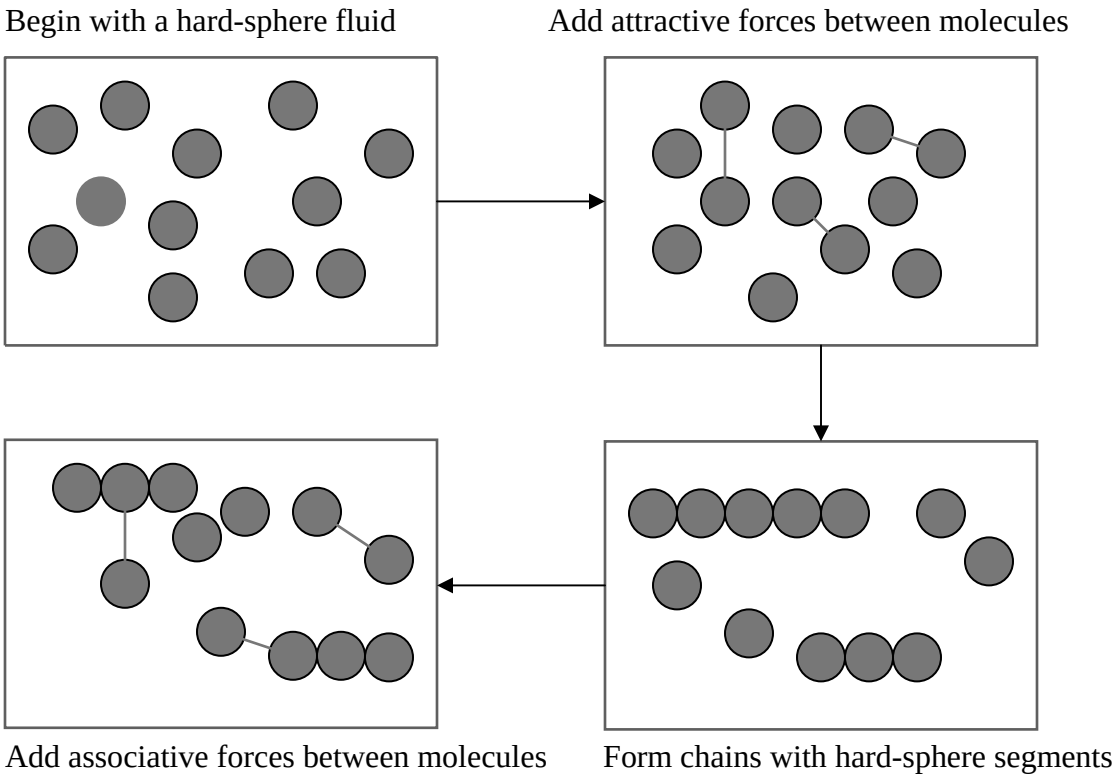


Figure 2.7 Molecular Model Underlying the Perturbed-Chain SAFT EOS

The spherical segments may possess association sites, exhibiting specific (often strong) short-range interactions, thus mimicking hydrogen-bonding. Moreover, they may carry partial charges. Dipolar segments have two partial charges (positive and negative), whereas quadruple segments carry three charges.

Statistical associating fluid theory (SAFT) is a molecularly based EOS that incorporates terms accounting for the molecular size and shape (e.g., chain length and degree of branching), association (e.g., hydrogen bonding) energy, and mean-field (e.g., dispersion) energy. A SAFT fluid is a collection of spherical segments that are not only exposed to repulsive (hard sphere) and attractive (dispersion) forces but can also aggregate through covalent bonds to form chains (chain effect) and through hydrogen-like bonds to form short lived clusters (association effect).

The reference part of SAFT includes the hard–sphere, chain, and association terms. The perturbation part of SAFT accounts for relatively weaker, mean-field dispersion-like effects. The SAFT residual Helmholtz free energy ($a^{res}$) relative to an ideal gas reference state is given by

$$a^{res} = a^{ref} + a^{disp} \tag{2.21}$$

with

$$a^{ref}(T,V,N) = a^{hs}(T,V,N) + a^{chain}(T,V,N) + a^{assoc}(T,V,N) \tag{2.22}$$

Using the thermodynamic relationship $\left(\partial a/\partial v\right)_T = -P$, SAFT can be expressed in terms of the compressibility factor, Z:

$$Z = \frac{Pv}{RT} = 1 + Z^{hs} + Z^{chain} + Z^{assoc} + Z^{disp} \tag{2.23}$$

where

$$Z^{hs} = m\left(4\eta - 2\eta^2\right)/\left(1-\eta^3\right) \tag{2.24}$$

$$Z^{chain} = \left(1-m\right)\left[\left(2.5\eta - \eta^2\right)/\left\{\left(1-\eta\right)\left(1-0.5\eta\right)\right\}\right] \tag{2.25}$$

$$Z^{assoc} = \rho\sum_{A}\left[\left\{\left(1/X^A\right) - 0.5\right\}\left(\partial X^A/\partial\rho\right)_T\right] \tag{2.26}$$

$$Z^{disp} = m\sum_{i}\sum_{j}\left[jD_{ij}\left(u/kT\right)^i\left(\eta/\tau\right)^i\right] \tag{2.27}$$

where $\eta$ is the reduced fluid density, $m$ is the number of segments per molecule, $\rho$ is the molar density, $v$ is the molar volume, $X^A$ is the mole fraction of molecules not bonded at site $A$, $u/k$ is a temperature dependant dispersion energy of interaction between segments, $D_{ij}$ and $\tau$ are constants, and the summation is over all the sites. The reduced density, $\eta$, of the fluid is defined as

$$\eta = 0.74048\rho m v^0 \tag{2.28}$$

where $v^0$ is the segmental molar volume at closed-packing, in units of cubic centimeter per mole of segments, given as

$$v^0 = v^{00}\left[1 - C\exp\left(\frac{-3u^0}{kT}\right)\right]^3 \tag{2.29}$$

where, $u^0/k$ is a temperature-independent parameter in Kelvins, $C$ is a constant set to 0.12, thus there are three unary parameters $v^{00}$, $u^0/k$, and $m$ for each component in the SAFT model.

Knowing $a^{res}$ and $Z$, $\varphi^i$ can be estimated from the following identity:

$$\ln \varphi_i = \left\{ \partial \left( a^{res} / RT \right) / \partial n_i \right\}_{T,V,n_j} - \ln Z \tag{2.30}$$

where $V$ is the total volume of the system and $n_i$ is the number of moles of substance $i$.

When using SAFT, the characteristic parameters for pure substances are determined by optimizing the predictions of vapor-liquid equilibrium (*VLE*) data. When *VLE* data is not available, which is usually the case for polymers, *PVT* data are used instead. Also, if there are no accurate *PVT* data available, the characteristic parameters can be estimated from the molecular weight only, which is a nice feature of SAFT. When SAFT is extended to mixtures, only one binary mixture parameter is needed. This parameter in SAFT is temperature independent in contrast to most of the lattice theories in which the interaction parameters are temperature dependant.

For mixtures, either volume fraction mixing rules or the van der Waals one-fluid (*VDW1*) mixing rules can be used in the model. Using the *VDW1* mixing rules, the dispersion energy of interaction is given by

$$\frac{u}{RT} = \frac{\sum_i \sum_j X_i X_j m_i m_j \left[ \frac{u_{ij}}{RT} \right] v_{ij}^0}{\sum_i \sum_j X_i X_j m_i m_j v_{ij}^0} \tag{2.31}$$

with

$$u_{ij} = \left( u_{ii} u_{jj} \right)^{1/2} \left( 1 - \xi_{ij} \right) \tag{2.32}$$

$$m_{ij} = \frac{\left( m_i + m_j \right)}{2} \left( 1 - \zeta_{ij} \right) \tag{2.33}$$

$$v_{ij}^0 = \left\{ \frac{1}{2} \left[ \left( v_i^0 \right)^{1/3} + \left( v_j^0 \right)^{1/3} \right] \right\}^3 \tag{2.34}$$

where $X_i$ and $m_i$ are the mole fraction and molecular segment number of component $i$ in the mixture, $\xi_{ij}$ is an empirical binary interaction parameter, $\zeta_{ij}$ is another empirical binary interaction parameter, $v_{ij}^{0}$ is the segment molar volume for the mixture, in which $v_i^{0}$ is temperature dependent segment molar volume and is related to the temperature independent segment molar volume $v_{ii}^{00}$ as written above in equation (2.29). SAFT is used to describe many real pure components and fluid mixtures, including supercritical and near-critical solutions of polymers.

# CHAPTER 3

# EXPERIMENTAL SYSTEM AND PROCEDURES

In this chapter, the experimental system, equipment setup, and procedures are described in detail, independently describing the instruments that constitute the system. Also, the procedure and the results of the calibration of the phase analyzer and its PLC controller are presented. Following this, the techniques for preparation of materials and chemicals are described. Finally, the procedure for observing and measuring the bubble points of the MMA-$CO_2$ system, and the cloud points of the PMMA-$CO_2$-MMA system at various temperatures for obtaining the appropriate solubility data is elaborated.

To emphasize again, the objectives of this work are, first, to develop a procedure and obtain experimental solubility data for a suitable polymer-SCF mixture which can be used for supercritical impregnation processes and, second, to test in a comprehensive and systematic way the available thermodynamic SAFT model for polymer-diluent mixtures, developed by Aslam and Sunol (2004). This is a technologically important field as polymer-diluent mixtures are frequently encountered in polymer processing and thermodynamic models for these systems play a pivotal role in the design of process equipment.

3.1. Experimental Apparatus Description

The apparatus used for measuring phase behavior of dilute polymer-supercritical fluid solutions is illustrated in Figure 3.1,

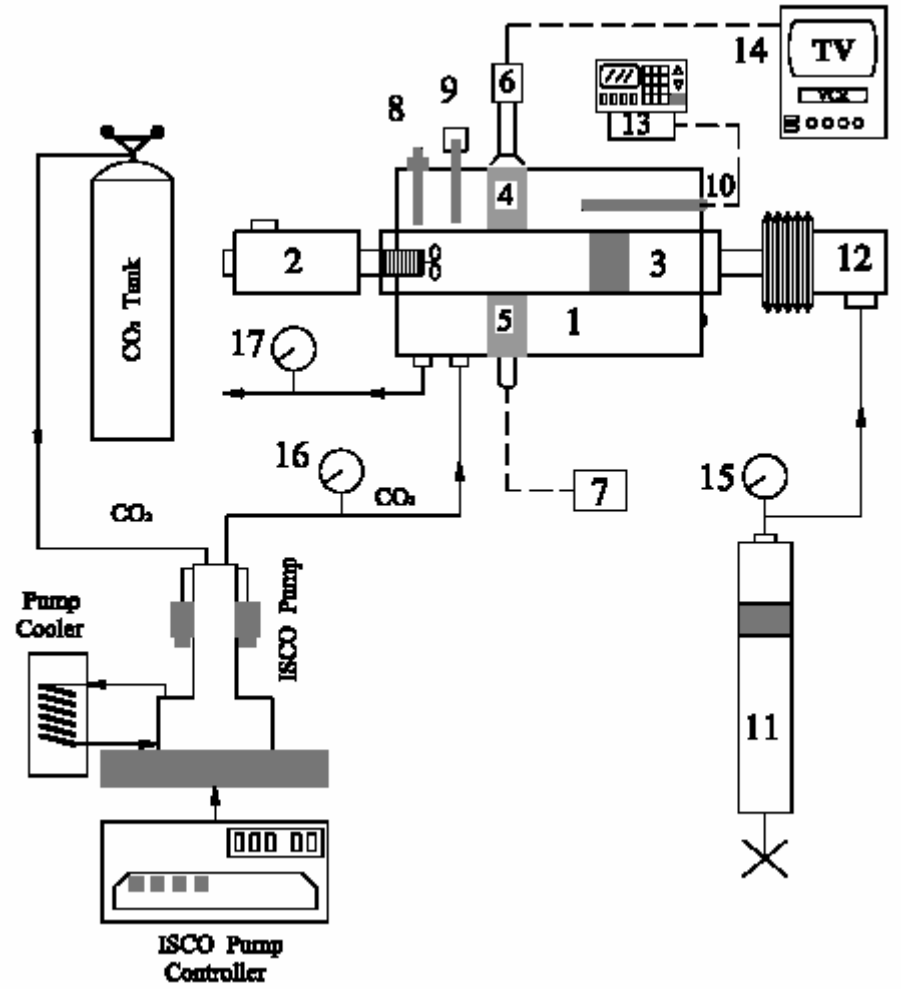


Figure 3.1 Schematic Diagram of the High-Pressure Phase Monitoring System: (1) variable-volume cell, (2) mixer, (3) piston, (4) camera sapphire window (5) light sapphire window, (6) borescope w/camera, (7) light source, (8) pressure transducer, (9) thermocouple, (10) heater, (11) hydraulic pump, (12) hydraulic lifting section, (13) controller, (14) TV/VCR, (15, 16, 17) pressure gauges at pump, cell inlet & outlet (vent).

### 3.1.1. Phase Monitor

The heart of the experimental system is the Phase Monitor SPM20 (manufactured by Thar Technologies, Inc., Pittsburgh, PA). It consists of a sealed, high-pressure, variable-volume cell, containing the polymer solution within the enclosure, the temperature of which is controlled programmatically up to a maximum of 150°C, and the pressure of which is adjusted via a movable piston. The pressure is controlled up to a maximum of 700 bar by a hydraulic hand pump (Model 2200, Ruska Instruments), which is used to raise and lower the hydraulic lifting section of the phase monitor carriage assembly. The vessel piston is attached to the lifting section, so that when the lifting section raises, the vessel piston moves into the vessel body thus reducing the vessel volume. As the vessel volume is reduced, the vessel pressure will increase, and vice versa. There is a volume displacement scale mounted on the carriage assembly, which displays the remaining vessel volume from the maximum of 15 ml down to a minimum of 5 ml. The pressure variations into the cell are measured by a pressure transducer mounted to the vessel body, and the signal is transferred to a portable PLC controller.

A mixer, rotated at variable speeds by an external motor, was used to mix the mixture in the high-pressure cell. Visual observation of phase phenomena occurring inside the cell was made on a video monitor using a camera coupled to a boroscope, placed directly over the sapphire window. The cell has two camera mounting adapter assemblies; one assembly holds the camera and the second holds the camera light source.

The vessel assembly is heated by four electrical heaters installed into the bottom of the vessel body, while the temperature is measured through a thermocouple mounted to the vessel body and whose heat conductive probe enters the interior of the vessel and gets into a direct contact with the fluid in the cell. The signal from the thermostat is transferred to the portable PLC controller, where the output is displayed in the unit 'bar'.

A photo of the high-pressure cell and the PLC controller is shown in Figure 3.2,

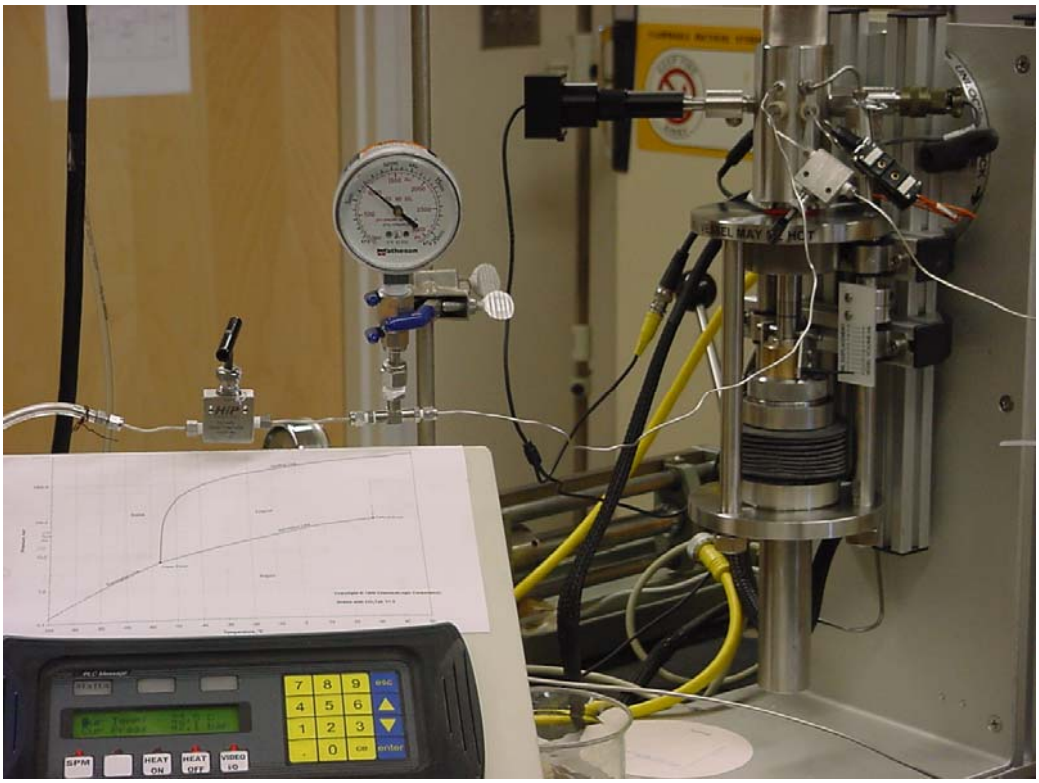


Figure 3.2 The Vessel Assembly and Controller of the Phase Monitor SPM20

The camera assembly, the inlet and outlet tubing connections, the pressure transducer and the thermocouple can be seen as they are connected to the vessel body. Also, there is a mechanical pressure gauge connected online to the vessel at the outlet tubing, for comparison and verification of the pressure measured by the pressure transducer which is being converted in bar units through the controller.

One advantage of using the variable-volume cell is that the concentration of the system remains constant during the experiment.

### 3.1.2. Tubing Reticulation

The 1/8” stainless steel tubing that starts from the carbon dioxide tank, goes through the high-pressure syringe pump (Model: 100DX, ISCO, Inc., Lincoln, NE), from where it continues through an outlet tubing, a manual valve, a tubing reducer and a connection to the vessel body through a vessel inlet port 1/16” Valco. All the tube fittings, including the crosses, tees, nuts, ferrules, back ferrules, reducers, plugs, connectors, bushings, are of 1/18” connection size, stainless steel fittings (Swagelok, Solon, OH) adapted for high-pressure applications. The minimum amount of fittings has been used throughout the system, so that the pressure drop introduced to the system is minimized and easy to compensate for by the syringe pump. There is another 1/16” connection port on the vessel body, which serves as an outlet from the vessel to let the $CO_2$ and other gas fumes leave the vessel body whenever the outlet valve is open. The released fumes are vented through the external ventilation system.

### 3.1.3. High Pressure Syringe Pump

The pump that delivers supercritical carbon dioxide to the system is a high-pressure syringe pump (Model: 100DX, ISCO, Inc., Lincoln, NE) equipped with a cooling jacket to assure that the carbon dioxide withdrawn from the gas cylinder is cooled down to a liquid state. The temperature of the cooling jacket is maintained below zero degrees Celsius by a Lauda Circulator (Lauda GMBH&CO.KG, Germany). The cooling is required to get the maximum efficiency from the syringe pump with liquefied carbon dioxide in order to get the desired supercritical pressure with the minimum possible compression and maximum possible volume. The pump comes with 1/8" standard Valco ports. The cylinder capacity of the pump is 102.93 $cm^3$. Modes of operation are constant flow within 0.01 μl/min to 50 ml/min (for any pressure from 0.6895 up to 689.5 bar). The flow rate accuracy is rated to be ± 0.3% with a flow rate display resolution of 0.01 μl/min. Usually the supercritical carbon dioxide is pumped in at a constant flow rate of 5 ml/min. The pump is operated with a controller (Model: D Series Controller, ISCO, Inc., Lincoln, NE), which is a microprocessor-based user interface, and a digital motor speed control system, by entering and monitoring set values during the pump operation.

### 3.1.4. Low-Temperature Circulator

The Ecoline low-temperature thermostat (Model: RE-120, Lauda Dr. R. Wobser GMBH & CO. KG, Germany) has both refrigeration and heating unit with adjustable flow rate ranging from 8 l/min to 17 l/min, and maximum discharge pressure of 0.4 bar. The capacity of the circulator is approximately 14 to 20 liters. The temperature range of

operation is –30 to 120 °C with a control accuracy of ± 0.05 °C at 20 °C. The unit is equipped with a pressure pump with variable drive. The refrigeration system consists essentially of a hermetically sealed compressor. Heat of condensation and motor heat are dissipated by a fan-cooled finned condenser.

### 3.1.5. Syringe Pump Controller

The pump setup and operation is regulated by the D Series Programmable Controller (Model: D Series Controller, ISCO, Inc., Lincoln, NE). Operating parameters are entered via the keypad on the front panel of the controller. Operating modes such as CONST FLOW, CONST PRESS, REFILL, START, and STOP all have dedicated keys on the controller keypad. The pump also allows user-programmed refill, as well as pumping rates. The filling of the vessel itself with supercritical $CO_2$ is monitored visually through the TV camera attached to the vessel body, and also by reading the pressure increase in the vessel during the filling. These observations give a good indication about when the system is full, thus when to switch the syringe pump off.

## 3.2. Calibration of the Phase Monitor's PLC Controller

After assembling, and test running of the phase monitoring experimental apparatus, it was discovered that the accuracy of the Phase Monitor's temperature and pressure PLC Controller was off. For calibration purposes, two manual pressure gauges were connected to the high-pressure cell, one at the inlet and one at the outlet. Both pressure gauges have shown a same pressure difference from the controller reading.

Throughout the working pressure range of the cell, the manual pressure gauges read about 20 bar higher pressures than those calculated by the controller. Nitrogen gas was used to do the low pressure measurements, from 0.5 to 50 bar, while liquid $CO_2$ was used for the high pressure measurements, 50 to 120 bar. With both gases, it was repeatedly shown that there's always about 20 bar difference throughout this pressure range.

This difference had to be accounted in the experimental measurements. Thus, for every pressure reading from the controller a 20 bar correction factor is added for representation of the results in this work. However, more accurate calibration could be performed by re-checking the software of the PLC controller itself, i.e. the equations used for calculation and conversion of the readings from the pressure transducer. The manufacturer of this controller should accept the responsibility of re-calibration of the instrument. Until that is done, however, we will apply our first hand calibration results to correct for the controller offset.

Therefore, the experimental conditions are predetermined during the calibration of the controller since same measurement conditions have to be attained as with the calibration conditions to be able to determine the right pressure in the system at the time of performing the experiments. The observations have shown that attaining and controlling a desired temperature is harder and error-wise more important, so that our efforts are focused on stabilizing the temperature in the system. The temperature was controlled to within ± 0.2 °C maximum. The pressure is always variable, depending on the hydraulic pump displacement of the piston and the cloud-point phase transition. The pressure reading is always fluctuating at the bubble-point and at the cloud-point, and it

takes a little bit of time to stabilize; therefore a number of repeated measurements is needed, where the average of those pressure readings is calculated and accepted as the actual pressure of the system at that point.

## 3.3. Experimental Section

In the following section, the preparation of the chemicals, the operation of the variable-volume cell, and the experimental measurements will be explained. This will be followed by a detailed experimental procedure and the observations obtained throughout the experimental run.

### 3.3.1. Materials Description

Carbon dioxide (99.8% purity) was obtained from Airgas and used as received. Methyl methacrylate (MMA) (99% purity) and poly(methyl methacrylate) (99% purity) that has weight-average molecular weight ($M_w$) of 93,000 and number-average molecular weight ($M_n$) of 46,000, therefore having a polydispersity index ($M_w/M_n$) of 2.02, were obtained from Aldrich and used as received. To prevent MMA polymerization, 4-methoxyphenol, that is, hydroquinone monomethyl ether, (Aldrich, 99% purity) was used as an inhibitor at a concentration of 0.0025 times the amount of MMA, which was added to the monomer as part of the manufacturing process. The chemical structure of each chemical is shown in Schemes 3.1, 3.2, and 3.3.

Acrylates are made from acrylate monomers, which contain vinyl groups, that is, two carbon atoms double bonded to each other, directly attached to the carbonyl carbon.

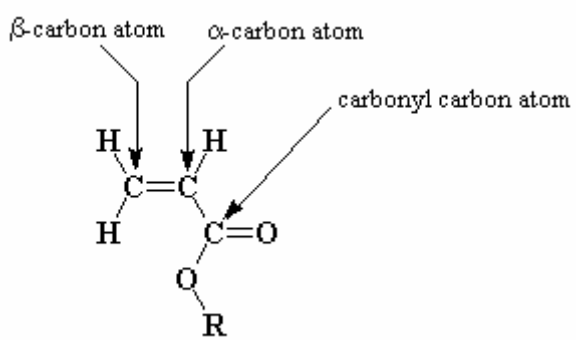


Scheme 3.1 Chemical Structure of acrylate Monomers

Some acrylates have an extra methyl group attached to the alpha carbon, and these are called *methacrylates*.

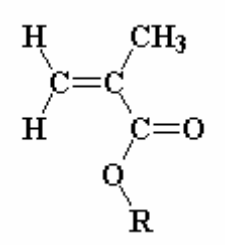


Scheme 3.2 Chemical Structure of a methacrylate

One of the most common methacrylate polymers is poly(methyl methacrylate), which is obtained by free radical vinyl polymerization of methyl methacrylate monomer,

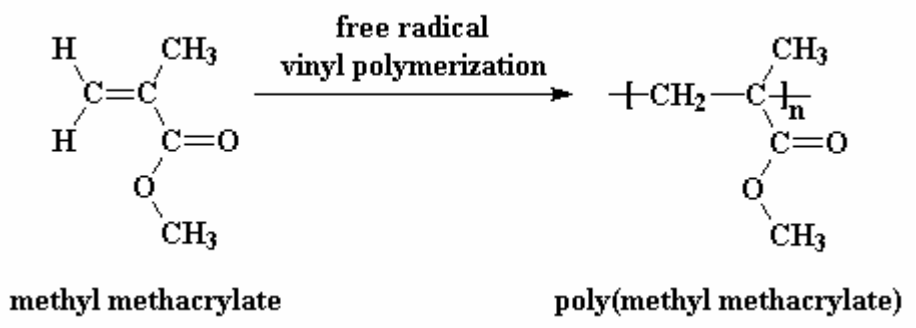


Scheme 3.3 Polymerization of methyl methacrylate to Get PMMA

Poly(methyl methacrylate), PMMA, is a clear, thermoplastic, linear polymer with no cross-links. The backbone of the chain is usually carbon atoms linked by covalent, single bonds. The degree of polymerization is the number of monomer units in a chain, normally $10^3$-$10^5$, and it can be calculated as,

$$\left(Degree\ of\ polymerization\right) = \frac{M_w\ of\ polymer}{M_r\ of\ monomer} \tag{3.1}$$

For the chemicals at hand, the degree of polymerization is calculated as,

$$DP = \frac{93000}{100.12} = 928.88$$

That is, there are approximately 1,000 MMA units in one single chain of PMMA of this study.

### 3.3.2. Experimental Procedure

There are two different experiments that were conducted using the same experimental setup. First, the methyl methacrylate-$CO_2$ equilibrium was studied, by determining the bubble point of the mixture at different temperatures.

The second system, PMMA-$CO_2$-MMA, was studied by determining the cloud-point data at different temperatures. In the first experiment, the first step was to load the methyl methacrylate monomer into the cell from the end that is capped with the variable speed mixer during the experiments. The amount of methyl methacrylate loaded into the cell was determined using a sensitive analytical balance, measurable to ± 0.001 g. The methyl methacrylate is loaded with a pipette from the top while the vessel is in its upright position. Then, the mixer assembly is screwed in position and the cell is purged slowly with carbon dioxide at pressures as low as 1 bar, to create just enough pressure difference to force the remaining air out of the system. After the purging is complete, the outlet valve is closed, and $CO_2$ is transferred from the gas cylinder into the cell volumetrically, at 5 ml/min constant flow rate, using a syringe pump and a controller. The contents of the cell are projected onto a video monitor using a camera coupled to a boroscope placed directly against the sapphire window. The filling of the cell with liquefied $CO_2$ is monitored on the TV monitor. As the $CO_2$ level reaches the top of the cell, the interior pressure in the vessel starts to build up quickly. At that point, the inlet valve must be closed, and the syringe pump stopped manually. In a few seconds, once the system reached thermal equilibrium, the initial pressure and temperature in the cell are recorded. The volume of the cell at this stage is usually at its maximum, that is, 15 ml. The initial temperature is the ambient temperature in the cell. The initial pressure is somewhere in the lower end of the supercritical region of carbon dioxide. Now, the vessel assembly is tilted in its horizontal position until the interface between the two phases in the cell is visible in the viewfinder of the camera. The cell is then heated to the desired

temperature, which is programmed by the temperature controller. Once thermal equilibrium is maintained in the cell, the contents of the cell are compressed into the one phase region by moving the piston forward via the hydraulic lifting section. The phase behavior is obtained in the pressure interval between the two-phase state and the one-phase fluid state. Once in the one-phase region, the pressure is lowered rapidly by moving the piston backwards i.e. increasing the volume until the first bubbles appear in the cell. The pressure at which the first bubbles appear is recorded, and that is the bubble point at the given temperature. Next, the temperature of the system is increased, and then the entire procedure is repeated to obtain more data points without reloading the cell. In this manner, without re-sampling, an isopleth (constant composition at various temperature and pressure) is obtained. The phase transition is representative of the mixture critical point if critical opalescence is observed during the transition process and if two phases of equal volume are present when the mixture phase separates. Bubble, dew, and critical point transitions for the $CO_2$-MMA mixtures are measured and reproduced at least three times to within ± 0.5 bar and ± 0.3 °C.

The same procedure is used in the second experiment for measuring the cloud points of the PMMA-$CO_2$-MMA mixture. The only difference is the addition of polymer into the system. The liquid MMA is measured to within ± 0.001 g in a small beaker. The glassy PMMA powder is also measured to ± 0.001 g accuracy, and added to the MMA in the beaker. The mixture is covered and stirred with a magnetic stirrer, at low speed, until the polymer beads are fully dissolved into the monomer. At the same time, the magnetic stirrer is heated slightly to aid the dissolution. Once a homogeneous mixture is obtained,

the solution is transferred slowly into the cell using a pipette. Then, the mixer assembly is screwed in position and the cell is purged slowly with carbon dioxide as already described. After the purging is complete, the outlet valve is closed, and $CO_2$ is transferred from the gas cylinder into the cell, as previously described. When the cell is full, the $CO_2$ is shut off, and the initial values of the temperature and pressure in the system are recorded. Then, the mixture in the cell is preheated up to about 105-110 °C, just above the glass transition temperature of the polymer. This is needed in order to avoid the nucleation of the polymer as a result of incompatibility issues related to the density differences between the $CO_2$ and the PMMA in the system. Once the system is preheated to this temperature, the mixer is turned on to agitate the solution until it becomes a homogeneous optically transparent mixture. The cell assembly is then lowered in its horizontal position, and the heater is switched off. The desired temperature at which the first cloud point would be measured is preset on the controller. The system cools down slowly until the temperature reaches the set point. At this point of time the mixture in the cell may have turned milky or cloudy, due to phase separation in the system. This is expected behavior and it will remain that way until the pressure is increased to bring the system back into the one phase region. Thus, once thermal equilibrium is maintained in the cell at the pre-set temperature, the contents of the cell are compressed into the one phase region where the mixture in the cell becomes transparent. Once in the one-phase region, the pressure is lowered rapidly by moving the piston backwards i.e. increasing the volume until the first appearance of a cloud in the cell.

The pressure at which the first cloudy look appears is recorded, and that is the cloud point of the system at the given temperature. After completing the measurement at a given temperature, the cell temperature is then stabilized at a new value, and the experimental procedure is repeated. Cloud points are measured and reproduced at least three times, but preferably five times, to within ± 2.5 bar and ± 0.3 °C. An average cloud point is then calculated from the multiple measurements. In this work, cloud point data was measured in ~15 °C increments i.e. decrements, and the above procedure was repeated, thus creating a pressure-temperature (P-T) cloud point curve at fixed PMMA, MMA, and $CO_2$ concentrations.

# CHAPTER 4

# RESULTS AND DISCUSSION

In this chapter, the experimental results obtained at several different temperatures and compositions are presented. The focus of this work is to measure the solubility of poly(methyl methacrylate) (PMMA) in supercritical $CO_2$.

## 4.1. Experimental Results

Experimental information is presented on the phase behavior of the $CO_2$-MMA system, and the PMMA-$CO_2$-MMA system. The primary reason for obtaining $CO_2$-MMA data is to determine whether $CO_2$ and MMA form multiple phases in the pressure-temperature-composition regions explored in the PMMA-$CO_2$-MMA studies. The $CO_2$-MMA data and the PMMA-$CO_2$-MMA data are modeled with the SAFT equation of state. The obtained results and the various phenomena associated with this kind of system are discussed in detail.

### 4.1.1. $CO_2$-MMA System

Table 4.1 and Figure 4.1 present the $CO_2$-MMA bubble-point data obtained from the experimental runs at 40, 80, and 105.5 °C.

Table 4.1 Experimental Data for the MMA-$CO_2$ System Obtained in this Study

| Temperature (°C) | MMA mole fraction | Pressure (bar) | Transition (bubble point) |
|---|---|---|---|
| 40.0 | 0.005 | 86.00 | BP |
| | 0.044 | 86.93 | BP |
| | 0.048 | 86.90 | BP |
| | 0.091 | 86.04 | BP |
| | 0.160 | 78.78 | BP |
| | 0.193 | 78.60 | BP |
| | 0.337 | 66.33 | BP |
| | 0.449 | 58.03 | BP |
| 80.0 | 0.091 | 119.30 | BP |
| | 0.337 | 100.40 | BP |
| | 0.600 | 60.00 | BP |
| 105.5 | 0.110 | 141.34 | BP |
| | 0.175 | 144.10 | BP |
| | 0.360 | 114.45 | BP |
| | 0.650 | 55.16 | BP |

The isotherms for the MMA-$CO_2$ system of this study, based on the experimental data from Table 4.1, are given in Figure 4.1, where the mole fractions of MMA are coupled with the appropriate bubble-point pressures measured in this experiment.

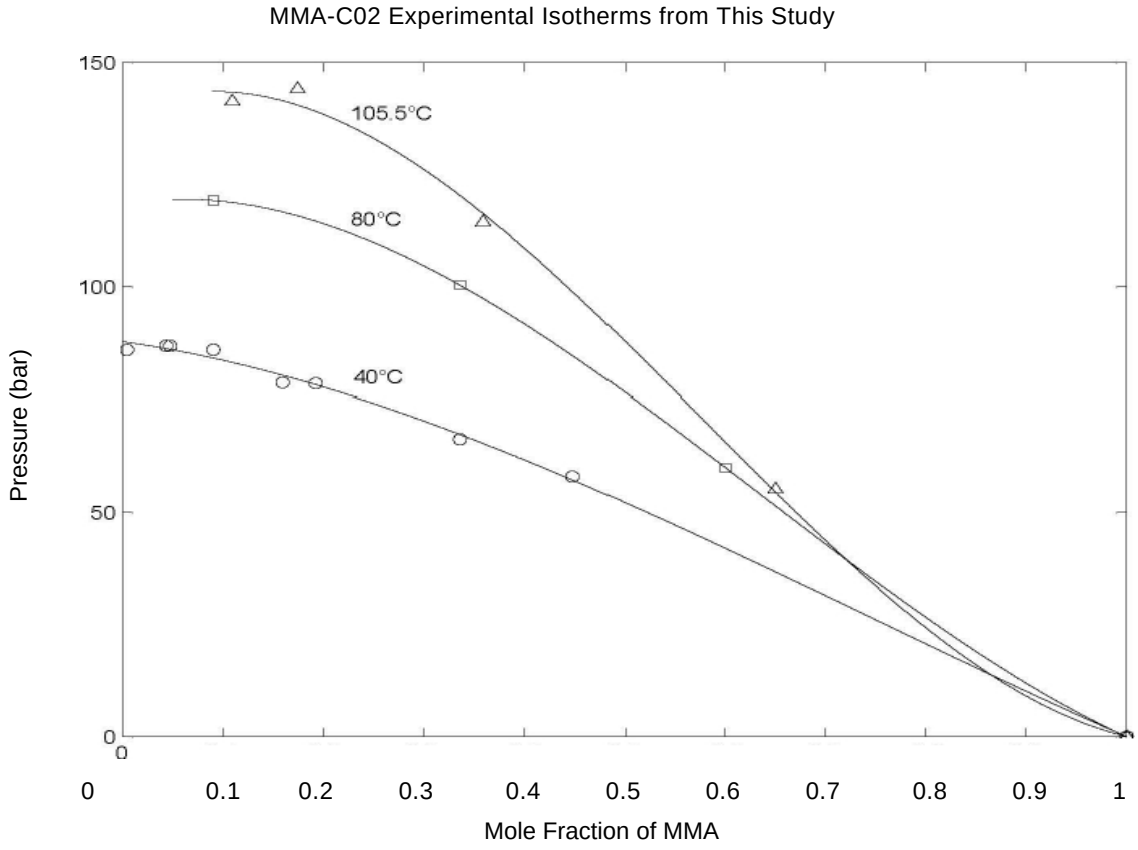


Figure 4.1 MMA-$CO_2$ Experimental Isotherms from This Study

For the purpose of making these P-x plots at different temperatures, the mole fraction of MMA needed to be calculated. This was done using the Peng-Robinson equation of state, given in Appendix A, to compute the compressibility factors Z for the pure component $CO_2$ at the required temperatures and pressures. These values for Z are further used to calculate the number of moles of $CO_2$ gas in the system, using the ideal

gas law, $n(CO_2)=PV/ZRT$. The number of moles of $CO_2$ is then used to calculate the mole fraction, the weight, and the weight fraction of $CO_2$, and the corresponding mole and weight fractions of monomer (MMA) and polymer (PMMA) in the system.

It is important to note that there is no solubility data available in the literature on the MMA-$CO_2$ and the PMMA-$CO_2$-MMA systems, other than the data published in 1999 by McHugh and coworkers [2], which, on the other hand, is largely inaccurate. All of their measurements show much lower bubble pressures than the results from the experiments in this work. Comparison plots are shown in Figure 4.2,

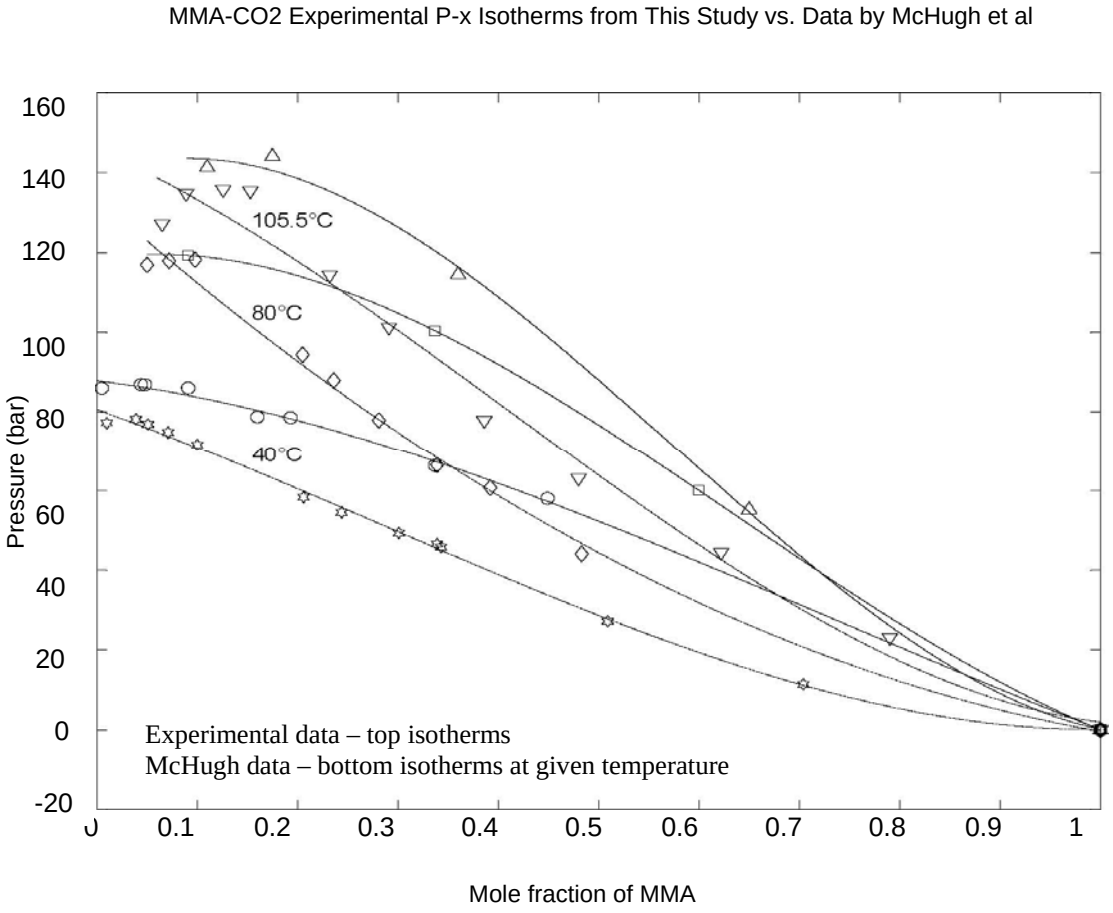


Figure 4.2 MMA-$CO_2$ Experimental Isotherms vs. Data by McHugh et al

For some reason, the abovementioned authors have experienced some experimental errors. This gives more room for publishing the corrected data. Also, the SAFT modeling of the PMMA-$CO_2$-MMA system performed by the same authors has a lot of shortcommings, since they could not get any closer results with regard to the solubility measurements. More on this will be elaborated in the next section.

### 4.1.2. PMMA-$CO_2$-MMA System

The data obtained in the second experiment by measuring the cloud-points of the PMMA-$CO_2$-MMA mixture is given in Table 4.2. Using this data, P-T cloud-point plots can be generated for each composition, as shown in Figure 4.3.

In order to obtain the number of moles, the volume, wt%, and mol% for each component in the system, the same calculation pattern as in the previous section is implemented. That is, the compressibility factors of the pure $CO_2$ at the given initial conditions, pressure and temperature, are computed using the Peng-Robinson equation of state, given in Appendix A. These values for Z are used to further calculate the number of moles of $CO_2$ gas in the system, using the ideal gas law, $n(CO_2)=PV/ZRT$. The number of moles of $CO_2$ are then used to calculate the mole fraction, weight, and weight fraction of $CO_2$, and the corresponding mole and weight fractions of monomer (MMA) and polymer (PMMA) in the system.

This calculation is repeated for all experimental conditions in order to obtain all appropriate mole fractions of MMA and PMMA. Detailed sample calculation for calculating the mole fractions is given in Appendix B.

Table 4.2 Experimental Cloud-points for the PMMA-$CO_2$-MMA System of This Study

| No. | MMA wt.% | MMA mol% | PMMA wt.% | PMMA mol% | Temperature (°C) | Pressure (bar) |
|---|---|---|---|---|---|---|
| Sample # 1128 | 45.4 | 27.7 | 2.5 | 1.56E-03 | 27 | 129.00 |
| | | | | | 45 | 210.00 |
| | | | | | 60 | 275.83 |
| | | | | | 75.5 | 312.00 |
| Sample # 1031 | 26.9 | 14.0 | 0.5 | 2.62E-04 | 27 | 66.50 |
| | | | | | 45 | 94.00 |
| | | | | | 60 | 119.60 |
| | | | | | 75.5 | 141.00 |
| Sample # 1101 | 26.8 | 13.9 | 0.2 | 1.02E-04 | 27 | 63.70 |
| | | | | | 45 | 88.30 |
| | | | | | 60 | 106.53 |
| | | | | | 75.5 | 125.00 |
| Sample # 1102 | 26.9 | 14.0 | 0.1 | 5.60E-05 | 27 | 62.00 |
| | | | | | 45 | 86.00 |
| | | | | | 60 | 102.00 |
| | | | | | 75.5 | 117.00 |

The cloud-point measurement represents an indirect way of presenting the solubility phase behavior of the polymer into the supercritical solvent. The direct way of obtaining the solubility of polymer in the supercritical $CO_2$ would be to calculate the solubility using an appropriate equation of state such as SAFT, which is capable of describing the complex interactions between the polymer and the low molecular solvent. The governing equations used in the SAFT model are described in more detail in the next section. The data given in Table 4.2, if plotted in a P-T diagram, will depict the cloud-point behavior of the system, as shown in Figure 4.3 below. The error related to pressure variations is observed to be around ±2 bar.

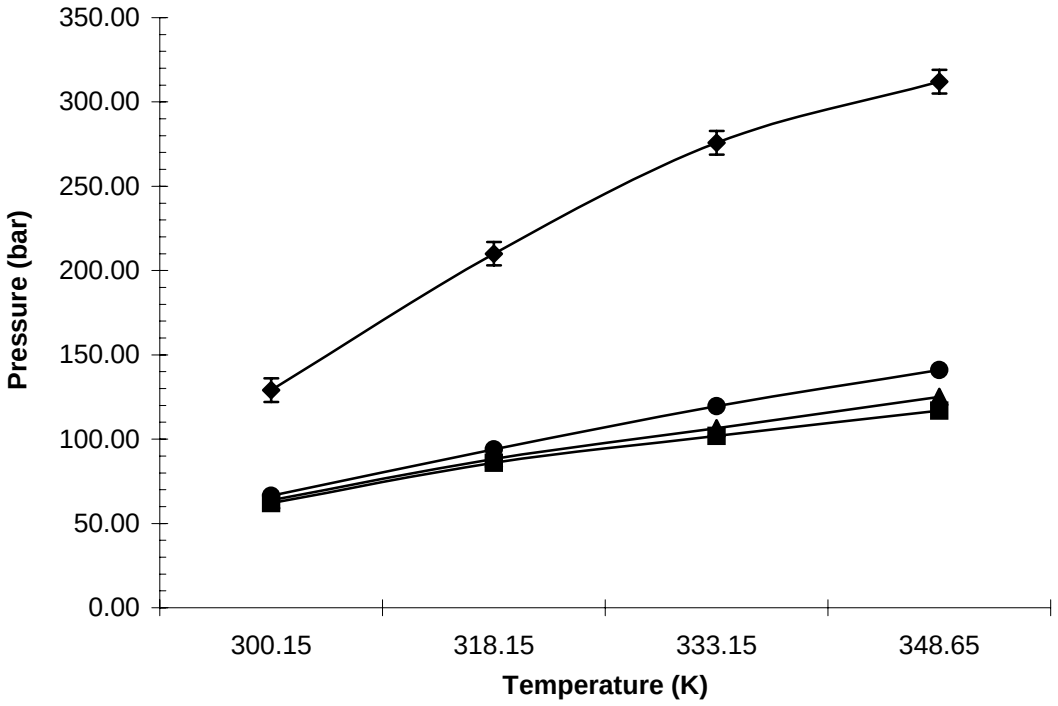


Figure 4.3 Experimental Cloud-point Curves for PMMA-$CO_2$-MMA

It is important to note that there is no solubility data available in the literature on the PMMA-$CO_2$-MMA system either, except the data published in 1999 by McHugh and coworkers [2], which, again, is largely inaccurate. Their measurements show much lower cloud-points than the results from this work. Comparison data is shown in Figure 4.4,

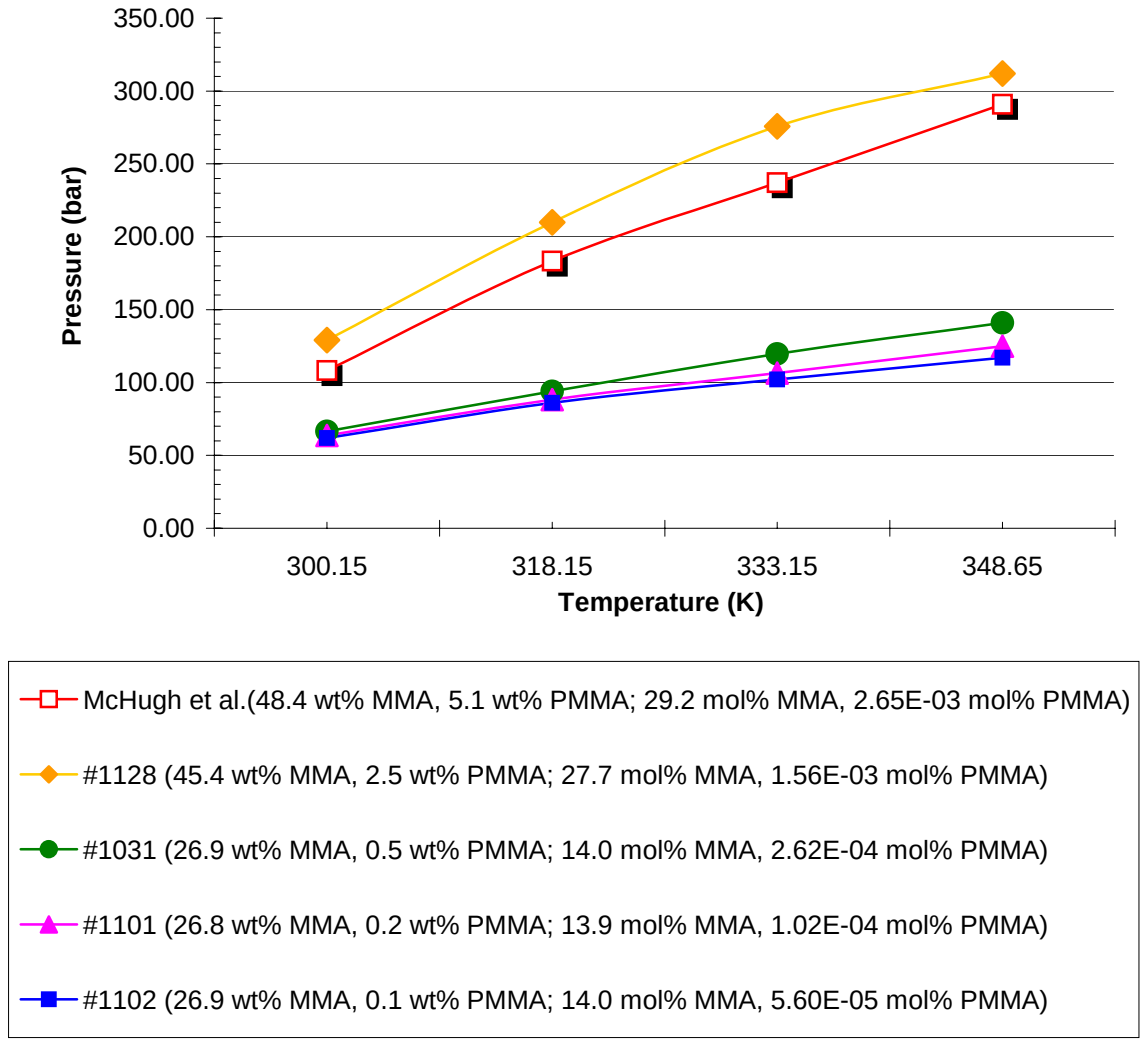


Figure 4.4 Experimental Cloud-point Curves for the PMMA-$CO_2$-MMA System of This Study vs. Cloud-point Data by McHugh et al

The experimental curve of this study (Sample # 1128: 'diamond' symbols,) can be analyzed against the data by McHugh and coworkers (open 'square' symbols). The data from this work was obtained at a 2.5 wt% concentration of PMMA, while the data by McHugh is at a 5.1 wt% PMMA, where the concentration of MMA for these data points is kept equal in both cases, at about 47.0 ± 1.5 wt%. It can be seen that the cloud-point pressures for Sample # 1128 of this study are much higher than those measured by McHugh and coworkers, even though the concentration of PMMA for the sample of this study is half the amount than what they have used. If we double the amount of PMMA, under the same conditions, then our measured pressure points would be even higher than what is already demonstrated with Sample # 1128. This leads to the conclusion that the referenced data by McHugh et al. is very much below the real cloud-point data.

## 4.2. Overview of the Equations Used for Computation of the Results

In this section, the governing equations used in the Peng-Robinson EOS and in the SAFT model are described in more detail, as well as the governing equations used in the solubility calculation.

### 4.2.1. The Peng-Robinson EOS with the Wong-Sandler Mixing Rules

The computation of the pure component parameters of the methyl methacrylate co-solvent used in this work has been performed by the Peng-Robinson equation of state (PR EOS). The general form of the PR EOS is,

$$P = \underbrace{\frac{RT}{v-b}}_{\text{Repulsive term}} - \underbrace{\frac{a(w,T)}{v(v+b)+b(v-b)}}_{\text{Attractive term}} \tag{4.1}$$

where $v$ is the molar volume, $a$ accounts for intermolecular interactions between the species in the mixture, and $b$ accounts for size differences between species of the mixture. The pure fluid parameters are given as,

$$a(w,T) = 0.45724 \frac{R^2 T_c^2}{P_c} \left[1 + m\left(1 - T_R^{0.5}\right)\right]^2 \tag{4.2}$$

and

$$b = 0.07780 \frac{RT_c}{P_c} \tag{4.3}$$

where,

$$m = 0.37464 + 1.54226w - 0.26992w^2 \tag{4.5}$$

where $T_R = T/T_c$ is the reduced temperature, and $w$ is the acentric factor for component $i$, available from literature for most of the low-to-moderate molecular weight hydrocarbons. The generalized PR EOS will take the form,

$$Z = \frac{V}{V-b} - \frac{a(T)V}{RT\left(V+\varepsilon b\right)\left(V+\sigma b\right)} \tag{4.6}$$

Implementing the Mathias-Copeman (1983) rules for $a(T)$ yields,

$$a(T) = a_c \alpha(T) \tag{4.7}$$

$$\alpha = \left[1 + C_1\left(1 - T_R^{0.5}\right) + C_2\left(1 - T_R^{0.5}\right)^2 + C_3\left(1 - T_R^{0.5}\right)^3\right]^2 \tag{4.8}$$

and using the Wong-Sandler (1992) mixing rules gives,

$$B(x_i,T)=\sum_i\sum_j x_i x_j B_{ij}(T)=\sum_i\sum_j x_i x_j\left(b_{ij}-\frac{a_{ij}}{RT}\right)=b-\frac{a}{RT} \tag{4.9}$$

$$b_{ij}-\frac{a_{ij}}{RT}=\frac{1}{2}\left[\left(b_{ii}-\frac{a_{ii}}{RT}\right)+\left(b_{jj}-\frac{a_{jj}}{RT}\right)\right]\left(1-k_{ij}\right) \tag{4.10}$$

Therefore, the cubic form of the PR EOS will take the form,

$$Z^3-(1-B)Z^2+\left(A-2B-3B^2\right)Z-\left(AB-B^2-B^3\right)=0 \tag{4.11}$$

where,

$$A=\frac{aP}{R^2T^2}\ ,\qquad B=\frac{bP}{RT} \tag{4.12}$$

For further thermodynamic calculations, the fugacity coefficient expression is given by,

$$\ln\varphi_i=\frac{b_i}{b}(Z-1)-\ln(Z-B)-\frac{A}{2\sqrt{2B}}\left(\frac{2\sum_j y_j a_{ji}}{a}-\frac{b_i}{b}\right)\ln\left(\frac{Z+\left(1+\sqrt{2}\right)B}{Z+\left(1-\sqrt{2}\right)B}\right) \tag{4.13}$$

For the purpose of this work, only the compressibility factors Z for the $CO_2$ are being calculated, at the appropriate initial temperatures and pressures, for the pure component. As mentioned before, these values for Z are used to further calculate the number of moles of $CO_2$ gas in the system, which are then used to calculate the mole fraction, the weight, and the weight fraction of $CO_2$, and the corresponding mole and weight fractions of monomer and polymer in the system.

### 4.2.2. Polymer - Supercritical Fluid Equilibria

Polymer solubility in supercritical fluids depends on temperature and pressure. In the supercritical pressure range, the solubility always increases with increasing

pressure. The effect of temperature is not as straightforward, however. At intermediate pressures, the free volume (density) effect is dominant and the solubility drops with increasing temperature ($(\partial \ln X / \partial T)_P < 0$). At higher pressures, the solubility increases with increasing the temperature.

As mentioned before, the starting point in determining the phase behavior of the system is the equilibrium criteria, which is defined by the equality of the fugacities, $f_i$, of each component in each phase,

$$\hat{f}_A^s = \hat{f}_A^g \tag{4.14}$$

$$\hat{f}_B^s = \hat{f}_B^g \tag{4.15}$$

where subscript *A* denotes the polymer and subscript *B* denotes the supercritical fluid, while the subscripts *s* and *g* are for solid and supercritical gas phases, respectively.

The assumptions involved in the study of the solubility phenomena are given:

- The supercritical fluid is insoluble in the solid polymer phase.
- The solid phase is incompressible; meaning the volume change of the solid due to increase of pressure above its equilibrium pressure is zero.
- Equilibrium pressure of a solid corresponds to the sublimation pressure for a solid supercritical fluid system.

These assumptions will lead to simplifications, which should be in good agreement with experimental observations. First, the equation (4.15) will drop because supercritical fluid ($CO_2$) is not distributed between phases. Thus, the remaining fugacity expression, Equation (4.14) can be rewritten as the equality of pure species fugacity in the solid phase to the partial fugacity of the solid in the supercritical gas phase,

$$f_A^s = \hat{f}_A^g \tag{4.16}$$

The left hand term, the solid phase fugacity for pure species, can be written as

$$f_A^s = \hat{\varphi}_A^{sub} P_A^{sub} \exp\left[\frac{V_A^s}{RT}\left(P - P_A^{sub}\right)\right] \tag{4.17}$$

where, the $P_A^{sub}$ is the solid vapor saturation pressure at the temperature $T$ of the system, or the sublimation pressure of the pure solid at the system temperature. $\hat{\varphi}_A^{sub}$ is the fugacity coefficient at $T$ and $P_A^{sub}$, and the exponential term is the Poynting correction for the fugacity of the pure solid. For a typical solid supercritical gas system, the solid vapor pressure is small, thus, for all practical purposes it can be considered as an ideal gas, which would reduce the $\hat{\varphi}_A^{sub}$ to unity, since the saturation pressure of a crystalline solid is normally much less than 1 bar. The right hand term of equation (4.16) is expressed as,

$$\hat{f}_A^g = y_A \hat{\varphi}_A^V P \tag{4.18}$$

Now, combining equations (4.17) and (4.18), yields

$$y_A = \frac{P_A^{sub}}{P} \frac{1}{\hat{\varphi}_A^V} \exp\left[\frac{V_A^s}{RT}\left(P - P_A^{sub}\right)\right] \tag{4.19}$$

where $y_A$ is the solubility of the solute in the supercritical gas, and it can be calculated using this equation. The $P_A^{sub}$ and $V_A^s$ are pure-species properties, either found from compiled data or estimated from a suitable correlation. The $\hat{\varphi}_A^V$, however, needs to be computed from a *PVT* equation of state, one that is capable of representing vapor-solute (polymer) mixtures at high pressures.

4.2.3. The SAFT Equation of State

Even for simple model fluids, like the Lennard-Jones fluid, it is not possible to derive exact and engineering-like (analytical) equations of state. The perturbation theories are therefore used to deliver simple approximate solutions for a given molecular model. The underlying idea is to divide the total intermolecular forces into repulsive and attractive contributions. The repulsive interactions are approximated through a 'reference-fluid', for which a reliable description has to be available. For perturbed chain equation, the *reference fluid* is the *hard chain fluid*. The attractive intermolecular forces in the Perturbed-Chain SAFT equation of state are further divided into different contributions, so that the reduced residual Helmholtz energy is written as

$$\frac{a^{res}}{kT} = \frac{a^{hc}}{kT} + \frac{a^{disp,chain}}{kT} + \frac{a^{assoc}}{kT} \qquad (4.20)$$

The right hand side of Equation (4.20) is composed of expressions for hard-chain fluid as well as contributions due to dispersion, association, dipolar and quadrupolar interactions. For a defined molecular model, theories from statistical thermodynamics can be applied for different contributions.

The *hard-chain reference fluid*, which is the first term in Equation (4.20), consists of chain-molecules with no attractive interactions. For chain comprising *m* segments, the reduced Helmholtz energy is given as

$$\frac{a^{hc}}{kT} = m\frac{a^{hs}}{kT} - \Sigma\, x_i\,(m_i - 1)\log g_{ii}^{hs}(\sigma_{ii}) \qquad (4.21)$$

where $x_i$ is the mole fraction of chains of component i, $m_i$ is the number of segments in a chain, $g_{ii}^{hs}$ is the radial pair distribution function for segments at collision-distance in

hard sphere system, and m is the mean segment number in the mixture.

$$m = \sum_i x_i \, m_i \tag{4.22}$$

The Helmholtz energy of the hard-sphere fluid required in Equation (4.21) is given as

$$\frac{a^{hs}}{kT} = \frac{1}{\zeta_0}\left[\frac{3\zeta_1\zeta_2}{(1-\zeta_3)} + \frac{\zeta_2^{\,3}}{\zeta_3(1-\zeta_3)^2} + \left(\frac{\zeta_2^{\,3}}{\zeta_3^{\,2}} - \zeta_0\right)\log(1-\zeta_3)\right] \tag{4.23}$$

while the radial distribution function of the hard-sphere fluid is:

$$g_{ij}^{\,hs} = \frac{1}{(1-\zeta_3)} + \left(\frac{d_i\, d_j}{d_i + d_j}\right)\frac{3\zeta_2}{(1-\zeta_2)} + \left(\frac{d_i\, d_j}{d_i + d_j}\right)^2 \frac{2\zeta_2}{(1-\zeta_3)^3} \tag{4.24}$$

with $\zeta_n$ defined as:

$$\zeta_n = \frac{\pi}{6}\rho\sum_i x_i \, m_i \, d_i^{\,n} \qquad\qquad n \in \{0,1,2,3\} \tag{4.25}$$

The segment diameter is a function of temperature and is given as follows

$$d_i = \sigma_i\left(1 - 0.12\exp\left(-3\frac{\varepsilon_i}{kT}\right)\right) \tag{4.26}$$

The *dispersion contribution for chain molecules*, which is the second term in Equation (4.20), is derived from the perturbation theory of Barker and Henderson (1983).

$$\begin{aligned}\frac{a^{disp,chain}}{kT} = & -2\pi\rho\left(\frac{\varepsilon}{kT}\right)\sigma^3\sum_\alpha^m\sum_\beta^m\int_1^\lambda g^{hc}{}_{\alpha\beta}(m, w, \rho)\, w^2\, dw \\ & - \pi\rho m kT\left(\frac{\partial\rho}{\partial P}\right)^{hc}\left(\frac{\varepsilon}{kT}\right)^2\sigma^3\frac{\partial}{\partial\rho}\left[\rho\sum_\alpha^m\sum_\beta^m\int_1^\lambda g^{hc}{}_{\alpha\beta}(m, w, \rho)\, w^2\, dw\right]\end{aligned} \tag{4.27}$$

with

$$kT\left(\frac{\partial\rho}{\partial P}\right) = \left(1 + m\frac{8\eta - 2\eta^2}{(1-\eta)^4} + (1-m)\frac{20\eta - 27\eta^2 + 12\eta^3 - 2\eta^4}{[(1-\eta)(2-\eta)]^2}\right)^{-1} \tag{4.28}$$

where $w$ is the reduced radial distance around the segments ($\mathrm{w} = \mathrm{r}/\sigma$), $\eta$ denotes the packing fraction (a dimensionless density, $\eta = \zeta_3$, and $\mathrm{g}^{\mathrm{hc}}{}_{\alpha\beta}(\mathrm{m}, \mathrm{w}, \rho)$ is the radial distribution function of the hard-chain reference fluid. For chain molecules, the overall intermolecular interaction is calculated as the sum of all individual segment-segment interactions in Equation (4.27). The integrals in Equation (4.27) are represented through simpler equations; the first integral is represented with $I_1$, and the second one with $I_2$.

$$\mathrm{I}_1(\eta, \mathrm{m}) = \sum_{\mathrm{i}=0}^{6} \mathrm{a}_\mathrm{i}(\mathrm{m})\, \eta^{\mathrm{i}} \tag{4.29}$$

$$\mathrm{I}_2(\eta, \mathrm{m}) = \sum_{\mathrm{i}=0}^{6} \mathrm{b}_\mathrm{i}(\mathrm{m})\, \eta^{\mathrm{i}} \tag{4.30}$$

where the coefficients $\mathrm{a}_\mathrm{i}(\mathrm{m})$ and $\mathrm{b}_\mathrm{i}(\mathrm{m})$ are functions of segment number.

$$\mathrm{a}_\mathrm{i}(\mathrm{m}) = \mathrm{a}_{0\mathrm{i}} + \frac{\mathrm{m}-1}{\mathrm{m}}\mathrm{a}_{1\mathrm{i}} + \frac{\mathrm{m}-1}{\mathrm{m}}\frac{\mathrm{m}-2}{\mathrm{m}}\mathrm{a}_{2\mathrm{i}} \tag{4.31}$$

$$\mathrm{b}_\mathrm{i}(\mathrm{m}) = \mathrm{b}_{0\mathrm{i}} + \frac{\mathrm{m}-1}{\mathrm{m}}\mathrm{b}_{1\mathrm{i}} + \frac{\mathrm{m}-1}{\mathrm{m}}\frac{\mathrm{m}-2}{\mathrm{m}}\mathrm{b}_{2\mathrm{i}} \tag{4.32}$$

The *association contribution*, i.e. the third term in Equation (4.20) is given as

$$\frac{a^{assoc}}{kT} = \sum_i x_i \sum_\alpha \left[ \sum_{Ai\alpha} \left( \ln X^{Ai\alpha} - \frac{X^{Ai\alpha}}{2} \right) + \frac{W_{i\alpha}}{2} \right] \tag{4.33}$$

where $\mathrm{W}_{\mathrm{i}\alpha}$ is the number of bonding sites of segment type $\alpha$.

The polymer-supercritical fluid system of this work (PMMA-$CO_2$-MMA), does not account for association terms, due to the fact that the functional groups of the polymer system are canceling themselves, and thus they do not exhibit association

interactions. There are no dipole effects either, which means there are only hard chain, hard sphere, and dispersion contributions.

## 4. 3. Modeling of the PMMA-$CO_2$-MMA System Using SAFT EOS

In this section, the PMMA-$CO_2$-MMA system is modeled using the statistical associating fluid theory (SAFT) model [19]. The fugacity coefficients of the supercritical fluid are obtained from this model, as a function of composition, temperature and pressure. By substituting the appropriate values for the molar fractions of $CO_2$, methyl methacrylate, and poly (methyl methacrylate), followed by the appropriate working temperature and pressure, the software gives a fugacity output for those given conditions. Detailed sample calculation procedure is given in Appendix E. The pure component critical temperature, pressure, and acentric factor for $CO_2$ and MMA is given in Table 4.3

Table 4.3 Critical Constants and Acentric Factor for $CO_2$ and MMA

| Component | $T_c$ (°C) | $P_c$ (bar) | Acentric Factor |
|---|---|---|---|
| $CO_2$ | 31.0 | 73.8 | 0.225 |
| MMA | 290.8 | 36.8 | 0.317 |

A detailed discussion of the mathematical form of the SAFT equation was given in the previous section, together with the expressions for the residual Helmholtz free energy, and for the fugacity coefficients. For each pure component there are potentially

five pure component parameters in the SAFT equation: $v^{oo}$, the temperature-independent volume of segment, $u^o/k$, the temperature-independent, nonspecific energy of attraction between two segments, $m$, the number of segments in a molecule, $\varepsilon/k$, the energy of association between sites on a molecule, and $v$, the volume of site-site association. Although spectroscopy data [2, 20] suggest the existence of a complex between $CO_2$ and the repeat units in MMA, the association parameters $\varepsilon/k$ and $v$ are nevertheless set equal to zero for this complex since it is rather weak and it would introduce more fitted parameters into the model.

The pure component parameters for $CO_2$ are available in the literature [21], while the pure component parameters for MMA and PMMA are not available in the literature and had to be estimated. They are all listed in Table 4.4 below,

Table 4.4 Pure Component Parameters Used in the SAFT Equation

| Component | $u^O/k$ (K) | $V^{oo}$ ($cm^3$/mole) | $m$ |
|---|---|---|---|
| $CO_2$ | 216.1 | 13.278 | 1.417 |
| MMA | 208.0 | 8.700 | 5.670 |
| PMMA | 240.0 | 9.560 | 2532 |

The values of the pure component parameters for low molecular weight components from a given chemical family usually follow trends that are directly related to the changes in structural features of each member of the family. Following that logic,

the above pure component parameters have been obtained by extrapolating the results found with the *n*-alkane parameters for similar polyolefins. Also, a simple group contribution method can be used to calculate the pure component parameters of polymers and their monomers, particularly for obtaining the number of segments, *m*, by calculating *m* for the base contributing groups in the molecule and adding them together.

As it can be seen from Table 4.4, there is a significant difference between the temperature-independent nonspecific energy of attraction between two segments, $u^0/k$, for PMMA and MMA. This can be due to the intra- and inter-segmental interactions of the many segments of PMMA that are affected by the excluded volume of the chains [2] relative to the small number of chains of MMA which is not as affected by excluded volume considerations.

The only experimental information available on the system PMMA-$CO_2$ is that PMMA is not soluble in pure $CO_2$ to temperatures as high as 255°C and pressures till 2550 bar, while the addition of monomer co-solvent to the polymeric system will greatly increase the solvating power of the supercritical $CO_2$ solvent. This has been proven experimentally in this work. The SAFT model should be able to predict the same findings, only through calculation. There are concerns in the literature though that the quantitative agreement between experimental data and calculations is not always good.

### 4.3.1. Solubility Behavior of the PMMA-CO2-MMA System

A detailed sample calculation of the sublimation pressure and the fugacity coefficients of the polymer system, using modified SAFT code, is given in Appendix E.

The software gives a fugacity output for the given conditions: composition, temperature, and pressure. The obtained sublimation pressure and the fugacity coefficients are further used in the solubility equation,

$$y_A = \frac{P_A^{sub}}{P}\frac{1}{\hat{\varphi}_A^V}\exp\left[\frac{V_A^s}{RT}\left(P - P_A^{sub}\right)\right]$$

By further successive substitution of all corresponding P-T cloud-points in the above equation, the solubility of PMMA is calculated for every combination of composition, pressure and temperature. The results are listed in Table 4.5,

Table 4.5 Solubility Data for the PMMA-$CO_2$-MMA System of this Study Calculated for all P-T-x Combinations Using the SAFT EOS

| Sample | 27 °C | | 45°C | | 60°C | | 75.5°C | |
|---|---|---|---|---|---|---|---|---|
| | $P_1$ | $y_1$ | $P_2$ | $y_2$ | $P_3$ | $y_3$ | $P_4$ | $y_4$ |
| #1128 | 129.00 | 1.976E-06 | 210.00 | 1.391E-05 | 275.83 | 6.518E-05 | 312.00 | 2.788E-04 |
| # 1031 | 66.50 | 4.445E-06 | 94.00 | 2.600E-05 | 119.60 | 1.006E-04 | 141.00 | 3.799E-04 |
| # 1101 | 63.70 | 4.574E-06 | 88.30 | 2.687E-05 | 106.53 | 1.059E-04 | 125.00 | 3.972E-04 |
| # 1102 | 62.00 | 4.606E-06 | 86.00 | 2.701E-05 | 125.00 | 1.073E-04 | 117.00 | 4.056E-04 |

Based on the calculated solubility results in Table 4.5, a P-y diagram is plotted in MATLAB depicting each isotherm for each appropriate pressure and solubility set, as shown in Figure 4.5.

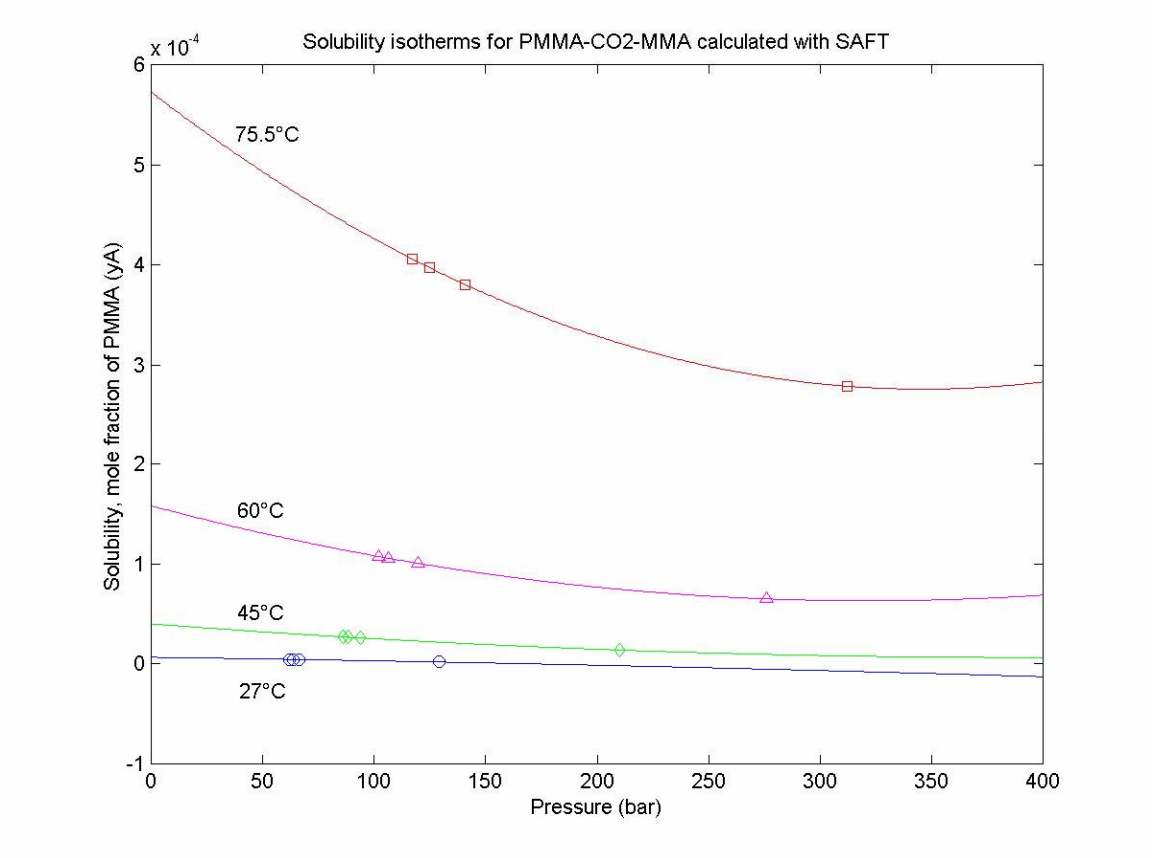


Figure 4.5 Solubility Isotherms for the PMMA-$CO_2$-MMA System of This Study Calculated Using the SAFT EOS Model

These isotherms can further be translated into a cloud-point data plot, making it more convenient to compare with the experimental cloud-point data. This can potentially be done using the same SAFT software with minor modifications for the pure component reduced density i.e. the segment or molecule packing factor, which is a function of the molar density. In the previous calculation of the vapor fugacity coefficients, the packing factor in the SAFT code is set to 0.232. Now, for calculating the fugacity coefficients of the liquid phase, the packing factor will be set to a much smaller value, 0.00026, which

would be representative of the liquid phase. A similar set of fugacity coefficients is calculated, and then both fugacity coefficients are used in the cloud-point flash calculation to obtain the cloud-point pressures. The calculated fugacity coefficients of the vapor and liquid phase are listed in Table 4.6,

Table 4.6 Fugacity Coefficients Calculated for the Vapor and the Liquid Phase for the PMMA-$CO_2$-MMA System of This Study Using the SAFT EOS

| Sample | 27 °C | | 45°C | | 60°C | | 75.5°C | |
|---|---|---|---|---|---|---|---|---|
| | $\varphi^V$ | $\varphi^L$ | $\varphi^V$ | $\varphi^L$ | $\varphi^V$ | $\varphi^L$ | $\varphi^V$ | $\varphi^L$ |
| #1128 | 0.1973 | 0.3696 | 0.2086 | 0.3696 | 0.2172 | 0.3697 | 0.2255 | 0.3697 |
| # 1031 | 0.1208 | 0.3692 | 0.1368 | 0.3693 | 0.1500 | 0.3693 | 0.1634 | 0.3693 |
| # 1101 | 0.1207 | 0.3692 | 0.1368 | 0.3693 | 0.1500 | 0.3693 | 0.1635 | 0.3693 |
| # 1102 | 0.1220 | 0.3692 | 0.1381 | 0.3693 | 0.1512 | 0.3693 | 0.1647 | 0.3693 |

This is an alternative approach and it may need to incorporate a new theory, because there is a fundamental problem in mapping the polymer solid phase to calculate the bubble point. This can be overcome by introducing some modifications to the existing SAFT code. Taking into consideration the current developments in SAFT modeling techniques, it is believed that soon it will be possible to perform this type of calculation with greater accuracy. In this study, an attempt was made to model the solubility behavior with SAFT, using a bubble-point algorithm. The calculated values are listed in Table 4.7,

Table 4.7 SAFT Modeled Solubility of Poly (Methyl) Methacrylate in $CO_2$ in the Presence of 2.0 wt % MMA

| x (27 C) | y (27 C) | P (27 C) | x (60 C) | y (60 C) | P (60 C) | x (76 C) | y (76 C) | P (76 C) |
|---|---|---|---|---|---|---|---|---|
| 0.999 | 4.86E-7 | 65 | 0.995 | 4.86E-6 | 65 | 0.99 | 1.12E-6 | 65 |
| 0.998 | 7.99E-7 | 89 | 0.982 | 6.32E-6 | 89 | 0.986 | 4.76E-6 | 89 |
| 0.983 | 1.98E-6 | 110 | 0.979 | 1.87E-5 | 110 | 0.973 | 1.88E-5 | 110 |
| 0.975 | 6.87E-6 | 138 | 0.973 | 9.86E-4 | 138 | 0.962 | 5.87E-5 | 138 |
| 0.972 | 8.99E-6 | 185 | 0.964 | 1.22E-3 | 185 | 0.959 | 8.87E-4 | 185 |
| 0.968 | 1.96E-5 | 198 | 0.958 | 3.98E-3 | 198 | 0.95 | 9.96E-4 | 198 |

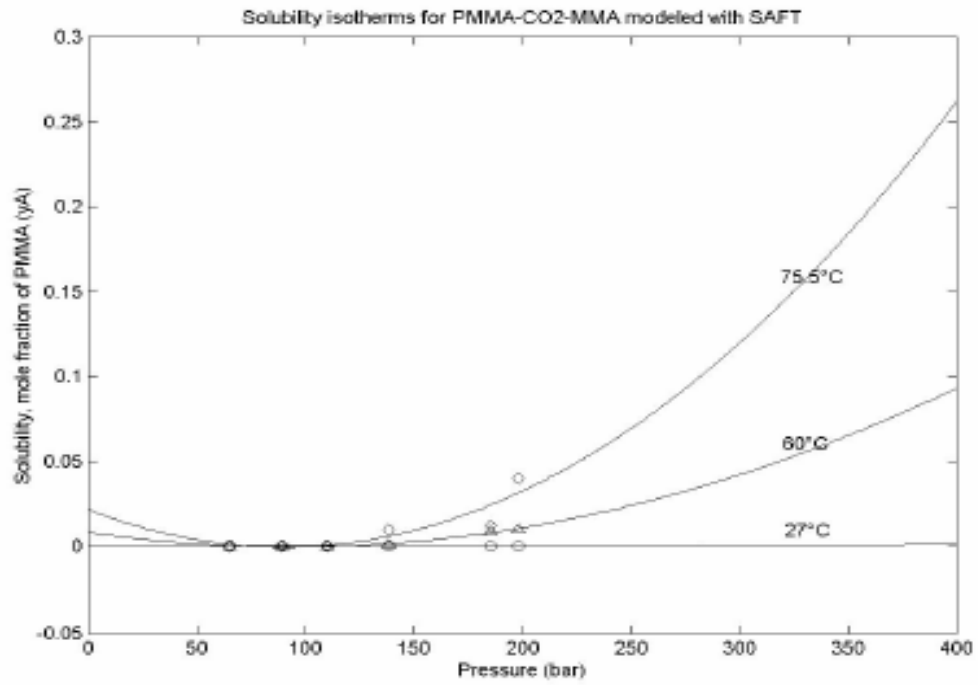


Figure 4.6 SAFT Modeled Solubility of PMMA-$CO_2$-MMA System

These curves show the quantitative agreement between experimental data and calculations. The predicted values in this study are very close to the experimental values. If we increase the amount of MMA in the calculations, the results would be even closer. It was proven experimentally that at 20wt% MMA and 40wt% MMA, solubility of poly (methyl methacrylate) increased significantly, due probably to the formation of a weak complex between the carboxylic oxygen in MMA and the carbon in $CO_2$. MMA co-solvent added to $CO_2$ significantly decreases the pressures needed to dissolve PMMA.

# CHAPTER 5

# CONCLUSIONS AND FUTURE WORK

To summarize, High Pressure Phase Monitoring System SPM20 has beeen used in this study to observe and measure phase behavior of a monomer-supercritical fluid and monomer-polymer-supercritical fluid systems. Solubility of poly (methyl methacrylate) (PMMA) in $CO_2$, plus methyl methacrylate as a cosolvent, was determined using cloud point measurements. The results are modeled using SAFT. Polymer processing in supercritical fluids has been a major interest for a portfolio of materials processing applications including their impregnation into porous matrices. Unfortunately they are only sparingly soluble in $CO_2$ unless one uses an entrainer or surfactant. This work focuses their solubility at rather mild conditions, low temperature and reduced pressures less than three.

Cloud-point measurement demonstrates that poly (methyl methacrylate) is hardly soluble in supercritical $CO_2$. Partial solubility of the polymer may be taking place, but it is far from soluble. The solubility improves with the addition of its own monomer, methyl methacrylate, to the system. Concentrations in the excess of 50 wt % (30 mol%) MMA have been employed, which resulted in single-phase systems, at relatively low pressures and temperatures (100-500 bar at corresponding 27-150 °C). It was noticed

that the polymer did not fully solubilize until the concentration of poly (methyl methacrylate) has been reduced more than ten times below the originally anticipated amount of 5.0 wt%. Cloud-point data for the dilute system of poly(methyl methacrylate) (PMMA)-$CO_2$-methyl methacrylate (MMA) are measured in the temperature range of 27-75.5 °C, and pressures as high as 320 bar, and with co-solvent concentrations of 27 and 48.4 wt% MMA, and varying concentrations of PMMA of 0.1, 0.2, and 0.5 wt%. Solubility data is reported for these systems. Peng-Robinson equation of state has been used to model the $CO_2$-MMA system, while SAFT equation of state is used to model the PMMA-$CO_2$-MMA system. Much closer qualitative match is achieved with the SAFT model used in this work, compared to the modeling results published by McHugh et al.

It is difficult to evaluate if the shortcomings of SAFT are caused by the equation itself or rather by the choice of parameters used in the calculation. SAFT does not account for chain stiffness [2, 6], whose contribution to the entropy of mixing can be of major importance. So far, the SAFT equation can possibly be used to show qualitatively the same trends as the experimental data, but it is not reliable enough to obtain an accurate quantitative agreement with the measured data. More substantial work is needed to extend and evaluate the group contribution method for estimating polymer, solvent, and co-solvent parameters if phase behavior is to be calculated reliably rather than measured experimentally. The findings presented in this work open up a new dimension for research in the thermodynamic analysis of polymeric systems.

REFERENCES


[1] McHugh, M. A., Krukonis, V. J., Eds. *Supercritical Fluid Extraction Principles and Practice, 2nd Ed.*; Butterworth-Heinemann: Boston, 1994.

[2] Lora M., McHugh M. A., Phase behavior and modeling of the poly(methyl methacrylate)-$CO_2$-methyl methacrylate system, *Fluid Phase Equilibria* 1999, *157*, 285-297.

[3] Kirby, F. C., McHugh, M. A., Phase Behavior of Polymers in Supercritical Fluid Solvents, *Chem. Rev*. 1999, *99*, 565-602.

[4] Tomasko, D. L., Li, H., Liu, D., Han, X., Wingert, M. J., Lee, L. J., Koelling, K. W., A Review of $CO_2$ Applications in the Processing of Polymers, *Ind. Eng. Chem. Res.* 2003, *42*, 6431-6456.

[5] Seung, N. J., Ji-Ung, P., Sun, Y. K., Ki-Pung, Y., High Pressure Behavior of Polymer-Solvent Systems with Addition of Supercritical $CO_2$ at Temperatures from 323.15 K to 503.15 K, *J. Chem. Eng. Data* 2002, *47*, 270-273.

[6] Rindfleisch, F., DiNoia T. P., McHugh, M. A., Solubility of Polymers and Copolymers in Supercritical $CO_2$, *J. Phys. Chem.* 1996, *100*, 15581-15587.

[7] Serifoglu, E. I., Theoretical and Experimental Investigation of Stefan Tube at Supercritical Conditions, Dissertation, University of South Florida, 2003.

[8] Walker, T. A., Spontak,R. J., Khan, S. A., Modification of Polymer Blend Phase Behavior with High-Pressure Carbon Dioxide, Dissertation, North Carolina State University, 2003.

[9] McHugh, M. A., Rindfleisch, F., Kuntz, P. T., Schmaltz, C., Buback, M., Cosolvent Effect of Alkyl Acrylates on the Phase Behavior of Poly(alkyl acrylates)-Supercritical $CO_2$ mixture, *Polymer* 1998, Vol. *39*, No. *24*, 6049-6052.

[10] Prausnitz, J. M., Lichtenthaler, R. N., de Azevedo, E. G., *Molecular Thermodynamics of Fluid-Phase Equilibria, 3rd Ed.*; Prentice Hall: Upper Saddle River, NJ, 1999.

[11] H. Obrey, C. P. Bokis, C.C. Chen, *Ind. Eng. Chem. Res.* 1998, *37*, 4481-4491.

[12] G. Luft, A. Lindner, *Angew. Makro. Chem.* 1976, *56*, 99.

[13] Voutsas, E. C., Pappa, G. D., Boukouvalas, C. J., Magoulas, K., Tassios, D. P., Miscibility in Binary Polymer Blends: Correlation and Prediction, *Ind. Eng. Chem. Res*. 2004, *43*, 1312-1321.

[14] Flory, P. J., *Principles of Polymer Chemistry*, Chapter 12. Cornell Univ. Press: Ithaca, New York, 1953.

[15] Sanchez, I. C., Statistical Thermodynamics of Polymer Blends, *Polymer Blends*, *Vol. 1*, Chapter 3. Academic Press: New York, 1978.

[16] Sanchez, I. C., Lacombe, R. H., *J. Phys. Chem.* 1976, *80*, 2352.

[17] Sanchez, I. C., Lacombe, R. H., *J. Polym. Sci. Polym. Lett. Ed.* 1977, *15*, 71.

[18] Lacombe, R. H., Sanchez, I. C., *J. Phys. Chem.* 1976, *80*, 2568.

[19] Aslam, N., SAFT, Dissertation, University of South Florida, 2005.

[20] Kazarian, S. G., Vincent, M. F., Bright, F. V., Liotta, C. L., Eckert, C. A., *J. Am. Chem. Soc.* 1996, *118*, 1729-1736.

[21] Huang, S. H., Radosz, M., Equation of State for Small, Large, Polydisperse, and Associating Molecules, *Ind. Eng. Chem. Res.* 1990, *29*, 2284-2294.

[22] Perry, R. H., Green, D., *Perry's Chemical Engineer's Handbook.*, 7th Ed., McGraw-Hill Book Company, New York, 1997.

[23] Orbey, H., Sandler, S. I., Modeling Vapor-Liquid Equilibria: Cubic Equations of State and Their Mixing Rules, Cambridge University Press: Cambridge, U.K., 1998.

BIBLIOGRAPHY


[1] Brunner, G., *Gas Extraction*, Steinkopff: Darmstadt-Springer: New York, 1994.

[2] Voutsas, E. C., Pappas, G. D., Boukouvalas, C. J., Magoulas, K., Tassios, D. P., Miscibility in Binary Polymer Blends: Correlation and Prediction, *Ind. Eng. Chem. Res.* 2004, *43*, 1312-1321.

[3] Sunol, A. K., Sunol, S. G., Substitution of Solvents by Safer Products and Processes, in Handbook of Solvents, Wypych, G., Ed., ChemTec Publishing, New York, 2001, 1419-1459.

[4] Day, C-Y., Chang, C. J., Chen, C-Y., Phase Equilibrium of Ethanol+$CO_2$ and Acetone+$CO_2$ at Elevated Pressures, *J. Chem. Eng. Data*, 1996, *41*, 839-843.

[5] Byun, H-S., Shin, J-S., Bubble-Point Measurement for $CO_2$+Vinyl Acetate and $CO_2$+Vynil Acrylate Systems at High Pressures, *J. Chem. Eng. Data*, 2003, *48*, 97-101.

[6] McHugh, M., Paulaitis, M. E., Solid Solubilities of Naphthalene and Biphenyl in Supercritical Carbon Dioxide, *J. Chem. Eng. Data*, 1980, *25*, 326-329.

[7] Byun, H. S., McHugh, M. A., Impact of "Free" Monomer Concentration on the Phase Behavior of Supercritical Carbon Dioxide-Polymer Mixtures., *Ind. Eng. Chem. Res.*, 2000, *39*, 4658-4662.

[8] Koak, N., Visser, R. M., de Loos, Th. W., *Fluid Phase Equilib*., 1999, *158-160*, 835-846.

[9] McHugh, M. A., Rindfleisch, F., Kunz, P. T., Schmaltz, C., Buback, M., Cosolvent Effect of Alkyl Acrylate on the Phase Behavior of Poly(alkyl acrylate)-Supercritical CO2 Mixtures., *Polymer,* 1998, *39*, 6049-6052.

[10] Xiong, Y., Kiran, E., *J. Applied Polymer Science*, 1995, *55*, 1805-1818.

[11] Sanchez, I. C., Lacombe, R., *J. Phys. Chem.*, 1976, *80*, 2352-2362.

[12] Sanchez, I. C., Lacombe, R., *Macromolecules*, 1978, *11*, 1145-1156.

[13] Folie, B., Radosz, M., *Ind. Eng. Chem. Res.*, 1995, *34*, 1501-1516.

[14] Condo, P. D., Radosz, M., *Fluid Phase Equilibria*, 1996, *117*, 1-10.

[15] Obrey, H., Bokis, C. P., Chen, C-C., *Ind. Eng. Chem. Res.* 1998, *37*, 4481-4491.

[16] Prausnitz, J. M., Lichtenthaler, R. N., de Azevedo, E. G., *Molecular Thermodynamics of Fluid Phase Equilibria*, 3rd Ed.; Prentice-Hall: Upper Saddle River, NJ, 1999.

[17] McHugh, M., Krukonis, V., *Supercritical Fluid Extraction*, 2nd Ed.; Butterworth-Heinemann: Stoneham, MA, 1994.

[18] Luft, G., Lindner, A., *Angew. Makro. Chem.* 1976, *56*, 99.

[19] Serifoglu, I. E., Theoretical and Experimental Investigation of Stefan Tube at Supercritical Conditions, Thesis (USF), 2003.

[20] Paul, D. R., Newman, S., Lacombe, S. I., *Polymer Blends*, Volume 1, Academic Press, Inc.(London) Ltd: 1978.

[21] Seung, N. J., Ji-Ung, P., Sun, Y. K., Ki-Pung, Y., High Pressure Behavior of Polymer-Solvent Systems with Addition of Supercritical $CO_2$ at Temperatures from 323.15 K to 503.15 K, *J. Chem. Eng. Data*, 2002, *47*, 270-273.

[22] Rindfleisch, F., DiNoia T. P., McHugh, M. A., Solubility of Polymers and Copolymers in Supercritical $CO_2$, *J. Phys. Chem.* 1996, *100*, 15581-15587.

[23] Sandler, S. I., Chemical and Engineering Thermodynamics, 3rd Ed., John Wiley & Sons, Inc., New York, 1999.

[24] Prausnitz, J., Anderson, T., Grens, E., Eckert, C., Hsieh, R., O'Connell, J., Computer Calculations for Multicomponent Vapor-Liquid and Liquid-Liquid Equilibrium., Prentice-Hall, Inc., Englewood Cliffs, NJ, 1980.

[25] Smith, J. M., Van Ness, H. C., Abbott, M. M., Introduction to Chemical Engineering Thermodynamics, 6th Ed., Tata McGraw-Hill Publishing Company Ltd., New Delhi, 2003.

[26] Benedek, P., Olti, F., Computer Aided chemical Thermodynamics of Gases and Liquids: Theory, Models, and Programs, John Wiley & Sons,Inc., New York, 1985.

[27] Tester, J. W., Modell, M., Thermodynamics and Its Applications, 3rd Ed., Prentice-Hall, Inc., Upper Saddle River, NJ, 1997.

[28] Clifford, T., Fundamentals of Supercritical Fluids, Oxford University Press, Inc., New York, 1999.

[29] Angus, S., Armstrong, B., de Reuck, K. M., Chapela, G. A., Rowlinson, J. S., International Thermodynamic Tables of the Fluid State Carbon Dioxide, IUPAC, Pergamon Press, New York, 1976.

[30] Hasch, B. M., Lee, S-H., McHugh, M. A., Strengths and Limitations of SAFT for Calculating Polar Copolymer-Solvent Phase Behavior, *Journal of Applied Polymer Science*, 1996, *59*, 1107-1116.

[31] Reid, R. C., Prausnitz, J. M., Poling, B. E., The Properties of Liquids and Gases, 4th Ed., McGraw-Hill, New York, 1987.

[32] Peng, D. Y., Robinson, D. B., A New Two-Constant Equation of State., *Ind. Eng, Chem. Fundam.*, 1976, *15*, 59-63.

# APPENDICES

Appendix A: MATLAB Program That Calculates the Z Values of Pure $CO_2$ Using the Peng-Robinson EOS with Wong-Sandler Mixing Rules

```
% Program Name: CO2.m
% ____________________________________________________________________
% This program provides the values for the compressibility % factors Z
% for the pure component CO2 in the system. The program calls for the
% PR EOS function "CO2.m". The subscript (1) stands for CO2; subscript
% (2) is for other solvent (Tc2, Pc2, w2 of a solvent must be entered)
% For the purpose of computing the Z factors of pure CO2 in the system,
% at the initial pressure and temperature of each experimental sample
% in the system, the amount of CO2 is fixed as 100%, while the other
% solvent portion is 0%. The output is the Z factors for the pure CO2.
% ____________________________________________________________________
clear all
function Z = CO2(x1,x2,P,T)

JFLG=1;
Tc1 = 304.25;  % critical temperature of CO2
Pc1 = 73.8;    % critical pressure of CO2
w1  = 0.225;   % acentric factor of CO2
Tc2 = 513.9;
Pc2 = 61.4;
w2  = 0.644;
Tr1 = T/Tc1;
Tr2 = T/Tc2;
k01 = 0.378893 + 1.4897153*w1-
0.17131848*w1^2+0.0196554*w1^3;
o1  = 0.04285;
o2  = -0.03374;
k02 = 0.378893 + 1.4897153*w2-
0.17131848*w2^2+0.0196554*w2^3;
k1  = k01 + o1*(1 + (Tr1)^0.5)*(0.7-Tr1);
k2  = k02 + o2*(1 + (Tr2)^0.5)*(0.7-Tr2);
alpha1 = [1 + k1*(1-(Tr1)^0.5)]^2;
R  = 83.14;
a1  = (0.457235*R^2*Tc1^2/Pc1)*alpha1;
b1 = 0.077796*R*Tc1/Pc1;
alpha2 = [1 + k2*(1-(Tr2)^0.5)]^2;
a2  = (0.457235*R^2*Tc2^2/Pc2)*alpha2;
b2 = 0.077796*R*Tc2/Pc2;
Alp12=0.30;
Alp21=0.30;
```

```
G12 = 1.909516*238.92;
G21 = 1.444729*238.92;
TAU12 = G12/(1.9872*T);
TAU21 = G21/(1.9872*T);
C   = -0.62323;
T12 = TAU12;
T21 = TAU21;
G01      = (x1*x2)*T21*G21;
G02      = x1*(1-G21) + G21;
G03      = (x1*x2)*T12*G12;
G04      = 1 - x1*(1-G12);
Gex      = G01/G02 + G03/G04;
I12 = -0.15;
I21 = -0.15;
F11 = x1^2*(b1 -a1/(R*T));
F12 = x1*(x2)*((b1+b2)-(a1+a2)/(R*T))*(1-I12)/2;
F21 = x1*(x2)*((b1+b2)-(a1+a2)/(R*T))*(1-I21)/2;
F22 = (x2)^2*(b2-a2/(R*T));
FOOO   = F11 + F12 + F21 + F22;
M11 = (x1*a1/(R*T*b1) + (x2)*a2/(R*T*b2));
M12 = Gex/C;
MOO   = 1 - M12 -M11;
b   = FOOO/MOO;
B   = b*P/(R*T);
M13 = Gex *R*T/C;
M14 = (x1*a1/b1 + (x2)*a2/b2);
M0  = M14 + M13;
a   = b*M0;
A   = a*P/(R*T)^2;
p1  = B-1;
p2  = A - 3*B^2-2*B;
p3  = B^3+B^2-A*B;
coeffs=[1 p1 p2 p3];
numz=roots(coeffs);
display(numz);
Z = numz(3)
display (A);
display (B);
fugacity = (Z-1) - log(Z-B)-A/(2.828*B)*log((Z+2.414*B)/(Z-
.414*B));
fugcoeff = log(fugacity);
display(fugcoeff);
```

## Appendix B: Sample Calculation to Determine the Mole Fractions of MMA or PMMA

For sample #1120 of this experiment, where the weight of MMA is m(MMA) = 1.0007 g,

n(MMA) = m/M = 1.0007/100.12 = 0.01 moles

V(MMA) = m/ρ= 1.0007/0.943 = 1.0612 ml

$V(CO_2)$ = 15 – V(MMA) = 15 - 1.0612 = 13.9388 ml

Using function Z = CO2(x1, x2, P, T) from the Matlab program CO2.m, from Appendix A.1., the compressibility of $CO_2$ , at initial pressure $P_{in}$ = 63.5 bar and initial temperature $T_{in}$ = 295.35 K, is calculated to be Z = 0.1645, as shown below:

Z = CO2 (x1, x2, P, T)

Z = CO2 (1, 0, 63.5, 295.35)

Z = 0.1645

Using this Z value, the number of $CO_2$ moles in the system is calculated,

$n(CO2) = (P_{in}V)/(ZRT_{in})$ = (63.5 x 13.9388) / (0.1645 x 83.1451 x 295.35) = 0.2191

Then, the mole fractions of $CO_2$ and MMA are calculated,

x1 ($CO_2$) = $n(CO_2)$ / [$n(CO_2)$+n(MMA)] = 0.2191/(0.2191+0.01) = 0.956

x2 (MMA) = n(MMA) / [$n(CO_2)$+n(MMA)] = 0.01/((0.2191+0.01) = 0.044

This calculation is further repeated for each experimental sample, at its corresponding MMA or PMMA weights, initial pressures and initial temperatures of the system, in order to obtain the appropriate mole fractions of MMA or PMMA for each experiment.

## Appendix C: Mole Fraction of Polymer Compared to the Corresponding Weight Fraction

For polymers, the mole fraction is often not very useful. For example, if we consider a mixture of 0.3 g PMMA of molecular weight 96,850 mixed with 5.5 g of MMA of molecular weight 100.12 and 6.32 g of supercritical $CO_2$ of molecular weight 44.01, the mole fraction of the polymer is,

$x$(PMM) = moles PMMA/(moles PMMA+moles MMA+moles $CO_2$) =

= (0.3/96,850) / (0.3/96,850 + 5.5/100.12 + 6.32/44.01) =

= 1.56E-05

where $x$ is mole fraction. While this seems like a vanishing amount of polymer, we can now consider the mass fraction of polymer in the mixture:

$m$(PMMA) = mass PMMA / (mass PMMA + mass MMA + mass $CO_2$) =

= 0.3 / (0.3 + 5.5 + 6.32) =

= 0.3/12.12 = 0.025

where $m$ is mass fraction. Although the mole fraction of polymer is tiny, the polymer occupies about 2.5% of the mass of the mixture. In terms of physical and thermodynamic properties, most of the times it is more meaningful to consider mass fractions than mole fractions of polymers.

Appendix D: The SAFT EOS Model Used in This Study

```
function T = SOFINAL(x1,x2,x3,T,P)

Z = 0.005;
dense = 0.232;
Tau =0.74048;
k = 1.381*10^-23;
NA = 6.023*10^23;
ek1 = 52.0;
ek2 = 10.0;
ek3 = 10.0;
m1 = 1.417;
m2 = 5.67;
m3 = 2532;
k12 = 0.23;
k13 = 0.059;
k23 = 0.12;
k21 = k12;
k31 = k13;
k32 = k23;
v100 = 13.278;
v200 = 8.7;
v300 = 9.56;
d11 = ((v100*6*Tau)/(3.14*NA))^0.33;    % Units cm
d22 = ((v200*6*Tau)/(3.14*NA))^0.33;    % Units cm
d33 = ((v300*6*Tau)/(3.14*NA))^0.33;    % Units cm
d1  = d11/(10^-8);
d2  = d22/(10^-8);
d3  = d33/(10^-8);
u10 = 216.1;
u20 = 208.0;
u30 = 240.0;
u11 = u10*(1+ek1/T);
u22 = u20*(1+ek2/T);
u33 = u30*(1+ek3/T);
u12 = (1-k12)*(u11*u22)^0.5;
u21 = (1-k21)*(u22*u11)^0.5;
u13 = (1-k13)*(u11*u33)^0.5;
u31 = (1-k31)*(u33*u11)^0.5;
u23 = (1-k23)*(u22*u33)^0.5;
u32 = (1-k32)*(u33*u22)^0.5;
v10 = v100*[1-0.12*exp(-3*u10/(T))]^3;
v20 = v200*[1-0.12*exp(-3*u20/(T))]^3;
v30 = v300*[1-0.12*exp(-3*u30/(T))]^3;

v110 = v10;
v220 = v20;
v330 = v30;
v120 = [0.5*[(v10)^0.33 + (v20)^0.33]]^3;
v210 = v120;
```

Appendix D (Continued):

```
v130 = [0.5*[(v10)^0.33 + (v30)^0.33]]^3;
v310 = v130;
v230 = [0.5*[(v20)^0.33 + (v30)^0.33]]^3;
v320 = v230;

m = m1*x1 + m2*x2 + m3*x3;
dmdx1 = m1;
dmdx2 = m2;
dmdx3 = m3;

z0t = (3.14/6)*(x1*m1*d1^0 + x2*m2*d2^0 + x3*m3*d3^0);
z1t = (3.14/6)*(x1*m1*d1^1 + x2*m2*d2^1 + x3*m3*d3^1);
z2t = (3.14/6)*(x1*m1*d1^2 + x2*m2*d2^2 + x3*m3*d3^2);
z3t = (3.14/6)*(x1*m1*d1^3 + x2*m2*d2^3 + x3*m3*d3^3);

rho = dense/(z3t);
z0  = z0t*rho;
z1  = z1t*rho;
z2  = z2t*rho;
z3  = z3t*rho;
I   = z3;
dz0tdx1 = (3.14/6)*(m1*d1^0);
dz1tdx1 = (3.14/6)*(m1*d1^1);
dz2tdx1 = (3.14/6)*(m1*d1^2);
dz3tdx1 = (3.14/6)*(m1*d1^3);
dz0tdx2 = (3.14/6)*(m2*d2^0);
dz1tdx2 = (3.14/6)*(m2*d2^1);
dz2tdx2 = (3.14/6)*(m2*d2^2);
dz3tdx2 = (3.14/6)*(m2*d2^3);
dz0tdx3 = (3.14/6)*(m3*d3^0);
dz1tdx3 = (3.14/6)*(m3*d3^1);
dz2tdx3 = (3.14/6)*(m3*d3^2);
dz3tdx3 = (3.14/6)*(m3*d3^3);

dz0dx1  = dz0tdx1*rho;
dz1dx1  = dz1tdx1*rho;
dz2dx1  = dz2tdx1*rho;
dz3dx1  = dz3tdx1*rho;
dz0dx2  = dz0tdx2*rho;
dz1dx2  = dz1tdx2*rho;
dz2dx2  = dz2tdx2*rho;
dz3dx2  = dz3tdx2*rho;
dz0dx3  = dz0tdx3*rho;
dz1dx3  = dz1tdx3*rho;
dz2dx3  = dz2tdx3*rho;
dz3dx3  = dz3tdx3*rho;

dIdx1 = dz3dx1;
dIdx2 = dz3dx2;
dIdx2 = dz3dx3;
```

Appendix D (Continued):

```
G1 =
x1^2*m1^2*[u11/(T)]*v110+x1*x2*m1*m2*[u12/(T)]*v120+x1*x3*m1*m3*[u13/(T
)]*v130+x2*x1*m2*m1*[u21/(T)]*v210+x2^2*m2^2*[u22/(T)]*v220+x2*x3*m2*m3
*[u23/(T)]*v230+x3*x1*m3*m1*[u31/(T)]*v310+x3*x2*m3*m2*[u32/(T)]*v320+x
3*x3*m3*m3*[u33/(T)]*v330;
G2 = x1^2*m1^2*v110 + x2^2*m2^2*v220 + x3^2*m3^2*v330 +
x1*x2*m1*m2*v120 + x1*x3*m1*m3*v130 + x2*x1*m2*m1*v210  +
x2*x3*m2*m3*v230 + x3*x1*m3*m1*v310 + x3*x2*m3*m2*v320;
G  = G1/G2;
ukT = G;

dG1dx1 = 2*x1*m1^2*[u11/(T)]*v110 + x3*m1*m2*[u13/(T)]*v130 +
x2*m2*m1*[u21/(T)]*v210 + x3*m3*m1*[u31/(T)]*v310;
dG1dx2 = x1*m1*m2*[u12/(T)]*v120 + x1*m1*m2*[u21/(T)]*v210 +
2*x2*m2^2*[u22/(T)]*v220 + x3*m2*m3*[u23/(T)]*v230;
dG1dx3 = x1*m1*m3*[u13/(T)]*v130 + x2*m3*m2*[u32/(T)]*v320 +
x1*m3*m1*[u31/(T)]*v310  + 2*x3*m3^2*[u33/(T)]*v330;

dG2dx1 = 2*x1*m1^2*v110 + x2*m1*m2*v120 + x3*m1*m3*v130 + x2*m2*m1*v210
+ x3*m3*m1*v310;
dG2dx2 = x1*m1*m2*v120 + x1*m2*m1*v210 + 2*x2*m2^2*v220 + x3*m2*m3*v230
+ x3*m3*m2*v320;
dG2dx3 = x1*m1*m3*v130 + x2*m2*m3*v230 + 2*x3*m3^2*v330 + x1*m3*m1*v310
+ x2*m3*m2*v320;

dGdx1 = (G2*dG1dx1 - G1*dG2dx1)/(G2^2);
dGdx2 = (G2*dG1dx2 - G1*dG2dx2)/(G2^2);
dGdx3 = (G2*dG1dx3 - G1*dG2dx3)/(G2^2);

dukTdx1 = dGdx1;
dukTdx2 = dGdx2;
dukTdx3 = dGdx3;

dIdx1 = dz3dx1;
dIdx2 = dz3dx2;
dIdx3 = dz3dx3;

D11 = -8.8043;
D12 = 4.16462;
D13 = -48.203;
D14 = 140.436;
D15 = -195.23;
D16 = 113.515;
D17 = 0.0;
D18 = 0.0;
D19 = 0.0;
D21 = 2.9396;
D22 = -6.086;
D23 = 40.137;
D24 = -76.23;
D25 = -133.70;
```

Appendix D (Continued):

```
D26 = 860.25;
D27 = -1535.32;
D28 = 1221.42;
D29 = -409.10;
D31 = -2.8225;
D32 = 4.7600;
D33 = 11.257;
D34 = -66.38;
D35 = 69.248;
D36 = 0.0;
D37 = 0.0;
D38 = 0.0;
D39 = 0.0;
D41 = 0.34;
D42 = -3.187;
D43 = 12.231;
D44 = -12.11;
D45 = 0.0;
D46 = 0.0;
D47 = 0.0;
D48 = 0.0;
D49 = 0.0;
Att11 = D11*[ukT]*[I/Tau];
Att12 = D12*[ukT]*[I/Tau]^2;
Att13 = D13*[ukT]*[I/Tau]^3;
Att14 = D14*[ukT]*[I/Tau]^4;
Att15 = D15*[ukT]*[I/Tau]^5;
Att16 = D16*[ukT]*[I/Tau]^6;
Att17 = D17*[ukT]*[I/Tau]^7;
Att18 = D18*[ukT]*[I/Tau]^8;
Att19 = D19*[ukT]*[I/Tau]^9;

dAtt11dx1 = D11*((dukTdx1)*(I/Tau) +   (ukT)*(1)*(dIdx1/Tau));
dAtt12dx1 = D12*((dukTdx1)*(I/Tau)^2 + (ukT)*2*(I/Tau)^1*(dIdx1/Tau));
dAtt13dx1 = D13*((dukTdx1)*(I/Tau)^3 + (ukT)*3*(I/Tau)^2*(dIdx1/Tau));
dAtt14dx1 = D14*((dukTdx1)*(I/Tau)^4 + (ukT)*4*(I/Tau)^3*(dIdx1/Tau));
dAtt15dx1 = D15*((dukTdx1)*(I/Tau)^5 + (ukT)*5*(I/Tau)^4*(dIdx1/Tau));
dAtt16dx1 = D16*((dukTdx1)*(I/Tau)^6 + (ukT)*6*(I/Tau)^5*(dIdx1/Tau));
dAtt17dx1 = D17*((dukTdx1)*(I/Tau)^7 + (ukT)*7*(I/Tau)^6*(dIdx1/Tau));
dAtt18dx1 = D18*((dukTdx1)*(I/Tau)^8 + (ukT)*8*(I/Tau)^7*(dIdx1/Tau));
dAtt19dx1 = D19*((dukTdx1)*(I/Tau)^9 + (ukT)*9*(I/Tau)^8*(dIdx1/Tau));

dAtt11dx2 = D11*((dukTdx2)*(I/Tau)   + (ukT)*(1)*(dIdx2/Tau));
dAtt12dx2 = D12*((dukTdx2)*(I/Tau)^2 + (ukT)*2*(I/Tau)^1*(dIdx2/Tau));
dAtt13dx2 = D13*((dukTdx2)*(I/Tau)^3 + (ukT)*3*(I/Tau)^2*(dIdx2/Tau));
dAtt14dx2 = D14*((dukTdx2)*(I/Tau)^4 + (ukT)*4*(I/Tau)^3*(dIdx2/Tau));
dAtt15dx2 = D15*((dukTdx2)*(I/Tau)^5 + (ukT)*5*(I/Tau)^4*(dIdx2/Tau));
dAtt16dx2 = D16*((dukTdx2)*(I/Tau)^6 + (ukT)*6*(I/Tau)^5*(dIdx2/Tau));
dAtt17dx2 = D17*((dukTdx2)*(I/Tau)^7 + (ukT)*7*(I/Tau)^6*(dIdx2/Tau));
dAtt18dx2 = D18*((dukTdx2)*(I/Tau)^8 + (ukT)*8*(I/Tau)^7*(dIdx2/Tau));
dAtt19dx2 = D19*((dukTdx2)*(I/Tau)^9 + (ukT)*9*(I/Tau)^8*(dIdx2/Tau));
```

Appendix D (Continued):

```
dAtt11dx3 = D11*((dukTdx3)*(I/Tau)   + (ukT)*(1)*(dIdx3/Tau));
dAtt12dx3 = D12*((dukTdx3)*(I/Tau)^2 + (ukT)*2*(I/Tau)^1*(dIdx3/Tau));
dAtt13dx3 = D13*((dukTdx3)*(I/Tau)^3 + (ukT)*3*(I/Tau)^2*(dIdx3/Tau));
dAtt14dx3 = D14*((dukTdx3)*(I/Tau)^4 + (ukT)*4*(I/Tau)^3*(dIdx3/Tau));
dAtt15dx3 = D15*((dukTdx3)*(I/Tau)^5 + (ukT)*5*(I/Tau)^4*(dIdx3/Tau));
dAtt16dx3 = D16*((dukTdx3)*(I/Tau)^6 + (ukT)*6*(I/Tau)^5*(dIdx3/Tau));
dAtt17dx3 = D17*((dukTdx3)*(I/Tau)^7 + (ukT)*7*(I/Tau)^6*(dIdx3/Tau));
dAtt18dx3 = D18*((dukTdx3)*(I/Tau)^8 + (ukT)*8*(I/Tau)^7*(dIdx3/Tau));
dAtt19dx3 = D19*((dukTdx3)*(I/Tau)^9 + (ukT)*9*(I/Tau)^8*(dIdx3/Tau));

Att21 = D21*[ukT]^2*[I/Tau];
Att22 = D22*[ukT]^2*[I/Tau]^2;
Att23 = D23*[ukT]^2*[I/Tau]^3;
Att24 = D24*[ukT]^2*[I/Tau]^4;
Att25 = D25*[ukT]^2*[I/Tau]^5;
Att26 = D26*[ukT]^2*[I/Tau]^6;
Att27 = D27*[ukT]^2*[I/Tau]^7;
Att28 = D28*[ukT]^2*[I/Tau]^8;
Att29 = D29*[ukT]^2*[I/Tau]^9;

dAtt21dx1 = D21*(2*(ukT)*(dukTdx1)*(I/Tau) + (ukT)^2*(1)*(dIdx1/Tau));
dAtt22dx1 = D22*(2*(ukT)*(dukTdx1)*(I/Tau)^2 +
(ukT)^2*2*(I/Tau)^1*(dIdx1/Tau));
dAtt23dx1 = D23*(2*(ukT)*(dukTdx1)*(I/Tau)^3 +
(ukT)^2*3*(I/Tau)^2*(dIdx1/Tau));
dAtt24dx1 = D24*(2*(ukT)*(dukTdx1)*(I/Tau)^4 +
(ukT)^2*4*(I/Tau)^3*(dIdx1/Tau));
dAtt25dx1 = D25*(2*(ukT)*(dukTdx1)*(I/Tau)^5 +
(ukT)^2*5*(I/Tau)^4*(dIdx1/Tau));
dAtt26dx1 = D26*(2*(ukT)*(dukTdx1)*(I/Tau)^6 +
(ukT)^2*6*(I/Tau)^5*(dIdx1/Tau));
dAtt27dx1 = D27*(2*(ukT)*(dukTdx1)*(I/Tau)^7 +
(ukT)^2*7*(I/Tau)^6*(dIdx1/Tau));
dAtt28dx1 = D28*(2*(ukT)*(dukTdx1)*(I/Tau)^8 +
(ukT)^2*8*(I/Tau)^7*(dIdx1/Tau));
dAtt29dx1 = D29*(2*(ukT)*(dukTdx1)*(I/Tau)^9 +
(ukT)^2*9*(I/Tau)^8*(dIdx1/Tau));

dAtt21dx2 = D21*(2*(ukT)*(dukTdx2)*(I/Tau) + (ukT)^2*(1)*(dIdx2/Tau));
dAtt22dx2 = D22*(2*(ukT)*(dukTdx2)*(I/Tau)^2 +
(ukT)^2*2*(I/Tau)^1*(dIdx2/Tau));
dAtt23dx2 = D23*(2*(ukT)*(dukTdx2)*(I/Tau)^3 +
(ukT)^2*3*(I/Tau)^2*(dIdx2/Tau));
dAtt24dx2 = D24*(2*(ukT)*(dukTdx2)*(I/Tau)^4 +
(ukT)^2*4*(I/Tau)^3*(dIdx2/Tau));
dAtt25dx2 = D25*(2*(ukT)*(dukTdx2)*(I/Tau)^5 +
(ukT)^2*5*(I/Tau)^4*(dIdx2/Tau));
dAtt26dx2 = D26*(2*(ukT)*(dukTdx2)*(I/Tau)^6 +
(ukT)^2*6*(I/Tau)^5*(dIdx2/Tau));
dAtt27dx2 = D27*(2*(ukT)*(dukTdx2)*(I/Tau)^7 +
(ukT)^2*7*(I/Tau)^6*(dIdx2/Tau));
```

Appendix D (Continued):

```
dAtt28dx2 = D28*(2*(ukT)*(dukTdx2)*(I/Tau)^8 +
(ukT)^2*8*(I/Tau)^7*(dIdx2/Tau));
dAtt29dx2 = D29*(2*(ukT)*(dukTdx2)*(I/Tau)^9 +
(ukT)^2*9*(I/Tau)^8*(dIdx2/Tau));

dAtt21dx3 = D21*(2*(ukT)*(dukTdx3)*(I/Tau) + (ukT)^2*(1)*(dIdx3/Tau));
dAtt22dx3 = D22*(2*(ukT)*(dukTdx3)*(I/Tau)^2 +
(ukT)^2*2*(I/Tau)^1*(dIdx3/Tau));
dAtt23dx3 = D23*(2*(ukT)*(dukTdx3)*(I/Tau)^3 +
(ukT)^2*3*(I/Tau)^2*(dIdx3/Tau));
dAtt24dx3 = D24*(2*(ukT)*(dukTdx3)*(I/Tau)^4 +
(ukT)^2*4*(I/Tau)^3*(dIdx3/Tau));
dAtt25dx3 = D25*(2*(ukT)*(dukTdx3)*(I/Tau)^5 +
(ukT)^2*5*(I/Tau)^4*(dIdx3/Tau));
dAtt26dx3 = D26*(2*(ukT)*(dukTdx3)*(I/Tau)^6 +
(ukT)^2*6*(I/Tau)^5*(dIdx3/Tau));
dAtt27dx3 = D27*(2*(ukT)*(dukTdx3)*(I/Tau)^7 +
(ukT)^2*7*(I/Tau)^6*(dIdx3/Tau));
dAtt28dx3 = D28*(2*(ukT)*(dukTdx3)*(I/Tau)^8 +
(ukT)^2*8*(I/Tau)^7*(dIdx3/Tau));
dAtt29dx3 = D29*(2*(ukT)*(dukTdx3)*(I/Tau)^9 +
(ukT)^2*9*(I/Tau)^8*(dIdx3/Tau));

Att31 = 1*D31*[ukT]^3*[I/Tau];
Att32 = 2*D32*[ukT]^3*[I/Tau]^2;
Att33 = 3*D33*[ukT]^3*[I/Tau]^3;
Att34 = 4*D34*[ukT]^3*[I/Tau]^4;
Att35 = 5*D35*[ukT]^3*[I/Tau]^5;
Att36 = 6*D36*[ukT]^3*[I/Tau]^6;
Att37 = 7*D37*[ukT]^3*[I/Tau]^7;
Att38 = 8*D38*[ukT]^3*[I/Tau]^8;
Att39 = 9*D39*[ukT]^3*[I/Tau]^9;

dAtt31dx1 = D31*(3*(ukT)^2*(dukTdx1)*(I/Tau) +
(ukT)^3*(1)*(dIdx1/Tau));
dAtt32dx1 = D32*(3*(ukT)^2*(dukTdx1)*(I/Tau)^2 +
(ukT)^3*2*(I/Tau)^1*(dIdx1/Tau));
dAtt33dx1 = D33*(3*(ukT)^2*(dukTdx1)*(I/Tau)^3 +
(ukT)^3*3*(I/Tau)^2*(dIdx1/Tau));
dAtt34dx1 = D34*(3*(ukT)^2*(dukTdx1)*(I/Tau)^4 +
(ukT)^3*4*(I/Tau)^3*(dIdx1/Tau));
dAtt35dx1 = D35*(3*(ukT)^2*(dukTdx1)*(I/Tau)^5 +
(ukT)^3*5*(I/Tau)^4*(dIdx1/Tau));
dAtt36dx1 = D36*(3*(ukT)^2*(dukTdx1)*(I/Tau)^6 +
(ukT)^3*6*(I/Tau)^5*(dIdx1/Tau));
dAtt37dx1 = D37*(3*(ukT)^2*(dukTdx1)*(I/Tau)^7 +
(ukT)^3*7*(I/Tau)^6*(dIdx1/Tau));
dAtt38dx1 = D38*(3*(ukT)^2*(dukTdx1)*(I/Tau)^8 +
(ukT)^3*8*(I/Tau)^7*(dIdx1/Tau));
dAtt39dx1 = D39*(3*(ukT)^2*(dukTdx1)*(I/Tau)^9 +
(ukT)^3*9*(I/Tau)^8*(dIdx1/Tau));
```

Appendix D (Continued):

```
dAtt31dx2 = D31*(3*(ukT)^2*(dukTdx2)*(I/Tau) +
(ukT)^3*(1)*(dIdx2/Tau));
dAtt32dx2 = D32*(3*(ukT)^2*(dukTdx2)*(I/Tau)^2 +
(ukT)^3*2*(I/Tau)^1*(dIdx2/Tau));
dAtt33dx2 = D33*(3*(ukT)^2*(dukTdx2)*(I/Tau)^3 +
(ukT)^3*3*(I/Tau)^2*(dIdx2/Tau));
dAtt34dx2 = D34*(3*(ukT)^2*(dukTdx2)*(I/Tau)^4 +
(ukT)^3*4*(I/Tau)^3*(dIdx2/Tau));
dAtt35dx2 = D35*(3*(ukT)^2*(dukTdx2)*(I/Tau)^5 +
(ukT)^3*5*(I/Tau)^4*(dIdx2/Tau));
dAtt36dx2 = D36*(3*(ukT)^2*(dukTdx2)*(I/Tau)^6 +
(ukT)^3*6*(I/Tau)^5*(dIdx2/Tau));
dAtt37dx2 = D37*(3*(ukT)^2*(dukTdx2)*(I/Tau)^7 +
(ukT)^3*7*(I/Tau)^6*(dIdx2/Tau));
dAtt38dx2 = D38*(3*(ukT)^2*(dukTdx2)*(I/Tau)^8 +
(ukT)^3*8*(I/Tau)^7*(dIdx2/Tau));
dAtt39dx2 = D39*(3*(ukT)^2*(dukTdx2)*(I/Tau)^9 +
(ukT)^3*9*(I/Tau)^8*(dIdx2/Tau));

dAtt31dx3 = D31*(3*(ukT)^2*(dukTdx3)*(I/Tau) +
(ukT)^3*(1)*(dIdx3/Tau));
dAtt32dx3 = D32*(3*(ukT)^2*(dukTdx3)*(I/Tau)^2 +
(ukT)^3*2*(I/Tau)^1*(dIdx3/Tau));
dAtt33dx3 = D33*(3*(ukT)^2*(dukTdx3)*(I/Tau)^3 +
(ukT)^3*3*(I/Tau)^2*(dIdx3/Tau));
dAtt34dx3 = D34*(3*(ukT)^2*(dukTdx3)*(I/Tau)^4 +
(ukT)^3*4*(I/Tau)^3*(dIdx3/Tau));
dAtt35dx3 = D35*(3*(ukT)^2*(dukTdx3)*(I/Tau)^5 +
(ukT)^3*5*(I/Tau)^4*(dIdx3/Tau));
dAtt36dx3 = D36*(3*(ukT)^2*(dukTdx3)*(I/Tau)^6 +
(ukT)^3*6*(I/Tau)^5*(dIdx3/Tau));
dAtt37dx3 = D37*(3*(ukT)^2*(dukTdx3)*(I/Tau)^7 +
(ukT)^3*7*(I/Tau)^6*(dIdx3/Tau));
dAtt38dx3 = D38*(3*(ukT)^2*(dukTdx3)*(I/Tau)^8 +
(ukT)^3*8*(I/Tau)^7*(dIdx3/Tau));
dAtt39dx3 = D39*(3*(ukT)^2*(dukTdx3)*(I/Tau)^9 +
(ukT)^3*9*(I/Tau)^8*(dIdx3/Tau));

Att41 = D41*[ukT]^4*[I/Tau];
Att42 = D42*[ukT]^4*[I/Tau]^2;
Att43 = D43*[ukT]^4*[I/Tau]^3;
Att44 = D44*[ukT]^4*[I/Tau]^4;
Att45 = D45*[ukT]^4*[I/Tau]^5;
Att46 = D46*[ukT]^4*[I/Tau]^6;
Att47 = D47*[ukT]^4*[I/Tau]^7;
Att48 = D48*[ukT]^4*[I/Tau]^8;
Att49 = D49*[ukT]^4*[I/Tau]^9;
```

Appendix D (Continued):

```
dAtt41dx1 = D41*(4*(ukT)^3*(dukTdx1)*(I/Tau) +
(ukT)^4*(1)*(dIdx1/Tau));
dAtt42dx1 = D42*(4*(ukT)^3*(dukTdx1)*(I/Tau)^2 +
(ukT)^4*2*(I/Tau)^1*(dIdx1/Tau));
dAtt43dx1 = D43*(4*(ukT)^3*(dukTdx1)*(I/Tau)^3 +
(ukT)^4*3*(I/Tau)^2*(dIdx1/Tau));
dAtt44dx1 = D44*(4*(ukT)^3*(dukTdx1)*(I/Tau)^4 +
(ukT)^4*4*(I/Tau)^3*(dIdx1/Tau));
dAtt45dx1 = D45*(4*(ukT)^3*(dukTdx1)*(I/Tau)^5 +
(ukT)^4*5*(I/Tau)^4*(dIdx1/Tau));
dAtt46dx1 = D46*(4*(ukT)^3*(dukTdx1)*(I/Tau)^6 +
(ukT)^4*6*(I/Tau)^5*(dIdx1/Tau));
dAtt47dx1 = D47*(4*(ukT)^3*(dukTdx1)*(I/Tau)^7 +
(ukT)^4*7*(I/Tau)^6*(dIdx1/Tau));
dAtt48dx1 = D48*(4*(ukT)^3*(dukTdx1)*(I/Tau)^8 +
(ukT)^4*8*(I/Tau)^7*(dIdx1/Tau));
dAtt49dx1 = D49*(4*(ukT)^3*(dukTdx1)*(I/Tau)^9 +
(ukT)^4*9*(I/Tau)^8*(dIdx1/Tau));

dAtt41dx2 = D41*(4*(ukT)^3*(dukTdx2)*(I/Tau) +
(ukT)^4*(1)*(dIdx2/Tau));
dAtt42dx2 = D42*(4*(ukT)^3*(dukTdx2)*(I/Tau)^2 +
(ukT)^4*2*(I/Tau)^1*(dIdx2/Tau));
dAtt43dx2 = D43*(4*(ukT)^3*(dukTdx2)*(I/Tau)^3 +
(ukT)^4*3*(I/Tau)^2*(dIdx2/Tau));
dAtt44dx2 = D44*(4*(ukT)^3*(dukTdx2)*(I/Tau)^4 +
(ukT)^4*4*(I/Tau)^3*(dIdx2/Tau));
dAtt45dx2 = D45*(4*(ukT)^3*(dukTdx2)*(I/Tau)^5 +
(ukT)^4*5*(I/Tau)^4*(dIdx2/Tau));
dAtt46dx2 = D46*(4*(ukT)^3*(dukTdx2)*(I/Tau)^6 +
(ukT)^4*6*(I/Tau)^5*(dIdx2/Tau));
dAtt47dx2 = D47*(4*(ukT)^3*(dukTdx2)*(I/Tau)^7 +
(ukT)^4*7*(I/Tau)^6*(dIdx2/Tau));
dAtt48dx2 = D48*(4*(ukT)^3*(dukTdx2)*(I/Tau)^8 +
(ukT)^4*8*(I/Tau)^7*(dIdx2/Tau));
dAtt49dx2 = D49*(4*(ukT)^3*(dukTdx2)*(I/Tau)^9 +
(ukT)^4*9*(I/Tau)^8*(dIdx2/Tau));

dAtt41dx3 = D41*(4*(ukT)^3*(dukTdx3)*(I/Tau) +
(ukT)^4*(1)*(dIdx3/Tau));
dAtt42dx3 = D42*(4*(ukT)^3*(dukTdx3)*(I/Tau)^2 +
(ukT)^4*2*(I/Tau)^1*(dIdx3/Tau));
dAtt43dx3 = D43*(4*(ukT)^3*(dukTdx3)*(I/Tau)^3 +
(ukT)^4*3*(I/Tau)^2*(dIdx3/Tau));
dAtt44dx3 = D44*(4*(ukT)^3*(dukTdx3)*(I/Tau)^4 +
(ukT)^4*4*(I/Tau)^3*(dIdx3/Tau));
dAtt45dx3 = D45*(4*(ukT)^3*(dukTdx3)*(I/Tau)^5 +
(ukT)^4*5*(I/Tau)^4*(dIdx3/Tau));
dAtt46dx3 = D46*(4*(ukT)^3*(dukTdx3)*(I/Tau)^6 +
(ukT)^4*6*(I/Tau)^5*(dIdx3/Tau));
```

Appendix D (Continued):

```
dAtt47dx3 = D47*(4*(ukT)^3*(dukTdx3)*(I/Tau)^7 +
(ukT)^4*7*(I/Tau)^6*(dIdx3/Tau));
dAtt48dx3 = D48*(4*(ukT)^3*(dukTdx3)*(I/Tau)^8 +
(ukT)^4*8*(I/Tau)^7*(dIdx3/Tau));
dAtt49dx3 = D49*(4*(ukT)^3*(dukTdx3)*(I/Tau)^9 +
(ukT)^4*9*(I/Tau)^8*(dIdx3/Tau));

Att1 = Att11 + Att12 + Att13 + Att14 + Att15 +  Att16 +  Att17 +  Att18
+  Att19 ; %
Att2 = Att21 + Att22 + Att23 + Att24 + Att25 +  Att26 +  Att27 +  Att28
+  Att29 ; %
Att3 = Att31 + Att32 + Att33 + Att34 + Att35 +  Att36 +  Att37 +  Att38
+  Att39 ;
Att4 = Att41 + Att42 + Att43 + Att44 + Att45 +  Att46 +  Att47 +  Att48
+  Att49 ;

dAtt1dx1 = dAtt11dx1 + dAtt12dx1 + dAtt13dx1 + dAtt14dx1 + dAtt15dx1 +
dAtt16dx1 +  dAtt17dx1 +  dAtt18dx1 +  dAtt19dx1 ;
dAtt2dx1 = dAtt21dx1 + dAtt22dx1 + dAtt23dx1 + dAtt24dx1 + dAtt25dx1 +
dAtt26dx1 +  dAtt27dx1 +  dAtt28dx1 +  dAtt29dx1 ;
dAtt3dx1 = dAtt31dx1 + dAtt32dx1 + dAtt33dx1 + dAtt34dx1 + dAtt35dx1 +
dAtt36dx1 +  dAtt37dx1 +  dAtt38dx1 +  dAtt39dx1 ;
dAtt4dx1 = dAtt41dx1 + dAtt42dx1 + dAtt43dx1 + dAtt44dx1 + dAtt45dx1 +
dAtt46dx1 +  dAtt47dx1 +  dAtt48dx1 +  dAtt49dx1 ;

dAtt1dx2 = dAtt11dx2 + dAtt12dx2 + dAtt13dx2 + dAtt14dx2 + dAtt15dx2 +
dAtt16dx2 +  dAtt17dx2 +  dAtt18dx2 +  dAtt19dx2 ;
dAtt2dx2 = dAtt21dx2 + dAtt22dx2 + dAtt23dx2 + dAtt24dx2 + dAtt25dx2 +
dAtt26dx2 +  dAtt27dx2 +  dAtt28dx2 +  dAtt29dx2 ;
dAtt3dx2 = dAtt31dx2 + dAtt32dx2 + dAtt33dx2 + dAtt34dx2 + dAtt35dx2 +
dAtt36dx2 +  dAtt37dx2 +  dAtt38dx2 +  dAtt39dx2 ;
dAtt4dx2 = dAtt41dx2 + dAtt42dx2 + dAtt43dx2 + dAtt44dx2 + dAtt45dx2 +
dAtt46dx2 +  dAtt47dx2 +  dAtt48dx2 +  dAtt49dx2 ;

dAtt1dx3 = dAtt11dx3 + dAtt12dx3 + dAtt13dx3 + dAtt14dx3 + dAtt15dx3 +
dAtt16dx3 +  dAtt17dx3 +  dAtt18dx3 +  dAtt19dx3 ;
dAtt2dx3 = dAtt21dx3 + dAtt22dx3 + dAtt23dx3 + dAtt24dx3 + dAtt25dx3 +
dAtt26dx3 +  dAtt27dx3 +  dAtt28dx3 +  dAtt29dx3 ;
dAtt3dx3 = dAtt31dx3 + dAtt32dx3 + dAtt33dx3 + dAtt34dx3 + dAtt35dx3 +
dAtt36dx3 +  dAtt37dx3 +  dAtt38dx3 +  dAtt39dx3 ;
dAtt4dx3 = dAtt41dx3 + dAtt42dx3 + dAtt43dx3 + dAtt44dx3 + dAtt45dx3 +
dAtt46dx3 +  dAtt47dx3 +  dAtt48dx3 +  dAtt49dx3 ;

a0dispRT = (Att1 + Att2 + Att3 + Att4) ; %
a0hsRT = (4*I - 3*I^2)/(1-I)^2; %
N = a0hsRT + a0dispRT ;   %
asegRT = m * N; %
achainRT = (1-m)*log((1-0.5*I)/(1-I)^3); %
U = asegRT + achainRT ; %
J = Z - 1;
```

Appendix D (Continued):

```
NNN1 = dAtt1dx1 + dAtt2dx1 + dAtt3dx1 + dAtt4dx1;
NNN2 = dAtt1dx2 + dAtt2dx2 + dAtt3dx2 + dAtt4dx2;
NNN3 = dAtt1dx3 + dAtt2dx3 + dAtt3dx3 + dAtt4dx3;

KKK1 = (-dmdx1)*log((1-0.5*I)/(1-I)^3) + (1-m)*[(1-I)^3/(1-0.5*I)]*[(-
0.5*(1-I)^3*dIdx1 - 3*(1-0.5*I)*(1-I)^2*(-dIdx1))/(1-0.5*I)^2] ;
KKK2 = (-dmdx2)*log((1-0.5*I)/(1-I)^3) + (1-m)*[(1-I)^3/(1-0.5*I)]*[(-
0.5*(1-I)^3*dIdx2 - 3*(1-0.5*I)*(1-I)^2*(-dIdx2))/(1-0.5*I)^2] ;
KKK3 = (-dmdx3)*log((1-0.5*I)/(1-I)^3) + (1-m)*[(1-I)^3/(1-0.5*I)]*[(-
0.5*(1-I)^3*dIdx3 - 3*(1-0.5*I)*(1-I)^2*(-dIdx3))/(1-0.5*I)^2] ;

NN1 = ((1-I)^2*(4*dIdx1 - 6*I*dIdx1) - ((4*I-3*I^2)*2*(1-I)*(-
dIdx1)))/(1-I)^4;
NN2 = ((1-I)^2*(4*dIdx2 - 6*I*dIdx2) - ((4*I-3*I^2)*2*(1-I)*(-
dIdx2)))/(1-I)^4;
NN3 = ((1-I)^2*(4*dIdx3 - 6*I*dIdx3) - ((4*I-3*I^2)*2*(1-I)*(-
dIdx3)))/(1-I)^4;

N1 = NN1 + NNN1 ;
N2 = NN2 + NNN2 ;
N3 = NN3 + NNN3 ;

KK1 = dmdx1 * N + m * N1;
KK2 = dmdx2 * N + m * N2;
KK3 = dmdx3 * N + m * N3;

K1 = KK1 + KKK1 ;
K2 = KK2 + KKK2 ;
K3 = KK3 + KKK3 ;
L = U + J + K1 - (x1*K1  + x2* K2  + x3* K3);
PHI3 = exp(L);
T = [PHI3];

End of SAFT code.
```

Appendix E: Hand Calculation of Pure Component Parameters and Solubility Data or the PMMA-$CO_2$-MMA System

Here is an Example of hand calculation of the pure component properties for the experimental Sample #1128, at T=333.15 K. The sublimation pressure of the polymer is temperature dependant, and is calculated using the following equation:

$$P_3^{sub} = \frac{10^{\left(A-\frac{B}{T}\right)}}{10^3}$$

Sample hand-calculation of the sublimation pressure is performed by substituting the working temperature and the appropriate coefficients in the above equation. The coefficients for poly(methyl methacrylate) are given as:

A=14.631;

B=4873.4;

Therefore, to calculate $P^{sub}$ at T = 333.15 K:

$$P^{sub} = \frac{10^{\left(A-\frac{B}{T}\right)}}{1000} = \frac{10^{\left(14.631-\frac{4873.4}{333.15}\right)}}{1000} = \frac{10^{(14.631-14.628)}}{1000} = \frac{10^{0.003}}{1000} = 1.0069E-03 = 0.001\ (bar)$$

The fugacity coefficient of the supercritical fluid, which is a function of composition, temperature and pressure, is calculated using the SAFT code, by substituting the appropriate values for molar fractions of $CO_2$, methyl methacrylate, and poly(methyl methacrylate), followed by the appropriate working temperature and pressure. The software will give fugacity output for the given conditions.

Appendix E (Continued):

For example, for Sample #1128 of this experiment, the composition is:

$x_1$ = 0.723 mol fraction $CO_2$

$x_2$ = 0.277 mol fraction MMA

$x_3$ = 1.56 x $10^{-5}$ mol fraction PMMA

Performing the calculation at T = 333.15 K, and P = 275.83 bar, (the cloud-point at 75.5°C), the SAFT code gives the appropriate fugacity coefficient:

φ = SOFINAL(x1, x2, x3, T, P)

φ = SOFINAL(0.723, 0.277, 1.56E-05, 333.15, 275.83)

φ = 0.2172

The Solubility equation is given as

$$y_A = \frac{P_A^{sub}}{P}\frac{1}{\hat{\varphi}_A^V}\exp\left[\frac{V_A^s}{RT}\left(P - P_A^{sub}\right)\right]$$

Substituting the sublimation pressure, and the fugacity coefficient in the solubility equation, together with the appropriate pressure and temperature conditions, gives:

$$y_A = \frac{0.001}{275.83}\frac{1}{0.2172}\exp\left[\frac{136.80}{83.1451\times 333.15}\left(275.83 - 0.001\right)\right] =$$

$$y_A = 1.66916\times 10^{-5}\exp(1.3622272)$$

$$y_A = 6.518\times 10^{-5}$$

Repeating this calculation procedure for all samples, and for all corresponding P-T cloud-points, we can calculate the solubility of PMMA for every combination of composition, pressure and temperature. The results are listed in Table 4.3.

Appendix F: MATLAB Program for Regression of Experimental Data

```
echo off; clc;
%-------------------------------------------------------------
% Algorithm:  (Least Squares Polynomial).
% Scope:    Curve Fitting of Experimental Data
%-------------------------------------------------------------
clc; clear all; format long e;
% - - - - - - - - - - - - - - - - - - - - - - - - - - - - - - -
%
% This program finds the least squares polynomial Pm(x),
% given a set of data points
% { (x , y ), (x , y ) ,..., (x , y ) }.
%    1   1     2   2          n   n
%
% The abscissas and ordinates are stored in X and Y,
% respectively.
%
% X = [x , x  ,..., x ];  Y = [y , y  ,..., y ];
%       1   2        n          1   2        n
%
% Note: lspoly.m is used for A.2.(Least Squares Polynomial)

pause % Press any key to continue.

clc;
% - - - - - - - - - - - - - - - - - - - - - - - - - - - - - - -
% Example: Find the least squares quadratic polynomial.
%
% Enter the abscissas for the points in  X.
%
% Enter the ordinates for the points in  Y.
%
% Enter the degree of the polynomial in  m.
% -------------------------------------------------------------
% Y = Pressure (bar)
% X = Mole fraction of MMA
%~~~~~~~~~~~~~~~~~~~~~~~~~~~~~~~~~~~~~~~~~~~~~~~~~~~~~~~~~~~~~~
```

Appendix F (Continued):

```
% fit1:(T=40°C)Experimental results obtained in this work

X1=[0.005 0.044 0.048 0.091 0.16  0.193 0.337 0.449  1];
Y1=[86.00 86.93 86.90 86.04 78.78 78.60 66.33 58.03  0];

m = 3;

C1 = lspoly(X1,Y1,m)';

pause % Press any key to find the least squares polynomial.

clc;

% ~ ~ ~ ~ ~ ~ ~ ~ ~ ~ ~ ~
% Prepare graphics arrays
% ~ ~ ~ ~ ~ ~ ~ ~ ~ ~ ~ ~
a = 0;
b = 1;
h = (b-a)/500;
Xs1 = a:h:b;
Ys1 = polyval(C1,Xs1);

clc; figure(1); clf;

%~~~~~~~~~~~~~~~~~~~~~~
% Begin graphics section
%~~~~~~~~~~~~~~~~~~~~~~
a = 0;
b =  1;
c =  0;
d =  120;
whitebg('w');
plot([a b],[0 0],'b',[0 0],[c d],'b');
axis([a b c d]);
axis(axis);
hold on;
plot(X1,Y1,'or',Xs1,Ys1,'-g');
xlabel('x');
xlabel('Mole fraction of MMA');
ylabel('Pressure (bar)');
Mx1 = 'Least squares polynomial: y = P';
Mx2 = [Mx1,num2str(m),'(x).'];
```

Appendix F (Continued):

```
title('Experimental isotherm for the MMA-CO2 system
obtained in this study at 40°C');
grid off;
hold off;
figure(gcf); pause % Press any key to continue.

points1 = [X1;Y1];

clc; format long e;

%.........................................
% Begin section to print the results.
% Diary commands are included which write all
% the results to the Matlab textfile   output
%.........................................

Mx1='y = P(x) = c(1)x^m + c(2)x^m-1 +...+ c(m)x + c(m+1)';
Mx2=['A polynomial of degree m = ',num2str(m),' has been
fit.'];
Mx3='The coefficients are stored in the array  C = ';
clc,echo off,diary output,...
disp(''),disp(Mx1),disp(Mx2),disp(Mx3),...
disp(''),disp(C1'),disp('The given x-y points:'),...
disp('      x         y'),disp(points1'),diary off,echo on
pause % Press any key to analyze the results.
% .. .. .. .. ..
% Prepare results
% .. .. .. .. ..

points2 = [X1;Y1;polyval(C1,X1);Y1-polyval(C1,X1)]';

clc; format short;
%.........................................
% Begin section to print the results.
% Diary commands are included which write all
% the results to the Matlab textfile   output
%.........................................

Mx4='    x(k)      y(k)      P(x(k))   error';
clc,echo off,diary output,...
disp(''),disp(Mx4),disp(points2),diary off,echo on
%~~~~~~~~~~~~~~~~~~~~~~~~~~~~~~~~~~~~~~~~~~~~~~~~~~~~~~~~~~~~~~~~
```

Appendix F (Continued):

```
%fit2:(T=80°C)Experimental results obtained in this work

X2=[  0.091      0.337    0.60     1];
Y2=[119.30     100.40    60.00     0];

m = 3;

C2 = lspoly(X2,Y2,m)';

pause % Press any key to find the least squares polynomial.

clc;

% ~ ~ ~ ~ ~ ~ ~ ~ ~ ~ ~ ~
% Prepare graphics arrays
% ~ ~ ~ ~ ~ ~ ~ ~ ~ ~ ~ ~
a = 0.1;
b = 1;
h = (b-a)/500;
Xs2 = a:h:b;
Ys2 = polyval(C2,Xs2);

clc; figure(1); clf;

%~~~~~~~~~~~~~~~~~~~~~~
% Begin graphics section
%~~~~~~~~~~~~~~~~~~~~~~
a = 0.1;
b =  1;
c =  0;
d =  120;
whitebg('w');
plot([a b],[0 0],'b',[0 0],[c d],'b');
axis([a b c d]);
axis(axis);
hold on;
plot(X2,Y2,'or',Xs2,Ys2,'-g');
xlabel('x');
xlabel('Mole fraction of MMA');
ylabel('Pressure (bar)');
Mx1 = 'Least squares polynomial: y = P';
Mx2 = [Mx1,num2str(m),'(x).'];
```

```
title('Experimental isotherms for the MMA-CO2 system
obtained in this study at 80°C');
grid off;
hold off;
figure(gcf); pause % Press any key to continue.

points1 = [X2;Y2];

clc; format long e;
%.........................................
% Begin section to print the results.
% Diary commands are included which write all
% the results to the Matlab textfile   output
%.........................................

Mx1='y = P(x) = c(1)x^m + c(2)x^m-1 +...+ c(m)x + c(m+1)';
Mx2=['A polynomial of degree m = ',num2str(m),' has been
fit.'];
Mx3='The coefficients are stored in the array  C = ';
clc,echo off,diary output,...
disp(''),disp(Mx1),disp(Mx2),disp(Mx3),...
disp(''),disp(C2'),disp('The given x-y points:'),...
disp('      x         y'),disp(points1'),diary off,echo on

pause % Press any key to analyze the results.
% .. .. .. .. ..
% Prepare results
% .. .. .. .. ..

points2 = [X2;Y2;polyval(C2,X2);Y2-polyval(C2,X2)]';

clc; format short;
%.........................................
% Begin section to print the results.
% Diary commands are included which write all
% the results to the Matlab textfile   output
%.........................................
Mx4='    x(k)      y(k)      P(x(k))   error';
clc,echo off,diary output,...
disp(''),disp(Mx4),disp(points2),diary off,echo on
%~~~~~~~~~~~~~~~~~~~~~~~~~~~~~~~~~~~~~~~~~~~~~~~~~~~~~~~~~~~~~~~~
```

Appendix F (Continued):

```
%fit3:(T=105.5°C)Experimental results obtained in this work

X3=[ 0.110      0.175     0.360  0.650   1];
Y3=[141.34     144.10    114.45  55.16    0];

m = 3;

C3 = lspoly(X3,Y3,m)';

pause % Press any key to find the least squares polynomial.

clc;

% ~ ~ ~ ~ ~ ~ ~ ~ ~ ~ ~ ~
% Prepare graphics arrays
% ~ ~ ~ ~ ~ ~ ~ ~ ~ ~ ~ ~
a = 0;
b = 1;
h = (b-a)/500;
Xs3 = a:h:b;
Ys3 = polyval(C3,Xs3);

clc; figure(1); clf;

%~~~~~~~~~~~~~~~~~~~~~~~
% Begin graphics section
%~~~~~~~~~~~~~~~~~~~~~~~
a = 0;
b =  1;
c =  0;
d =  120;
whitebg('w');
plot([a b],[0 0],'b',[0 0],[c d],'b');
axis([a b c d]);
axis(axis);
hold on;
plot(X3,Y3,'or',Xs3,Ys3,'-g');
xlabel('x');
xlabel('Mole fraction of MMA');
ylabel('Pressure (bar)');
Mx1 = 'Least squares polynomial: y = P';
Mx2 = [Mx1,num2str(m),'(x).'];
```

```
title('Experimental isotherms for the MMA-CO2 system
obtained in this study at 105.5°C');
grid off;
hold off;
figure(gcf); pause % Press any key to continue.

points1 = [X3;Y3];

clc; format long e;

%.........................................
% Begin section to print the results.
% Diary commands are included which write all
% the results to the Matlab textfile   output
%.........................................

Mx1='y = P(x) = c(1)x^m + c(2)x^m-1 +...+ c(m)x + c(m+1)';
Mx2=['A polynomial of degree m = ',num2str(m),' has been
fit.'];
Mx3='The coefficients are stored in the array  C = ';
clc,echo off,diary output,...
disp(''),disp(Mx1),disp(Mx2),disp(Mx3),...
disp(''),disp(C3'),disp('The given x-y points:'),...
disp('      x         y'),disp(points1'),diary off,echo on
pause % Press any key to analyze the results.
% .. .. .. .. ..
% Prepare results
% .. .. .. .. ..

points2 = [X3;Y3;polyval(C3,X3);Y3-polyval(C3,X3)]';

clc; format short;
%.........................................
% Begin section to print the results.
% Diary commands are included which write all
% the results to the Matlab textfile   output
%.........................................
Mx4='    x(k)      y(k)      P(x(k))   error';
clc,echo off,diary output,...
disp(''),disp(Mx4),disp(points2),diary off,echo on
%~~~~~~~~~~~~~~~~~~~~~~~~~~~~~~~~~~~~~~~~~~~~~~~~~~~~~~~~~~~~
```

```
%fit4:(T=40°C)Published results by McHugh et al(1999)
% in Fluid Phase Equilibria

X4=[0.010  0.039  0.051  0.071   0.1    0.206    0.244
0.301    0.339   0.343   0.509  0.704   1];
Y4=[77.2   78.2   76.9   74.8   71.7    58.3     54.5
49.3      46.5    45.8    27.2  11.4    0];

m = 3;
C4 = lspoly(X4,Y4,m)';

pause % Press any key to find the least squares polynomial.

clc;

% ~ ~ ~ ~ ~ ~ ~ ~ ~ ~ ~ ~
% Prepare graphics arrays
% ~ ~ ~ ~ ~ ~ ~ ~ ~ ~ ~ ~
a = 0.0;
b = 1;
h = (b-a)/500;
Xs4 = a:h:b;
Ys4 = polyval(C4,Xs4);

clc; figure(1); clf;

%~~~~~~~~~~~~~~~~~~~~~~
% Begin graphics section
%~~~~~~~~~~~~~~~~~~~~~~
a = 0.07;
b =  1;
c =  0;
d =  120;
whitebg('w');

plot([a b],[0 0],'b',[0 0],[c d],'b');
axis([a b c d]);
axis(axis);
hold on;
plot(X4,Y4,'or',Xs4,Ys4,'-g');
xlabel('x');
xlabel('Mole fraction of MMA');
```

```
ylabel('Pressure (bar)');
Mx1 = 'Least squares polynomial: y = P';
Mx2 = [Mx1,num2str(m),'(x).'];
title('Experimental isotherms for the MMA-CO2 system as per
McHugh at 40°C');
grid off;
hold off;
figure(gcf); pause % Press any key to continue.

points1 = [X4;Y4];

clc; format long e;
%.............................................
% Begin section to print the results.
% Diary commands are included which write all
% the results to the Matlab textfile   output
%.............................................
Mx1='y = P(x) = c(1)x^m + c(2)x^m-1 +...+ c(m)x + c(m+1)';
Mx2=['A polynomial of degree m = ',num2str(m),' has been
fit.'];
Mx3='The coefficients are stored in the array  C = ';
clc,echo off,diary output,...
disp(''),disp(Mx1),disp(Mx2),disp(Mx3),...
disp(''),disp(C4'),disp('The given x-y points:'),...
disp('      x         y'),disp(points1'),diary off,echo on

pause % Press any key to analyze the results.
% .. .. .. .. ..
% Prepare results
% .. .. .. .. ..
points2 = [X4;Y4;polyval(C4,X4);Y4-polyval(C4,X4)]';

clc; format short;
%.............................................
% Begin section to print the results.
% Diary commands are included which write all
% the results to the Matlab textfile   output
%.............................................
Mx4='    x(k)      y(k)      P(x(k))   error';
clc,echo off,diary output,...
disp(''),disp(Mx4),disp(points2),diary off,echo on
%~~~~~~~~~~~~~~~~~~~~~~~~~~~~~~~~~~~~~~~~~~~~~~~~~~~~~~~~~~~~~~~~
```

```
%fit5:(T=80°C)Published results by McHugh et al(1999)Fluid
Phase Equilibria

X5=[0.05  0.072  0.098  0.205  0.236  0.281  0.339  0.392
0.483  1];
Y5=[116.9 117.9  118.2  94.4   87.9   77.9   66.5   60.7
44.1   0];

m = 2;

C5 = lspoly(X5,Y5,m)';

pause % Press any key to find the least squares polynomial.

clc;

% ~ ~ ~ ~ ~ ~ ~ ~ ~ ~ ~ ~ ~
% Prepare graphics arrays
% ~ ~ ~ ~ ~ ~ ~ ~ ~ ~ ~ ~ ~
a = 0.07;
b = 1;
h = (b-a)/500;
Xs5 = a:h:b;
Ys5 = polyval(C5,Xs5);

clc; figure(1); clf;

%~~~~~~~~~~~~~~~~~~~~~~
% Begin graphics section
%~~~~~~~~~~~~~~~~~~~~~~
a = 0.07;
b =  1;
c =  0;
d =  120;
whitebg('w');
plot([a b],[0 0],'b',[0 0],[c d],'b');
axis([a b c d]);
axis(axis);
hold on;
plot(X5,Y5,'or',Xs5,Ys5,'-g');
xlabel('x');
xlabel('Mole fraction of MMA');
```

```
ylabel('Pressure (bar)');
Mx1 = 'Least squares polynomial: y = P';
Mx2 = [Mx1,num2str(m),'(x).'];
title('Experimental isotherms for the MMA-CO2 system as per
McHugh at 80°C');
grid off;
hold off;
figure(gcf); pause % Press any key to continue.

points1 = [X5;Y5];

clc; format long e;
%.........................................
% Begin section to print the results.
% Diary commands are included which write all
% the results to the Matlab textfile   output
%.........................................

Mx1='y = P(x) = c(1)x^m + c(2)x^m-1 +...+ c(m)x + c(m+1)';
Mx2=['A polynomial of degree m = ',num2str(m),' has been
fit.'];
Mx3='The coefficients are stored in the array  C = ';
clc,echo off,diary output,...
disp(''),disp(Mx1),disp(Mx2),disp(Mx3),...
disp(''),disp(C5'),disp('The given x-y points:'),...
disp('      x         y'),disp(points1'),diary off,echo on
pause % Press any key to analyze the results.
% .. .. .. .. ..
% Prepare results
% .. .. .. .. ..
points2 = [X5;Y5;polyval(C5,X5);Y5-polyval(C5,X5)]';

clc; format short;
%.........................................
% Begin section to print the results.
% Diary commands are included which write all
% the results to the Matlab textfile   output
%.........................................
Mx4='    x(k)      y(k)      P(x(k))   error';
clc,echo off,diary output,...
disp(''),disp(Mx4),disp(points2),diary off,echo on
%~~~~~~~~~~~~~~~~~~~~~~~~~~~~~~~~~~~~~~~~~~~~~~~~~~~~~~~~~~~~~~~
```

```
%fit6:(T=105.5°C)Published results by McHugh et
al(1999)Fluid Phase Equilibria

X6=[0.065  0.089  0.126  0.153  0.232  0.291  0.386  0.480
0.622  0.790   1];
Y6=[127.2  134.8  135.8  135.5  114.4  101.3  77.9   63.1
44.5    23.1   0];

m = 3;

C6 = lspoly(X6,Y6,m)';

pause % Press any key to find the least squares polynomial.

clc;

% ~ ~ ~ ~ ~ ~ ~ ~ ~ ~ ~ ~
% Prepare graphics arrays
% ~ ~ ~ ~ ~ ~ ~ ~ ~ ~ ~ ~
a = 0.00;
b = 1;
h = (b-a)/500;
Xs6 = a:h:b;
Ys6 = polyval(C6,Xs6);

clc; figure(1); clf;

%~~~~~~~~~~~~~~~~~~~~~~
% Begin graphics section
%~~~~~~~~~~~~~~~~~~~~~~
a = 0.00;
b =  1;
c =  0;
d =  120;
whitebg('w');
plot([a b],[0 0],'b',[0 0],[c d],'b');
axis([a b c d]);
axis(axis);
hold on;
plot(X6,Y6,'or',Xs6,Ys6,'-g');
xlabel('x');
xlabel('Mole fraction of MMA');
```

```
ylabel('Pressure (bar)');
Mx1 = 'Least squares polynomial: y = P';
Mx2 = [Mx1,num2str(m),'(x).'];
title('Experimental isotherms for the MMA-CO2 system as per
McHugh at 105.5 °C');
grid off;
hold off;
figure(gcf); pause % Press any key to continue.

points1 = [X5;Y5];

clc; format long e;
%.........................................
% Begin section to print the results.
% Diary commands are included which write all
% the results to the Matlab textfile   output
%.........................................

Mx1='y = P(x) = c(1)x^m + c(2)x^m-1 +...+ c(m)x + c(m+1)';
Mx2=['A polynomial of degree m = ',num2str(m),' has been
fit.'];
Mx3='The coefficients are stored in the array  C = ';
clc,echo off,diary output,...
disp(''),disp(Mx1),disp(Mx2),disp(Mx3),...
disp(''),disp(C6'),disp('The given x-y points:'),...
disp('      x         y'),disp(points1'),diary off,echo on
pause % Press any key to analyze the results.
% .. .. .. .. ..
% Prepare results
% .. .. .. .. ..
points2 = [X6;Y6;polyval(C6,X6);Y6-polyval(C6,X6)]';

clc; format short;
%.........................................
% Begin section to print the results.
% Diary commands are included which write all
% the results to the Matlab textfile   output
%.........................................
Mx4='    x(k)      y(k)      P(x(k))   error';
clc,echo off,diary output,...
disp(''),disp(Mx4),disp(points2),diary off,echo on
%~~~~~~~~~~~~~~~~~~~~~~~~~~~~~~~~~~~~~~~~~~~~~~~~~~~~~~~~~~~~~~~
```

Appendix F (Continued):

```
%fit123MMA (individual plots)

plot(X1,Y1,'or',Xs1,Ys1,'-r',X2,Y2,'sr',Xs2,Ys2,'-
r',X3,Y3,'^r',Xs3,Ys3,'-r',...
   X4,Y4,'ob',Xs4,Ys4,'-b',X5,Y5,'sb',Xs5,Ys5,'-
b',X6,Y6,'^b',Xs6,Ys6,'-b');
xlabel('Mole fraction of MMA');
ylabel('Pressure (bar)');
title('MMA-CO2 experimental isotherms from this study (red)
at 40, 80 & 105.5 °C, vs. data by McHugh et al.(blue)');

gtext('40°C')
gtext('80°C')
gtext('105.5°C')

pause %press any key to continue
%~~~~~~~~~~~~~~~~~~~~~~~~~~~~~~~~~~~~~~~~~~~~~~~~~~~~~~~~~~~~~~~~~~~~
```